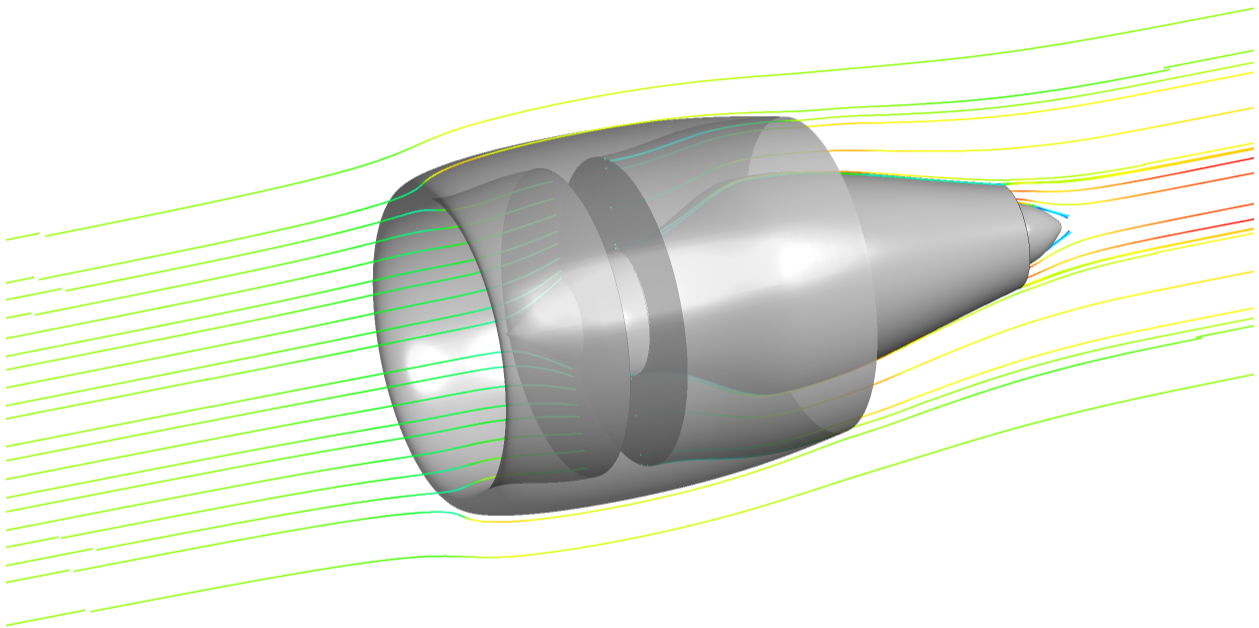




CHALMERS
UNIVERSITY OF TECHNOLOGY



Aerodynamic Evaluation of Nacelles for Engines with Ultra High Bypass Ratio

Master's thesis in Applied Mechanics

ANDREAS PETRUSSON

MASTER'S THESIS 2017:02

Aerodynamic Evaluation of Nacelles for Engines with Ultra High Bypass Ratio

ANDREAS PETRUSSON



Department of Applied Mechanics
Division of Fluid Dynamics
CHALMERS UNIVERSITY OF TECHNOLOGY
Göteborg, Sweden 2017

Aerodynamic Evaluation of Nacelles for Engines with Ultra High Bypass Ratio
ANDREAS PETRUSSON

© ANDREAS PETRUSSON, 2017.

Supervisor: Anders Lundbladh, GKN Aerospace
Examiner: Olivier Petit, Chalmers University of Technology

Master's Thesis 2017:02
Department of Applied Mechanics
Division of Fluid Dynamics
Chalmers University of Technology
SE-412 96 Göteborg
Telephone +46 31 772 1000

Cover: Visualisation of an axisymmetric turbofan geometry constructed in this project and streamlines from CFD simulations.

Typeset in L^AT_EX
Göteborg, Sweden 2017

Abstract

The aim in this project is to gain deeper understanding of nacelle drag for engines with ultra high bypass ratio. 2D axisymmetric nacelles with different fan cowl thickness and length are studied to investigate how these parameters affect the nacelle drag. Some different fan pressure ratios is also investigated. Furthermore, the drag for an aircraft fuselage with a fan and fan cowl at the rear that ingest the boundary layer of the fuselage is studied. This is the last part of the project and therefore this work still requires further study.

First the geometries of the nacelles are designed. The fan cowl and inlet profiles of the nacelle are designed using a CST method, based on fourth order Bernstein polynomials. This allows for specifying the initial curvature radius of the profile, along with maximum radius and trailing edge position and slope. A core engine cowl and a bypass channel are also designed using these curves, but the internal parts of the core engine are not included in this project and the core nozzle is only considered as an outlet boundary. These geometries are simulated in an axisymmetric section using CFX, and the drag was computed from the flow state and pressure forces on the nacelle surfaces. The geometries of the boundary layer ingestion cases are constructed in a similar manner to the nacelles. For these cases, a whole aircraft fuselage is placed in front of a nacelle, with the rear of the fuselage going into the inlet of the nacelle. The fan diameter is varied to study the effect on drag, which means that different portions of the boundary layer are ingested by the fan.

It is concluded that only shortening the fan cowl does not lower nacelle drag, since the aft core cowl should also be considered to contribute to the drag. Redesigning the aft core cowl could give a lower drag for the shorter and thinner cowl that are investigated, but the designs in this project does not take this into account. For the boundary layer ingestion cases, the drag is decreased more if a larger portion of the boundary layer is ingested. However, it could be more efficient if only some part of the boundary layer is ingested.

Keywords: Turbofan, Nacelle, Drag, Ultra-high bypass ratio, CFX, CST curve.

Acknowledgments

My first thanks goes to Anders Lundbladh at GKN Aerospace for his great support throughout the project. It was at his initiative the project was started, and without his guidance the project would not have been as successful. At GKN I would also like to thank Lars Ellbrant and Bernard Gustavsson for their support and our discussions regarding the CFD simulations. My last thanks goes to my examiner Olivier Petit for his dedication to the project and his feedback on my work.

Andreas Petrusson, Göteborg, January 2017

Contents

List of Figures	xiii
List of Tables	xv
Nomenclature	xvii
1 Introduction	1
1.1 Background	1
1.2 Problem Definition	2
1.3 Aim of the Project	2
1.3.1 Limitations	3
1.3.2 Method	3
2 Theory	5
2.1 Turbofan engine	5
2.1.1 Flow Physics	5
2.1.2 Installation Performance	6
2.2 Thrust and Drag	8
2.2.1 Thrust and Drag Components	8
2.2.1.1 Profile and Wave Drag	8
2.2.1.2 Spillage Drag	8
2.2.1.3 Interference Drag	9
2.2.2 Forces on an Isolated Nacelle	9
2.2.2.1 Single Streamtube Nacelle	9
2.2.2.2 Two streamtube Nacelle	11
2.2.3 Book Keeping System	12
2.2.4 Extracting Thrust and Drag from CFD	13
2.3 Nacelle Cowl Profiles	13
2.3.1 NACA 1-series Nacelle Cows	14
2.3.2 Class-Shape Transformation Based Nacelle Cows	15
3 Method	19
3.1 Creating Axisymmetric Geometries	19
3.1.1 Fan Cowl Profile Design	19
3.1.1.1 ESDU Method	20
3.1.1.2 Class-Shape Transformation Curve Method	21

3.1.2	Engine Core Geometry Design	22
3.1.2.1	Preliminary Core Geometry Design	22
3.1.2.2	Parametric Core Geometry Design	24
3.1.3	Bypass Channel Design	25
3.1.4	Nacelle Test Case Design	26
3.1.4.1	Parameterisation	27
3.1.5	Boundary Layer Ingestion Test Case Design	28
3.1.5.1	Fuselage Design	29
3.1.5.2	Parameterisation	30
3.2	Case Definitions	31
3.2.1	Nacelle Test Cases	32
3.2.1.1	Nacelle Test Cases Motivation	32
3.2.1.2	Turbofan Engine Cycle Design	33
3.2.1.3	The Eight Test Case Nacelles	34
3.2.2	Boundary Layer Ingestion Test Cases	34
3.2.2.1	Motivation of BLI Test Cases	35
3.2.2.2	The Four BLI Test Case Geometries	36
3.3	Computational Fluid Dynamics	36
3.3.1	Meshing	36
3.3.1.1	Geometry	37
3.3.1.2	Mesh Strategy	37
3.3.1.3	Mesh Convergence Study	38
3.3.2	Model setup	39
3.3.2.1	Schemes	39
3.3.2.2	Boundary Conditions	39
3.3.2.3	Convergence	40
3.3.3	Post Processing	40
4	Results	41
4.1	Convergence	41
4.2	Evaluation of Different Fan Cowl Length and Thickness	44
4.3	Evaluation of Different Fan Pressure Ratio	47
4.3.1	Cycle Designed FPR	48
4.3.2	Throttled FPR	50
4.4	Evaluation of Only Changing Fan Cowl Thickness	52
4.5	Evaluation of Effects from Flight Mach Number	55
4.6	Evaluation of Different Nacelle Length and Thickness at End of Runway	57
4.7	Engine Performance of Nacelle Test Cases	60
4.7.1	Inlet, Fan, and Bypass Pressure Ratios	60
4.7.2	Discharge Coefficient	62
4.7.3	Thrust	63
4.8	Boundary Layer Ingestion	64
4.8.1	BLI Engine Performance	68
5	Conclusion	71
5.1	Concluding Remarks on the Nacelle Test Cases	71
5.2	Concluding Remarks on the BLI Test Cases	71

5.3	Future Work	72
5.3.1	Improvements and Further Investigations of Nacelles	72
5.3.2	Improvements and Further Investigations of BLI	72
	Bibliography	75
A	MATLAB function used to generate cowl profiles	I
B	MATLAB function for generating core geometries	V
C	MATLAB script for generating nacelle test cases	VII
D	MATLAB code for generating core geometries for BLI cases	XV
E	MATLAB script for generating geometries of BLI test cases	XVII
F	Cycle data used in the project	XXVII
F.1	FPR 1.4 cycle, 2m fan	XXVII
F.2	FPR 1.3 cycle, 2m fan	XXXVI
G	Table used to evaluate discharge and thrust coefficient	XXXIX
H	Table of drag and thrust components	XLV
I	Table with pressures and pressure ratios	XLIX

List of Figures

2.1	Layout of a turbofan engine	5
2.2	Station numbering in a turbofan engine	7
2.3	Single streamtube nacelle	10
2.4	Two stream nacelle	11
2.5	Definition of surfaces on the nacelle for drag and thrust book keeping system	12
2.6	CST and NACA 1 cowl curve comparison	17
3.1	Example of nacelle profile from ESDU based method	20
3.2	Example of nacelle profile from CST curve based method	21
3.3	Preliminary geometries based on the CFM56-7B and UltraFan engine	23
3.4	Illustration of input parameters for parametric core engine geometry generation	25
3.5	The BLI nacelle and rear fuselage geometry, with station numbering .	29
3.6	The fuselage geometry of the BLI cases	30
3.7	Geometries used in nacelle test cases	35
3.8	Geometries used in boundary layer ingestion test cases	36
3.9	Mesh around the nacelle in test case 2	38
4.1	Pressure wave propagation in computational domain	42
4.2	Development of integrated pressure on nacelle surface during simulation	43
4.3	Development of integrated pressure on fuselage surface during simulation	44
4.4	Mach number contour for different sized nacelles	46
4.5	Comparison of drag for the four nacelle geometries	47
4.6	Mach number contour for different designed fan pressure ratios	49
4.7	Comparison of drag for different fan pressure ratios	49
4.8	Mach number contour for different throttled fan pressure ratios . . .	51
4.9	Mach number contour for different thickness of nacelles	53
4.10	Comparison of drag for different thickness of nacelles	54
4.11	Mach number contour for different flight Mach numbers	56
4.12	Comparison of drag for different flight Mach numbers	57
4.13	Mach number contour for different sized nacelles at end of runway . .	59
4.14	Comparison of drag for different sized nacelles at end of runway . . .	60
4.15	Contours of Mach number around BLI	65
4.16	Contours of total pressure around BLI	66

4.17	Comparison of drag for boundary layer ingestion	67
4.18	The decrease of drag relative the increase of F_{nps} for the BLI test cases	68

List of Tables

2.1	NACA 1 series cowl ordinates	14
3.1	Input to ESDU method	20
3.2	Input to CST method	22
3.3	Input parameters that define the core engine geometry	24
3.4	Parameterisation constants used in the geometry generating MAT-LAB code	27
3.5	Constants used to parameterise the BLI case geometries	31
3.6	Definitions of nacelle test cases	32
3.7	Summary of main parameters from cycle designs	33
3.8	Definitions of nacelle test cases	36
4.1	Status on convergence criteria in simulation cases	41
4.2	Summary of parameters for nacelle test cases with different nacelle length and thickness	44
4.3	Fan cowl wall shear and wall shear relative fan cowl and pre-entry force for nacelle test cases 1 to 4	47
4.4	Summary of parameters for nacelle test cases with different fan pressure ratios	48
4.5	Fan cowl wall shear and wall shear relative fan cowl and pre-entry force for nacelle test cases 3.0 and 5	50
4.6	Fan cowl wall shear and wall shear relative fan cowl and pre-entry force for nacelle test cases 3.0, and 3.1 to 3.4	50
4.7	Summary of parameters for nacelle test cases with different nacelle thickness	52
4.8	Fan cowl wall shear and wall shear relative fan cowl and pre-entry force for nacelle test cases 3.0, 6, and 7	54
4.9	Summary of parameters for nacelle test cases with different nacelle thickness	55
4.10	Summary of parameters for nacelle test cases with different nacelle length and thickness	58
4.11	Fan pressure ratios obtained in simulations for the nacelle test cases .	60
4.12	Inlet pressure recovery obtained in simulations for the nacelle test cases	61
4.13	Bypass pressure ratio obtained in simulations for the nacelle test cases	62
4.14	Bypass nozzle discharge coefficients obtained in simulations for the nacelle test cases	62

4.15	Bypass nozzle thrust coefficients obtained in simulations for the nacelle test cases	63
4.16	Fan cowl wall shear and wall shear relative fan suction force for BLI test cases	67
4.17	Engine performance parameters for the BLI cases	68
4.18	Fan energy output for BLI test cases	69
G.1	Nozzle quantities, and thrust and drag coefficients for nacelle test cases	XXXIX
G.2	Nozzle quantities, and thrust and drag coefficients for BLI test cases .	XLIII
H.1	Components of thrust and drag for nacelle test cases	XLV
H.2	Components of thrust and drag for BLI test cases	XLVII
I.1	Pressures [Pa] and pressure ratios of nacelle test cases	XLIX
I.2	Pressures [Pa] and pressure ratios of BLI test cases	LI

Nomenclature

Abbreviations

BLI	Boundary layer ingestion
BPR	Bypass ratio
CST	Class shape transformation
FPR	Fan pressure ratio
OPR	Overall pressure ratio
TO	Take Off, referring to end of runway test cases
UHBR	Ultra high bypass ratio

Greek Letters

β	The angle of a tangent to a curve
γ	Heat capacity ratio
ϕ	Resulting force on surface
ρ	Density
τ	Wall shear

Latin Letters

\dot{m}	Mass flow
C_D	Discharge coefficient
C_F	Thrust coefficient
A	Area
BP	Bernstein polynomial
bp	Bernstein polynomial weighting coefficients
C	Class function
D	Drag
F	Thrust
M	Mach number
n	Normal vector

P	Pressure
S	Surface
u	Velocity normal to surface
V	velocity

Subscripts

∞	Far down stream condition
0	Far upstream condition
0	Free stream condition
1	Condition at the engine inlet plane
18	Condition at the engine bypass nozzle exit
2	Condition at the engine fan face
8	Condition at the engine core nozzle exit
a	After-body
acc	Aft core cowl
f	Fore-body
hi	Indicating variable located at the fan cowl highlight
n	Polynomial order
nps	Net propulsive system
plug	Exhaust plug
ref	Reference condition
s	Referring to static quantity
t	Referring to total quantity
te	Indicating variable located at the fan cowl trailing edge

Chapter 1

Introduction

1.1 Background

In 2015, at the Paris climate conference, the first legally binding deal for climate change was adopted [1]. One important part was to limit the increase of average global temperature to well below 2°C. The EU has set a target to reduce their green house gas emissions by at least 40% relative 1990's emissions levels by 2030. Approximately 3% of EU's green house emissions come from aviation [2]. The emissions from aviation is predicted to increase around 70% relative 2005's emissions levels by 2020. To lower green house emissions from the aviation industry, research is aimed at lowering fuel consumption and increase efficiency.

One way to lower fuel consumption and increase the propulsive efficiency of turbofan engines is to lower the fan pressure ratio (FPR) [3]. This can be done by lowering the rotational speed of the fan, which has been made possible by placing a gear box between the low pressure turbine and the fan [4]. To achieve the same thrust with a lower FPR, a larger mass flow through the engine is needed, which means that the diameter of the fan increases. The larger mass flow also means that a smaller portion of the flow goes through the core which powers the fan. The ratio of the flow going through the bypass and the core is called the bypass ratio (BPR).

During the period 1975 to 2015 the BPR increased from approximately 6 to 12 and is expected to increase further [4]. An example is the UltraFan concept by Rolls Royce, which is expected to have a BPR exceeding 15 [5]. Engines with BPR of this size are called Ultra High Bypass Ratio (UHBR) engines. Increasing BPR means increasing the diameter of the engine. In turn this would result in a larger and heavier nacelle. The benefits sought by increasing the bypass ratio is a better propulsive efficiency and thus fuel efficiency, which would be lessened by a heavier engine with higher aerodynamic drag because of its increased size. To gain further increases in fuel efficiency the nacelle could be made shorter and thinner, thus reducing weight and drag.

There could be complications to the stability of the flow around and into the engine if the nacelle is made too short. Regarding the flow around the engine, flow separation on the outside surface would give an increased drag. This limits the curvature on the outside of the nacelle and thus also the nacelle length. Since parts essential for the operation of the engine is placed in the nacelle, it can not be made too thin, which means that a short nacelle might need to be the same thickness as a longer

nacelle. Then the outside would have a high curvature and the risk for separation would be high, and in that case a somewhat longer nacelle could be beneficial.

In [6] the limitations of short inlet nacelle design are discussed. The efficiency of the fan is dependent on the flow condition in the inlet. An even pressure profile into the fan give best performance, but it is required that the flow is attached and have a low fan rotor incidence. If the flow separates, the core engine can be subjected to high wear. The requirement on the inlet flow limits the nacelle thickness and inlet length since the flow must be able to follow the surface. The risk for separation becomes most critical at high angle of attack, for example at take off, at the lower part of the inlet. This is the reason a nacelle is generally thicker at the bottom.

An other concept that could potentially lower fuel consumption is to implement a third turbofan engine at the rear end of the aircraft. A part of the aircraft boundary layer is then ingested into this engine, reducing the boundary layer thickness while the slower moving air of the boundary layer also increases the propulsive efficiency of the engine [7]. Instead of using a turbofan cycle, it has also been proposed to drive the fan of this engine with an electric motor, which in turn is powered by the main engines under the wings.

1.2 Problem Definition

To understand the development in UHBR turbofan nacelles, system level performance parameters such as external drag and thrust will be evaluated for different nacelle lengths and thicknesses, at different fan pressure ratios and bypass ratios. Furthermore, system level performance of a boundary layer ingesting turbofan will be evaluated. What drag reduction can be obtained by reducing the nacelle size, and how the drag is affected by FPR and BPR will be studied. For the different nacelles, any effect on the thrust will also be studied. In the case of boundary layer ingestion, the benefit of reduced fuselage drag will be studied.

1.3 Aim of the Project

The aim of this project is to evaluate the aerodynamics around the nacelle, in the inlet, and in the bypass channel of turbofan engines of varying design. The aerodynamics will be evaluated in a 2D axisymmetric case using computational fluid dynamic (CFD) simulations. The evaluation will consist of a cruise design point case, that is at 35 000 feet and Mach 0.8, and at end-of-runway case, that is at sea level and Mach 0.25. In addition, a part of the project is to evaluate the aerodynamics of an electrically driven fan that ingest the boundary layer of an aircraft fuselage.

1.3.1 Limitations

In this project the geometries and flow cases are limited to 2D axisymmetric, which means that no angle of attack, scarfing, or different thicknesses around the nacelle can be considered, nor any parts for mounting the engine to the aircraft. The geometries will not be that of any existing design, but will try to mimic some geometric relations by using a parametric design method. When looking at the performance of the engine, the drag and thrust will be the main parameters of interest, and the weight and its effect on over all performance of the aircraft will not be included.

1.3.2 Method

To evaluate the 2D axisymmetric aerodynamics of nacelles, first a geometry is needed. This will be created from cycle data of turbofan engines extracted from the design tool GasTurb 9. Parameters that are needed are temperatures, pressures, mass flows, and nozzle exit areas. These, together with some geometric relations, for example length of fan cowl trough fan diameter, will be changed to generate different geometries for test cases. The geometry will be constructed in MATLAB, and then exported to the meshing tool ICEM. The simulations will then be done using ANSYS CFX and using ANSYS CFD-post results of interest, such as drag, will be extracted.

Chapter 2

Theory

2.1 Turbofan engine

In this section a short introduction to the turbofan engine, and the general flow around a nacelle, both in 3D and 2D, is made. A layout of a turbofan nacelle can be seen in Figure 2.1, where also the different parts of the engine are presented. Note that the fan guide vanes are not included in this figure, since these are considered to be a part of the fan system, marked by "Fan" in the figure, in this project. These should otherwise be placed behind the fan in the bypass channel. The focus will in this section be on the nacelle, bypass channel, fan, and nozzle exits. In this context the nacelle refers to all external parts of the engine, that is the outside of the fan cowl, the aft core cowl and the exhaust plug. The core engine would for a geared fan consist of two compressors: the booster and high pressure compressor (HPC), the combustor, and two turbines: the high pressure turbine (HPT) and low pressure turbine (LPT). The HPT drives the HPC, and the LPT drives both the booster and the fan through the gear.

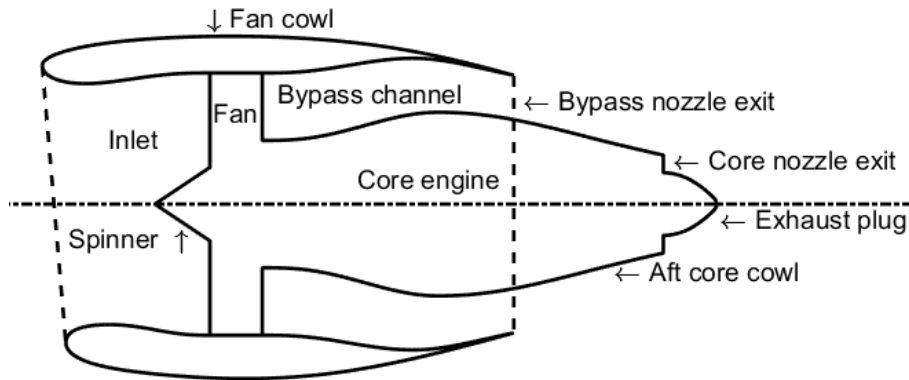


Figure 2.1: Layout of a turbofan engine

2.1.1 Flow Physics

The shape of a turbofan nacelle is in itself non-symmetric and 3-dimensional, resulting in a 3D flow. The potential flow around the wing of an airplane results in an

upwash, which gives an angle of attack of the free stream relative to the rotational axis of the engine [6]. That means that it would not be possible to fly at cruise, with the air flowing towards the intake with an angle perpendicular to the fan face. In turn, this means that an axisymmetric turbofan nacelle would not be optimal. One way that a nacelle compensates for this is scarfing, which means that the angle of the plane at the edge of the inlet is tilted (see front of nacelle in Figure 2.1) so that it is perpendicular to the flow at cruise. The scarfing also compensates for some of the angle of attack at take-off.

Looking at the nacelle as a series of airfoils in a circle, the airfoil on the underside will experience a negative angle of attack, while the airfoil on the top side will experience a positive angle of attack. It is required that the flow remains attached in the inlet and this sets conditions on the thickness of the profile of the lower part of the nacelle. This requirement is not critical on the top part, because of the positive angle of attack, but here separation on the outside of the nacelle needs to be avoided. Therefore the angle of the centerline in the front of the top profile is adjusted so that no separation occurs. Both these conditions must be fulfilled at take-off, where the angle of attack is the highest.

If the pressure in the intake is non symmetric due to separation in the lower part at a high angle of attack, the flow through the fan and subsequent compressors can become unstable [8]. This can in turn lead to vibrations in compressor blades, inefficient combustion, and decrease in overall efficiency and thrust. This is most critical at take-off where the most thrust is needed, while the risk for separation in the inlet is highest.

The wing will affect the flow around the engine in other ways than just upwash. There will also be some installation effects. The pressure on the rear of the nacelle will be affected by the low pressure under the wing, which also means that the jet from the nozzles is affected. Furthermore, the air has to flow around the mount, or the pylon, between the engine and wing.

A 2-dimensional axisymmetric turbofan engine cannot have a fan cowl with different camber angle or thickness at different positions around the cowl, nor any scarfing, as described above, and the risk for flow separation would be high at high angle of attack. But, to simplify the flow around the turbofan to a 2D axisymmetric case the angle-of-attack has to be zero. In turn, this means that both the flight angle at take-off and the effects from the wing and pylon needs to be neglected.

2.1.2 Installation Performance

All components in the engine have some efficiency, but also the performances of the inlet and nozzles are described using some efficiency parameters. For the inlet a pressure recovery parameter is used, which is the total pressure just in front of the inlet divided by the total pressure at the fan. Using the station numbering presented in Figure 2.2, the pressure recovery becomes P_2/P_1 . The same type of pressure ratio can be used to describe the bypass nozzle performance, that is the nozzle pressure ratio is P_{18}/P_{13} . Note that the station 13 is located after the fan guide vanes, but

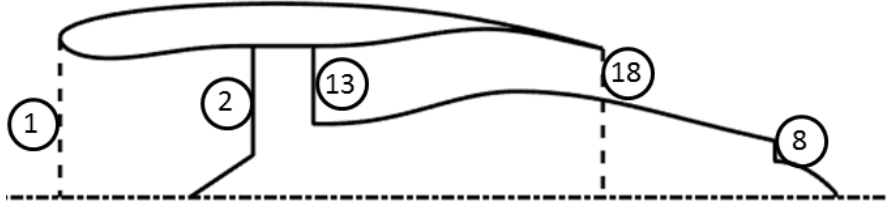


Figure 2.2: Station numbering in a turbfan engine

as these are not a part of the geometry the station is placed at the outlet of the fan. The effects from the guide vanes are here considered as a part of what happens in the fan.

The performance of the nozzles can also be described by discharge coefficients and thrust coefficients. The discharge coefficient is

$$C_D = \frac{A_{ideal}}{A_{actual}} \quad (2.1)$$

where A_{actual} is the exit area of the nozzle and A_{ideal} is the ideal exit area of the nozzle for that flow state [9]. The ideal area for a given mass flow can be calculated from the ideal exit velocity,

$$A_{ideal} = \frac{\dot{m}}{\rho V_{ideal}} \quad (2.2)$$

The ideal velocity can be found from the dynamic temperature, that is

$$V_{ideal} = \sqrt{2C_P(T_t - T_s)} \quad (2.3)$$

How the density and static temperature are obtained depend on whether the nozzle is choked or not. If the nozzle is choked

$$\frac{P_t}{P_s} = \left(1 - \frac{\gamma - 1}{\gamma + 1}\right)^{-\frac{\gamma}{\gamma - 1}} \quad (2.4)$$

where γ is the heat capacity ratio. Knowing the exit total pressure this gives the static pressure and in turn the density from the ideal gas law. If the nozzle instead is unchoked, the exit static pressure is the ambient static pressure and from knowing both the static and total pressure, the static temperature is

$$T_s = T_t \left(\frac{P_t}{P_0}\right)^{-\frac{\gamma - 1}{\gamma}} \quad (2.5)$$

From these equations the discharge coefficient can be computed knowing the mass flow, exit total temperature and pressure, and C_P .

When the ideal quantities above have been determined, an ideal thrust can be computed as

$$F_{ideal} = V_{ideal}\dot{m} + A_{ideal}(P_{s,exit} - P_0) \quad (2.6)$$

and from this the nozzle discharge coefficient

$$C_F = \frac{F_{actual}}{F_{ideal}} \quad (2.7)$$

If the actual thrust is known from experiment or simulation, the coefficient of thrust is then given. The second term of equation (2.6) only occurs if the nozzle is choked. Otherwise, the pressure at the exit is the same as the free stream pressure, that is $(P_{s,exit} - P_0) = 0$.

2.2 Thrust and Drag

This section will deal with the theory behind defining the thrust and drag of a turbofan engine at a steady flow condition. It is important that the definitions of thrust and drag are consistent, with a clear book keeping method to differentiate between different effects. The importance of separating rearward force from drag is stresses in [9]. If the normal pressure force on a part of a closed body is considered, the resulting force is not considered drag if it is countered by an opposite force on a different part of the body.

2.2.1 Thrust and Drag Components

The drag of an isolated nacelle can be split into three components: profile drag, wave drag, and spillage drag, but an installed nacelle can be affected by the parts around it, giving one more drag components: interference drag.

2.2.1.1 Profile and Wave Drag

If the flow around the cowl is attached and subsonic, the profile drag, which is the sum of the skin friction and pressure drag acting on the outer surface of the nacelle, is the only component of drag [10, 9]. The pressure drag, sometimes called the form drag, arises from changes in pressure along the surface due to boundary layer growth, but possibly also flow separation at some part of the surface [9]. In the case where the flow becomes supersonic as it is accelerated along the outside of the nacelle, shock waves may occur which modifies the pressure distribution giving an increase in drag. This drag increase is the wave drag. The third component, the spillage drag, is a result of the flow at the inlet of the nacelle and will be discussed in more detail in Section 2.2.1.2.

2.2.1.2 Spillage Drag

At some operating point, the turbofan engine will ingest a certain amount of flow. For example at cruise the relative velocity at the inlet of the engine is lower than the free stream velocity. This deceleration could be represented by an expanding

streamtube, starting at a free stream condition and ending at the front of the inlet. Because of this the flow will not be parallel to the free stream at the leading edge of the fan cowl. As the flow then has to turn around the fan cowl, a lower pressure is expected further back on the fan cowl. Thus the risk of separation on the outside of the fan cowl increases as a higher relative velocity in the free stream or a lower relative velocity at the inlet is experienced. The increase of drag due to the higher pressure in front of the inlet is referred to as spillage drag [9]. To be able to measure spillage drag, a reference condition is needed. This reference condition should then per definition have no spillage drag, which would be achieved if the streamtube entering the inlet is completely straight. If separation occurs on the outside of the fan cowl, a rapid rise in spillage drag will be experienced [10]. Separation can still occur at the rear of the fan cowl even if there is no spillage drag due to a bad design.

2.2.1.3 Interference Drag

An installed engine under the wing of an airplane will experience an increased drag compared to the isolated nacelle, both due to the pylon, which holds the engine under the wing, and the presence of interference drag. The drag contribution of the pylon could be considered as separate from the nacelle, but the interference drag can be seen as a reflection in surfaces, resulting in a change in pressure. According to [8] the interference drag will give a negative contribution to the net propulsive force, which would suggest that the total drag of an installed nacelle should include this term. But, the definitions of net propulsive force and drag presented in this section will be for an isolated nacelle, thus no interference drag will be considered.

2.2.2 Forces on an Isolated Nacelle

From the drag descriptions in Section 2.2.1, it is clear that the nacelle drag can be extracted from the pressure distribution on its surface.

2.2.2.1 Single Streamtube Nacelle

The resulting forces on a single streamtube nacelle can be divided into three parts: pre-entry, nacelle, and post-exit forces. These correspond to ϕ_{pre} , $\phi_{nacelle}$, and ϕ_{post} , shown in Figure 2.3. The pre-entry force can be evaluated by looking at the pressure forces and the momentum flux acting on the streamtube in front of the nacelle, which is the tube enclosed by the dashed lines between stations 0 and 1 in Figure 2.3. Newton's second law then gives the pre-entry force and in the same way the post-exit force

$$\phi_{pre} = \int_{A_1} P dA + \dot{m}_1 V_1 - \left(\int_{A_0} P dA + \dot{m}_0 V_0 \right) \quad (2.8)$$

$$\phi_{post} = \int_{A_\infty} P dA + \dot{m}_\infty V_\infty - \left(\int_{A_8} P dA + \dot{m}_8 V_8 \right) \quad (2.9)$$

The nacelle force is the force exerted on the outside surface of the nacelle, which is the sum of pressure and shear forces

$$\phi_{nacelle} = \int_{S_{nacelle}} (P - P_0) + \tau dA \quad (2.10)$$

Now the drag of the nacelle is

$$D_{nacelle} = \phi_{pre} + \phi_{nacelle} + \phi_{post} \quad (2.11)$$

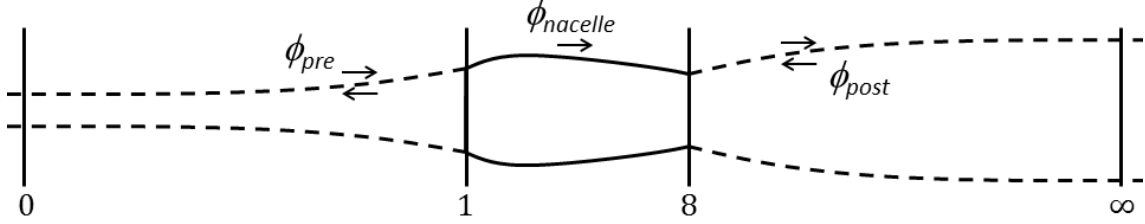


Figure 2.3: Single streamtube nacelle

Considering the nacelle in Figure 2.3, the forces at the front and back of the nacelle are usually accounted separately [9]. The nacelle is divided into a fore-body, stretching from the front end to the maximum radius, and an after-body, stretching from the maximum radius to the rear end. The drag for each part can be expressed as

$$D_{nacelle,f} = \phi_{pre} + \phi_{nacelle,f}, \quad (2.12)$$

$$D_{nacelle,a} = \phi_{nacelle,a} + \phi_{post} \quad (2.13)$$

The net propulsive force is the total thrust force on the propulsion system including the drag of the nacelle ($D_{nacelle}$) and the net thrust (F_{net}),

$$F_{nps} = F_{net} - D_{nacelle} \quad (2.14)$$

where the net thrust is the force at the exit nozzle plane minus the free stream momentum, or ram drag. Assuming the nozzle is choked

$$F_{net} = F_{gross} - D_{ram} = \int_{A_8} (\rho u^2 + (P - P_a)) dA - \dot{m} V_0 \quad (2.15)$$

Here u is the velocity normal to the nozzle exit plane. On its simplest form the net propulsive force does not consider contributions from the post term, that is

$$F_{nps} = F_{net} - \phi_{pre} - \phi_{nacelle} \quad (2.16)$$

This means that the influence from the far field condition in the jet (∞ in Figure 2.3) is not accounted for. It is motivated to use this accounting since it is difficult to determine the far field condition, both in experiments and simulations. Inserting equation (2.12) gives

$$F_{nps} = F_{net} - (D_{nacelle,f} + \phi_{nacelle,a}) \quad (2.17)$$

which is called the hybrid force accounting system, where the sum of the drag for the fore-body and the force on the after-body of the nacelle is counted as the drag. The hybrid drag for a single streamtube nacelle is defined as

$$D_{hybrid} = D_{nacelle,f} + \phi_{nacelle,a} \quad (2.18)$$

Looking at a flow condition where the streamtube between stations 0 and 1 in Figure 2.3 is straight, that is no expansion or compression of the flow occurs, the spillage drag must be zero from the definition in Section 2.2.1.2. Using this as a reference condition, the spillage drag can be defined as the difference between the experienced drag of the fore-body and that of the reference condition ($D_{nacelle,f,ref}$)

$$D_{spill} = D_{nacelle,f} - D_{nacelle,f,ref} \quad (2.19)$$

2.2.2.2 Two streamtube Nacelle

A turbofan engine can be represented by a two streamtubes nacelle, where one streamtube enters and two leave the nacelle; one from the bypass and one from the core nozzle. The nacelle also has two external parts at the rear of the nacelle: the aft core cowl and the exhaust plug. The forces on these parts are denoted ϕ_{acc} and ϕ_{plug} , respectively, in Figure 2.4. The forces on these parts may contribute to drag or thrust, depending on accounting system.

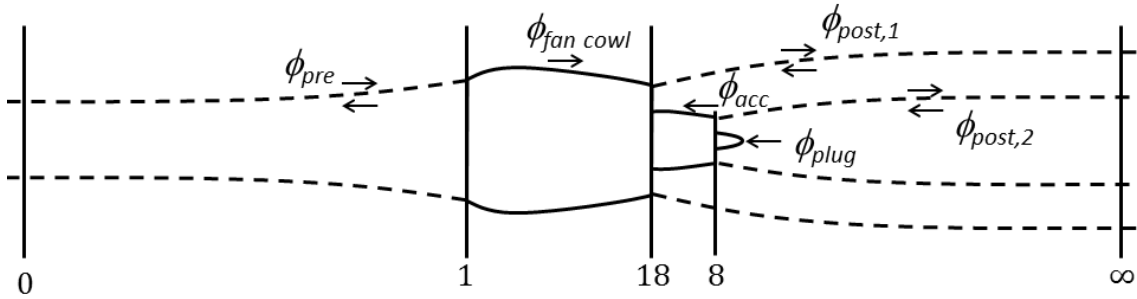


Figure 2.4: Two stream nacelle

Because there are two streamtubes exiting the nacelle, two different post-exit forces are defined: $\phi_{post,1}$ for the bypass stream and $\phi_{post,2}$ for the core stream. In this case it becomes even more complicated to determine these forces and, as for the single streamtube nacelle, a hybrid force accounting where these forces are not considered is often used. The hybrid drag for a two streamtube nacelle, which compares to a turbofan nacelle, is obtained by replacing $\phi_{nacelle,a}$ in equation (2.18) by the forces acting on the rear of the nacelle in Figure 2.4. The drag then becomes

$$D_{hybrid} = D_{fan\ cowl,f} + \phi_{fan\ cowl,a} + \phi_{acc} + \phi_{plug} \quad (2.20)$$

Choosing to account the forces on the aft core cowl and exhaust plug as drag, the gross thrust can be expressed as the sum of impulse and pressure contributions from

the two exhausts, that is

$$F_{gross} = \int_{A_{18}} (\rho u^2 + (P - P_0)) dA + \int_{A_8} (\rho u^2 + (P - P_0)) dA$$

which gives the net thrust by subtracting the ram drag

$$F_{net} = \int_{A_{18}} (\rho u^2 + (P - P_0)) dA + \int_{A_8} (\rho u^2 + (P - P_0)) dA - \dot{m}_{inlet} V_0 \quad (2.21)$$

Accounting the forces on the aft core cowl and exhaust plug as thrust, a modified hybrid drag can be defined as

$$D_{modified\ hybrid} = D_{fan\ cowl,f} + \phi_{fan\ cowl,a} \quad (2.22)$$

Choosing this type of accounting would mean that the thrust depends on the design of the nacelle, which would make designing a turbofan engine cycle more difficult as it would have to include a design of the aft core cowl and exhaust plug. It is therefore preferable to use the previous accounting method, where the forces on these parts are counted as contributions to drag.

2.2.3 Book Keeping System

From the definitions of thrust and drag in Section 2.2.2, a book keeping system for an axisymmetric turbofan can be established. For the accounting of thrust to be consistent to a cycle design tool, only the nozzles are considered to contribute to thrust. Furthermore, the nozzle exit planes are assumed to be perpendicular to the rotational axis of the engine so that the axial velocity component will give the impulse at the nozzle exit. This also means that the forces acting on the aft core cowl and the exhaust plug are considered drag. Figure 2.5 shows how the surfaces on a nacelle are defined using this book keeping system.

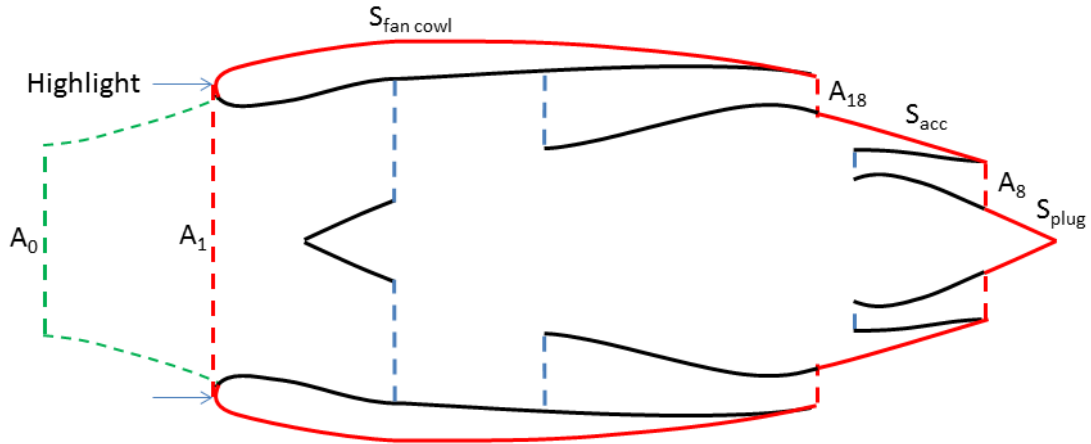


Figure 2.5: Definition of surfaces on the nacelle for drag and thrust book keeping system

When computing the pre-entry force, the inlet plane should be located at the point where the flow is split into internal and external flow, that is the stagnation point at the front of the fan cowl. This is not a fixed point and will change with the flow conditions, but as the pressure term in the integral of the pre-entry force will be very similar if the inlet plane is moved to a location a small distance away from the stagnation point, the inlet plane is assumed to be fixed at the highlight of the fan cowl. Looking at the inlet of the nacelle in Figure 2.5, the difference between the location of the highlight and the stagnation point (where the streamtube entering the inlet connects to the fan cowl) can be seen.

The accounting system presented here uses equation (2.21) as the definition of net thrust, where in this case u is the axial velocity at the exit planes of the nozzles and (2.20) as the definition of drag. It is equivalent to summing the forces acting on a control volume enclosed by the surface A_0 , the surface of the streamtube between A_0 and A_1 , and the surfaces $S_{fan\ cowl}$, A_{18} , S_{acc} , A_8 , and S_{plug} in Figure 2.4.

2.2.4 Extracting Thrust and Drag from CFD

Extracting thrust from CFD simulations is quite straight forwards using the accounting system described in Section 2.2.3. By placing planes perpendicular to the flight direction covering the nozzle exits and using for example equation (2.21), the net thrust for the turbofan can be computed.

The drag components discussed earlier in this chapter are difficult to separate in a CFD solution, but the hybrid drag accounting can be evaluated from the flow field around the nacelle. Pressure forces, shear forces and impulses at inlet and nozzle exits give the forces on the nacelle which are needed to compute the forces on different parts. The fan cowl fore-body drag in equation (2.20) can be computed as

$$D_{fan\ cowl,f} = \int_{A_1} \rho u^2 + (P - P_0) dA - \dot{m}_1 V_0 + \int_{S_{fan\ cowl,f}} (\tau_x + n_x(P - P_0)) dA \quad (2.23)$$

where τ_x is the wall shear in the axial direction and n_x is the axial component of the outward facing surface normal vector. Expressing equation (2.20) in integrals then gives that

$$D_{hybrid} = \int_{A_1} \rho u^2 + (P - P_0) dA - \dot{m}_1 V_0 + \int_{S_{fan\ cowl} \cup S_{acc} \cup S_{plug}} (\tau_x + n_x(P - P_0)) dA \quad (2.24)$$

2.3 Nacelle Cowl Profiles

Looking at a nacelle cross section, the profile is similar to a wing profile. There are different methods of constructing this profile curve, but two are presented in this section. The first is a method based on a well tested profile with high critical speed,

which is used as the fore-body. The second is a class-shape transformation based method, where the profile curve is built from a polynomial curve.

2.3.1 NACA 1-series Nacelle Cowls

The NACA-1 cowl provides a profile for the fore-body of the cowl. In [10] the whole cowl geometry is defined in three parts: the fore-body being a NACA-1 cowl, then a cylindrical mid-body, and finally a after-body either described by a circular arc ending in a straight line or a parabolic curve.

Table 2.1 shows the ordinates for a NACA-1 cowl profile, with a nose radius of $0.025Y$ [11]. Y is the height and X is the length of the fore-body of the cowl and both are measured from the highlight radius to the maximum radius. The highlight is the furthest most point on the profile. Results from wind tunnel tests, in the form of charts, are presented in [11]. These charts makes it possible to design a cowl with a certain critical Mach number, which is the flight Mach number causing sonic flow somewhere on the cowl, given fluid properties, diameter of the cowl, and the mass flow needed in the engine \dot{m}_1 . For example, requiring a critical Mach number $M_{crit} = 0.83$, and a mass flow coefficient $(\dot{m}_1/(\rho_0 F V_0)) = 0.130$, gives an inlet to cowl diameter ratio of 0.526 and a cowl length to cowl diameter ratio of 1.16. F is the cross sectional area of the cowl.

Table 2.1: NACA 1 series cowl ordinates

x/X [%]	y/Y [%]	x/X [%]	y/Y [%]	x/X [%]	y/Y [%]	x/X [%]	y/Y [%]
0.0	0.00	13.0	41.94	34.0	69.08	60.0	89.11
0.2	4.80	14.0	43.66	35.0	70.05	62.0	90.20
0.4	6.63	15.0	45.30	36.0	71.05	64.0	91.23
0.6	8.12	16.0	46.88	37.0	72.00	66.0	92.20
0.8	9.33	17.0	48.40	38.0	72.94	68.0	93.11
1.0	10.38	18.0	49.88	39.0	73.85	70.0	93.95
1.5	12.72	19.0	51.31	40.0	74.75	72.0	94.75
2.0	14.72	20.0	52.70	41.0	75.63	74.0	95.48
2.5	16.57	21.0	54.05	42.0	76.48	76.0	96.16
3.0	18.31	22.0	55.37	43.0	77.32	78.0	96.79
3.5	19.94	23.0	56.66	44.0	78.15	80.0	97.35
4.0	21.48	24.0	57.92	45.0	78.95	82.0	97.87
4.5	22.96	25.0	59.15	46.0	79.74	84.0	98.33
5.0	24.36	26.0	60.35	47.0	80.50	86.0	98.74
6.0	27.01	27.0	61.52	48.0	81.25	88.0	99.09
7.0	29.47	28.0	62.67	49.0	81.99	90.0	99.40
8.0	31.81	29.0	63.79	50.0	82.69	92.0	99.65
9.0	34.03	30.0	64.89	52.0	84.10	94.0	99.85
10.0	36.13	31.0	65.97	54.0	85.45	96.0	99.93
11.0	38.15	32.0	67.03	56.0	86.73	98.0	99.98
12.0	40.09	33.0	68.07	58.0	87.95	100.0	100.00

2.3.2 Class-Shape Transformation Based Nacelle Cows

This method for designing a nacelle fan cowl is based on a class-shape transformation (CST) curve. A class function determines the outline of the curve, and then this is transformed using shape functions. The class function used in this method is

$$C(\psi) = \psi^{0.5} (1 - \psi) \quad (2.25)$$

which is a class function for a general round nosed airfoil [12]. As shape functions Bernstein polynomials are used, which are constructed as

$$\begin{aligned} BP_{i,n} &= K_{i,n} \psi^i (1 - \psi)^{n-i} \\ BP(\psi) &= \sum_{i=1}^n BP_{i,n} \end{aligned} \quad (2.26)$$

n is the order of the Bernstein polynomials and $K_{i,n}$ are the so called binomial coefficients defined as

$$K_{i,n} = \frac{n!}{i!(n-i)!} \quad (2.27)$$

The CST curve is now constructed from weighting each part of the Bernstein polynomials before summing them and then multiplying the class function, so

$$\xi(\psi) = \psi^{0.5} (1 - \psi) \sum_{i=1}^n bp_i BP_{i,n} + \psi \Delta \xi_{te} \quad (2.28)$$

where bp_i are the weighting coefficients and the term $\psi \Delta \xi_{te}$ is added to modify the ordinate of the trailing edge. If all weights are equal to one, the shape functions would not affect the class function, since the sum of the Bernstein polynomials always is one everywhere. By setting constraints on the profile curve, that is ξ , the weights bp_i can be solved from a system of equations.

The method presented in [13] uses fourth order Bernstein polynomials ($n = 4$), giving five unknown weighting coefficients. Five conditions are required to solve these, but two conditions can directly give two of the coefficients. The first is the initial fore-body radius r_{if} , which can be related to bp_0 as

$$bp_0 = \sqrt{\frac{2r_{if}}{L_{cowl}}} \quad (2.29)$$

where L_{cowl} is the length of the cowl profile [12]. The second is the angle β_{te} and vertical position $\Delta \xi_{te}$ of the curve at the trailing edge, which can be related to bp_n [12], n being the order of the polynomials, so in this method

$$bp_4 = \tan(\beta_{te}) + \frac{\Delta \xi_{te}}{L_{cowl}} \quad (2.30)$$

The maximum of the curve and the second derivative are used to solve the remaining coefficients. Setting the position of the maximum and knowing that the gradient must be zero at this point gives one equation on $\xi(\psi)$ and one on its derivative, and

the third is given by assuming that the second derivative at the trailing edge is zero. Rewriting equation (2.28) on matrix form and moving known terms to the left hand side gives

$$B = AX \quad (2.31)$$

$$B = \begin{bmatrix} b_1 \\ b_2 \\ b_3 \end{bmatrix} \quad A = \begin{bmatrix} a_{1,1} & a_{1,2} & a_{1,3} \\ a_{2,1} & a_{2,2} & a_{2,3} \\ a_{3,1} & a_{3,2} & a_{3,3} \end{bmatrix} \quad X = \begin{bmatrix} bp_1 \\ bp_2 \\ bp_3 \end{bmatrix}$$

Writing out the terms in the B and A matrices, they are

$$b_1 = \xi(\psi) - (bp_0 BP_{i=0,4}(\psi) + bp_4 BP_{i=4,4}(\psi)) C(\psi) - \psi \Delta \xi_{te} \quad (2.32)$$

$$b_2 = \frac{d}{d\psi} b_1 \quad b_3 = \frac{d^2}{d\psi^2} b_1$$

$$a_{1,j} = (BP_{i=1,4}(\psi) + BP_{i=2,4}(\psi) + BP_{i=3,4}(\psi)) C(\psi) - \psi \Delta \xi_{te} \quad (2.33)$$

$$a_{2,j} = \frac{d}{d\psi} a_{1,j} \quad a_{3,j} = \frac{d^2}{d\psi^2} a_{1,j}$$

where $j = 1, 2, 3$. Evaluating b_1 , $a_{1,j}$, b_2 , and $a_{2,j}$ at the position for the maximum, and b_3 and $a_{3,j}$ at the trailing edge and solving equation (2.31) gives the weighting coefficients. When these are known, the CST curve can be constructed.

Figure 2.6 shows the NACA 1 cowl ordinates presented in Table 2.1 together with a CST curve with the same initial curvature, and similar after-body, that is the angle at the trailing edge is similar to that of a parabolic curve. At around $x/X = 0.5$, the curvature of the CST curve is higher which might cause higher acceleration of the flow around this point, thus also a higher Mach number, suggesting a lower critical speed for this profile.

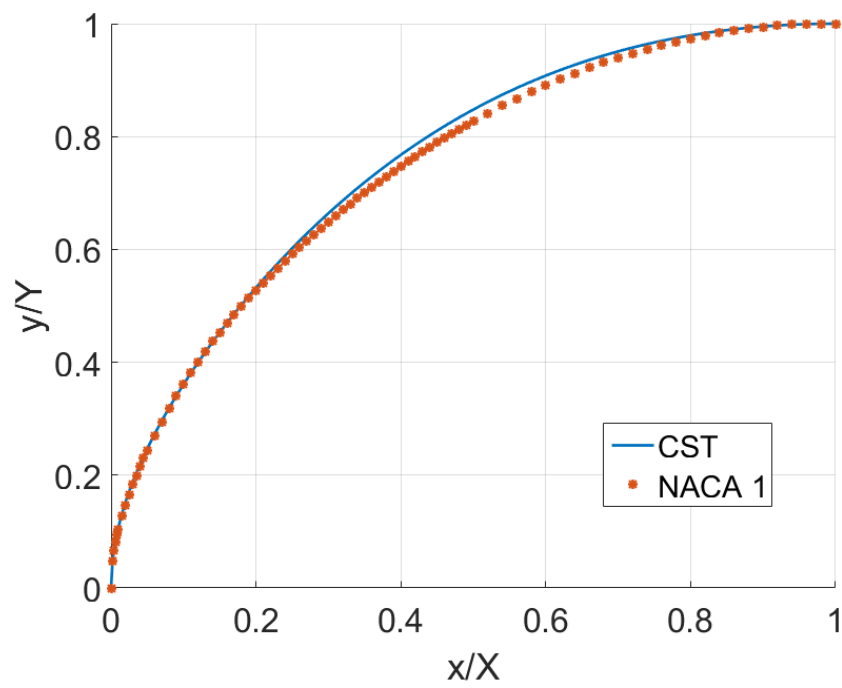


Figure 2.6: CST and NACA 1 cowl curve comparison

Chapter 3

Method

3.1 Creating Axisymmetric Geometries

The nacelle test case geometry is generated from the design parameters and output from the cycle design. While developing the method for creating axisymmetric geometries, the design was based on the CFM56-7B and UltraFan engines. Preliminary geometries representing these engines were created. These are not simulated in CFD, but only used to create a parameterisation of input variables for later designs used in test cases.

Variants of the CFM56-7B turbofan engine are used on the Boeing 737 next generation airliners, which seat between around 130 and 220 passengers [14]. These engines have a BPR of around 5.3, a fan diameter of approximately 1.55 meters [15]. This is not in the range of BPR classifying as ultra-high, but this engine is commonly used and therefore used in this project as a baseline for the nacelle design. The Rolls-Royce UltraFan engine, on the other hand, is not yet in use, but is expected to come into service in 2025 [5]. This engine will have a UHBR, since the BPR is expected to exceed 15[5], and a much larger fan diameter [16]. These are the main reasons that this concept was also used in the preliminary design.

3.1.1 Fan Cowl Profile Design

The curves for the outside of the nacelle and the inlet were constructed using one of two methods, which here are called "the ESDU method" and "the CST method". The first is based on [10], and the second is based on [17, 13]. The methods were implemented as MATLAB functions, and what method is used is specified in the input to the function. The code of this function can be seen in Appendix A. The input parameters are different depending on which method is used as no time was spent to refine this function so that the same input could be used for both the methods, but the output is in both cases the ordinates for the profile, which then need to be scaled in an appropriate way described below. Generally the CST method was used to generate test cases for this project.

3.1.1.1 ESDU Method

This method was based on the ESDU report [10], which uses a NACA 1-series cowl fore-body, a cylindrical mid-body, and a parabolic after-body. The NACA 1-series cowl dimensionless ordinates were taken from [11] and scaled with the desired height and length of the fore-body. No cylindrical mid-body was used, and thus the after-body begins at the end of the fore-body and extends to the trailing edge of the nacelle. An example of the outer profile of a fan cowl with the trailing edge 10% lower than the highlight is shown in Figure 3.1. The inlet was generated using the same method and in that case the trailing edge is located at the tip of the fan, which is the same as the highlight radius in the example.

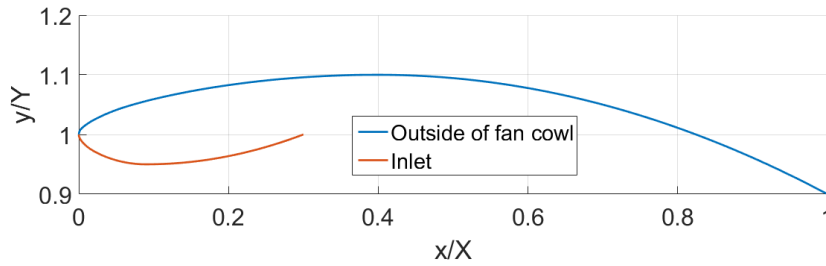


Figure 3.1: Example of nacelle profile from ESDU based method

The generation of these profiles were done in MATLAB. The function made for this purpose have four input parameters placed in a vector g , which can be seen in Table 3.1. A separate input parameter is used to specify that this method should be used. The first determines how large portion of the cowl profile will be the fore-body and thus is the length of the NACA-1 cowl. The second parameter is in this project zero, but it was included so the function also could be used to generate profiles with a cylindrical mid-body portion. The third parameter is then the remaining length of the cowl, which is where the after-body is placed. A parabolic curve was chosen for this part as it is simple to create in a line of code. The last parameter is the difference between the highlight and trailing edge radius, relative the height of the cowl profile.

Table 3.1: Input to ESDU method

Input	Definition
$g(1)$	L_f/L_{tot}
$g(2)$	L_c/L_{tot}
$g(3)$	L_a/L_{tot}
$g(4)$	$(r_{hi} - r_{te})/(r_{max} - r_{hi})$

The function output is the cowl profile ordinates, so the horizontal ordinates (ψ) are then scaled with the total length and the vertical ordinates (ξ) are scaled by the height of the desired profile, that is $r_{max} - r_{hi}$. Finally, the highlight radius is also added to the vertical coordinates, since the ordinates always start at zero. In the case where the inlet profile is generated, the maximum radius is the throat

radius $r_{inlet,t}$ and the height with which the vertical ordinates are scaled is instead $r_{hi} - r_{inlet,t}$. The scaling done can be summarised in these equations

$$\begin{aligned} x_{fan\ cowl} &= \psi L_{fan\ cowl}, \\ y_{fan\ cowl} &= r_{hi} + \xi (r_{max} - r_{hi}), \\ x_{inlet} &= \psi L_{inlet}, \\ y_{inlet} &= r_{hi} - \xi (r_{hi} - r_{inlet,t}). \end{aligned}$$

3.1.1.2 Class-Shape Transformation Curve Method

This method was based on [17, 13], and the theory of it is described in more detail in Section 2.3.2. The fan cowl profile curve is generated from a fourth order polynomial with boundary conditions at the highlight, at maximum height of the fan cowl, and at the trailing edge. Figure 3.2 shows an example of an outer fan cowl and inlet profile generated using this method. The largest difference to using the ESDU method described above, is that the initial fore-body radius and the angle of the curve at the trailing edge and at the fan face now can be specified. Furthermore, the curvature is constant along the curve, which is not the case for a curve generated using the ESDU method and is an advantage aerodynamically [17].

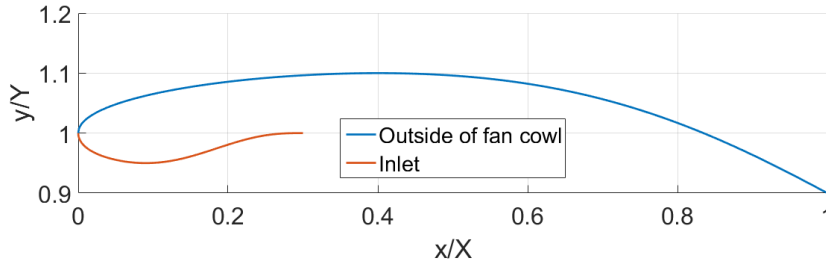


Figure 3.2: Example of nacelle profile from CST curve based method

The MATLAB function that generates these curves has five input parameters, using the same parametrisation as described in [17]. Table 3.2 shows the non dimensional input parameters to the function, which are all collected in a vector g . The first input parameter is used to specify the height of the profile. The second is used to specify the location of the maximum as a portion of the total length and this is used as the first condition to solve the weighting coefficients in the shape functions used to create the CST curve. The third is a non dimensional initial fore-body radius. This parameter was calculated for the preliminary geometries from engine sketches, and later a compromise of the values from the two geometries was chosen, $f_{if} = 1.092$ and kept constant for all test case designs. The fourth and fifth input parameters specify the vertical displacement and the angle/slope of the curve at the trailing edge.

The value of f_{if} is higher than for the NACA-1 cowl where $f_{if} = 0.546$, and thus a larger relative initial fore-body radius is used in all test cases generated using the CST curve fan cowl. A f_{if} around 0.796 should according to CFD simulations in [17]

Table 3.2: Input to CST method

Input	Definition
$g(1)$	r_{max}/r_{hi}
$g(2)$	f_{max}
$g(3)$	$f_{if} = \frac{(r_{if} f_{max} l_{tot})}{(r_{max} - r_{hi})^2}$
$g(4)$	$(r_{te} - r_{hi})/r_{hi}$
$g(5)$	β_{te}

give better drag performance for these CST cowl. The value from the preliminary design is higher still, but not higher than the maximum value tested in [17] (1.115), and could therefore give a somewhat higher drag in some cases. Since the preliminary design was based on sketches there is a margin of error in the value used for the test cases, but it should not be more than a few percent.

Because this parameterisation is used, both the height and length are scaled to the length of the profile. This means that the ordinates output by the MATLAB function; ψ and ξ , are scaled by the profile length, and as when the NACA-1 profile is used: the vertical ordinates by the height of the cowl and the horizontal ordinates by the length. The vertical coordinates ξ still need to be displaced by the highlight radius. The scaling done to the ordinates in this case can be summarised by the following equations

$$\begin{aligned}
x_{fan\ cowl} &= \psi L_{fan\ cowl}, \\
y_{fan\ cowl} &= r_{hi} + \xi L_{fan\ cowl}, \\
x_{inlet} &= \psi L_{inlet}, \\
y_{inlet} &= r_{hi} - \xi L_{inlet}.
\end{aligned}$$

3.1.2 Engine Core Geometry Design

The core engine geometry was based on two different engines, but also based on some relations which are more general for turbofan engines. First some preliminary designs, already shown in Figure 3.3, were created, and based on these a parametric core engine geometry was created. This was later used in all the test cases, but as the input parameters change, the design of the core also changes. The MATLAB code used to create the parametric core engine geometries can be seen in Appendix B.

3.1.2.1 Preliminary Core Geometry Design

The first steps to creating a 2D axisymmetric turbofan geometry were to define what parts should be included in the design and what proportions they should have. To do this, sketches of two engines with nacelles in particular was used: a CFM56-7B and a Rolls-Royce UltraFan engine sketch. From these the relative length of different parts were established. To generate a core with a certain length and height, the

parts were then scaled equally with that height and length. To be able to specify a set core nozzle area, this part was scaled first so that when the whole geometry is scaled with the height later, the core nozzle obtain the right proportions. Figure 3.3 shows the preliminary geometries that were generated from sketches mentioned here.

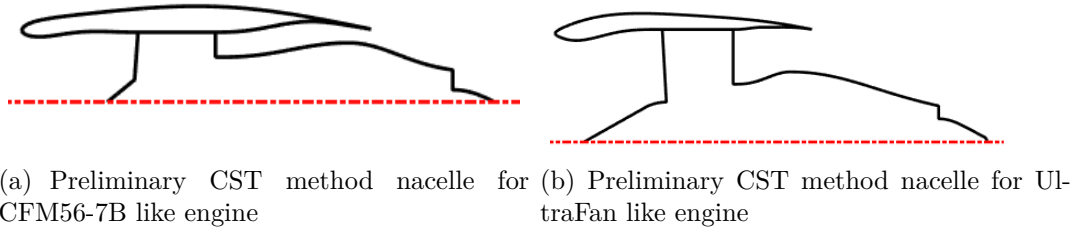


Figure 3.3: Preliminary geometries based on the CFM56-7B and UltraFan engine

As the flow around different sizes of fan cowls was going to be evaluated, it was deemed important that both the inlet and the bypass channel was included in the geometry. For the core geometry this means that the spinner and the whole core cowl, and not just the aft core cowl, needed to be designed. The spinner looks different on different engines. In the sketch of CFM56-7B it has a simple conical shape and on the UltraFan sketch it begins as a cone, but is then curved near the fan inlet face. The core cowl in the geometry starts after the fan guide vanes and has a maximum radius inside the bypass channel. It then curves inwards and end at the outer end of the core nozzle. The slope of the end of the core cowl curve is different in the two sketches, with the CFM56-7B core cowl ending in an almost axial direction, while the UltraFan core cowl have a relatively high slope at the end. It was found that a high curvature of the aft core cowl could cause shocks and instabilities in the bypass jet flow, and thus a aft core cowl similar to the UltraFan was later used to be able to generate shorter core cowl.

The exhaust plug is also different in the two sketches. The one on the CFM56-7B ends in a cylindric shape, while the UltraFan has a more conical shape and a half spherical end. This part is assumed to have a small effect on parameters such as drag and thrust. Similar to the aft core cowl, the curvature of the exhaust plug at the core nozzle exit affect the jet flow. Also in this case a shape similar to that of the UltraFan was later used. It was made from a parabolic function ending in a circular arc starting where the slope is negative 45° . In summary, from the preliminary core geometry design the aft core cowl and the exhaust plug from the UltraFan design was used in the next step of the geometry design process: the parametric geometry. But, as no clear reason to use a more complicated spinner shape than a cone in this project, the spinner shape of the CFM56-7B was used.

3.1.2.2 Parametric Core Geometry Design

The core geometry was generated from 15 input parameters, collected in an input vector "center_input", shown in Table 3.3. The spinner is assumed to have a conical shape and is defined by a length and a radius. The function allows for specifying different fan tip radii at the inlet and exit of the fan system, but in this project these are always equal. The angles of the fan faces can also be specified, but for most cases these are kept as 90° , so that both faces are perpendicular to the symmetry axis of the geometry. Furthermore, the length between these faces at the tip of the fan system is specified by the l_fan_system parameter, which means that if an angle is specified, the length of the spinner and/or the core cowl will be affected, but the total length of the core remains the same.

Table 3.3: Input parameters that define the core engine geometry

Input	Parameter	Description
center_input(1)	r_spinner	radius of the spinner
center_input(2)	l_spinner	length of the spinner
center_input(3)	r_fan	radius of fan tip at fan inlet face
center_input(4)	alpha_fan_inlet_face	angle of the line representing the fan inlet face relative to the center axis
center_input(5)	l_fan_system	total length of the fan system, that is fan and fan guide vanes
center_input(6)	alpha_fan_exit_face	angle of the line representing rear end of the fan system relative the center axis
center_input(7)	r_outer_fan_exit	radius of the tip at the rear end of the fan system
center_input(8)	r_inner_fan_exit	radius of the hub of the rear end of the fan system
center_input(9)	r_max_core_cowl	maximum radius of the core cowl
center_input(10)	l_core_cowl	length of the core cowl
center_input(11)	f_max_core_cowl	position of the maximum as a portion of the length of the core cowl
center_input(12)	beta_rear_core_cowl	angle/slope at the rear of the core cowl
center_input(13)	r_outer_core_nozzle	outer radius of the core nozzle
center_input(14)	r_inner_core_nozzle	inner radius of the core nozzle
center_input(15)	l_plug	length of the exhaust plug

Figure 3.4 also shows the locations of all the center_input parameters. The number in the figure corresponds to the number of the input in Table 3.3. The inner radius of the core nozzle is also the radius of the exhaust plug, so this radius and the length input parameter for this part define the size of it, and the shape for it is taken from the UltraFan preliminary core geometry. The part remaining now is the core cowl, which is generated using the CST curves previously used to generate fan cowl profiles. Here the angle of the curve both at the fan face and at the core cowl rear end was specified by creating two CST curves: one starting at the fan system exit face and ending at the core nozzle, and one starting at the core nozzle and ending

at the fan system exit face. The maximum of both curves were placed at the same location so that if the fore-bodies of the profiles are removed, one curve remains where the angle both at the fan and the rear end of the core cowl is specified. Note that only the second angle is an input to the MATLAB function. The first angle is always zero, so that the core cowl and thus the bypass always starts horizontally.

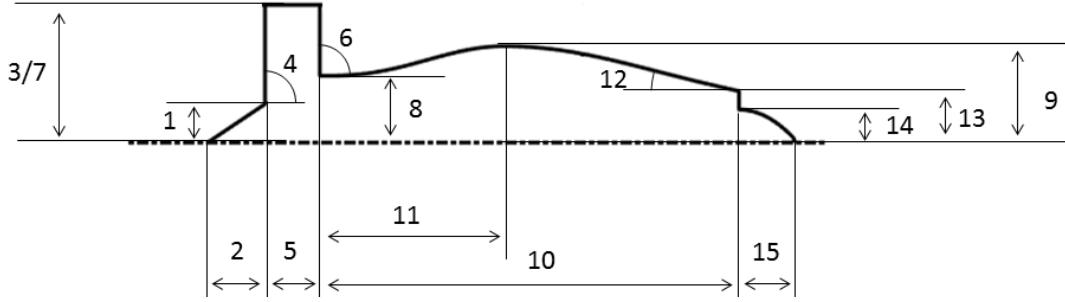


Figure 3.4: Illustration of input parameters for parametric core engine geometry generation

When comparing the length of the fan system of the parametric designed core geometry to that generated from engine sketches, it is much shorter in the parametric case. This is because of simulation reasons. If the fan system and fan cowl are short, the bypass channel becomes short and has to contract rapidly and thus the flow have to turn rapidly over the maximum radius of the core cowl. Because this caused high pressures in portions of the bypass, the fan system was shortened, while the initial part of the bypass was kept roughly at a constant area so the flow in the bypass can stabilize after entering the domain and then have room to turn over the core maximum radius over a larger distance. Also, it is important to note that the fan system exit face area becomes larger relative to the inlet face area for the lower FPR engines. Thus this shortening of the fan system becomes even more critical if the maximum radius of the core cowl remain the same relative to the fan diameter.

The placement of the maximum radius could also be critical. If it is placed too far back, either right at the bypass nozzle exit or further back on the core cowl, the flow could separate as the curvature of the aft fore cowl is too large. The same could happen if the angle of the rear end of the core cowl is too large, resulting again in a too high curvature of the aft core cowl. This was experienced in the first designs that were run in CFD software and the angle was reduced. The separation at the aft core cowl also created unstable chocks in the bypass nozzle jet and no good accuracy could be achieved using steady state simulations.

3.1.3 Bypass Channel Design

The inner part of the bypass channel is designed automatically in the core geometry design, but the outer part, that is the inside of the rear part of the fan cowl, is not

yet defined. This curve is created in a similar manner as the core cowl curve. Two CST curve profiles are created: one starting at the fan system exit and ending at the trailing edge of the fan cowl, and one starting at the trailing edge of the fan cowl and ending at the top of the fan system exit. The location of the maximum is the same for both curves. The fore-bodies of the profiles are then removed to leave one curve left, where the angle at both ends can be specified. As for the core cowl, the angle at the fan system exit is set to zero, making the bypass area vary very little near the fan system. The angle at the trailing edge was chosen as a portion of the outer fan cowl profile trailing edge angle so that the fan cowl has a thickness all the way to the trailing edge. This also minimizes the risk of the curve of this part crossing the outside curve.

3.1.4 Nacelle Test Case Design

Generating geometries by combining the core engine, fan cowl, inlet and bypass channel geometries using only the methods presented thus far would result in specifying a lot of input parameters. From the preliminary design the relations between all these parameters could be established. From these and some trends in turbofan engine sizes, the input was parameterised so it would be enough to only specify a few variables to get the entire geometry. As the aim of this project was to investigate the effects of the size of the fan cowl on drag, the thickness and the length of the fan cowl as a portion of the fan diameter was chosen as the only input parameters to the parameterisation function. The fan cowl thickness is defined as the radial distance from the fan tip to the maximum radius of the cowl, and the length is the axial distance between the highlight and the trailing edge of the cowl. The code used to generate nacelle test cases can be seen in Appendix C.

To make the geometry compatible to an actual engine turbofan engine cycle, the nozzle areas were assumed to be specified beforehand. The core geometry was created first, and from that the radius at the trailing edge of the fan cowl was computed from the bypass exit area. The inner radius at the fan system exit is computed from the mass flow, total pressure, total temperature and Mach number at this point given from cycle data. The area of this section is first given by

$$\frac{\dot{m}\sqrt{RT_t}}{A P_t} = \sqrt{\gamma} M \left(1 + \frac{\gamma - 1}{2} M^2\right)^{-\frac{\gamma+1}{2(\gamma-1)}}, \quad (3.1)$$

and then the radius could be computed. The Mach number is not given in cycle data, but it was assumed to be approximately 0.465 at a cruise Mach number of 0.78. This comes from the preliminary design related to CFM56-7B, where equation (3.1) was used to calculate the Mach number given the area and cycle parameters. The Mach number at the fan system exit was assumed to be higher at a higher flight Mach number, and the engine cycles designed for cruise at Mach 0.8 were given a fan exit Mach number of 0.4739. This implies the same ratio between flight Mach number and fan system exit Mach number as seen in for the preliminary geometry with lower flight Mach number.

3.1.4.1 Parameterisation

From only the length and thickness of the fan cowl relative to the fan diameter, all other input for generating first the core engine or center geometry, then the fan cowl and inlet, and lastly the outer part of the bypass channel, needed to be specified. This was done by parameterising the other variables. Table 3.4 shows the list of constants and relations that was used for this.

Table 3.4: Parameterisation constants used in the geometry generating MATLAB code

Variable	Value	Description
C(1)	0.2	$r_{hi} = r_{fan} + C(1)h_{cowl}$
C(2)	0.4	$f_{max,nac}$, assumed constant
C(3)	1.092	f_{if} , assumed constant
C(4)	1.2	$\beta_{rear\ core\ cowl} = \text{atan}\left(C(4)\frac{(r_{max,core\ cowl}-r_{outer,core\ nozzle})}{(l_{core\ cowl}(1-f_{max,core\ cowl}))}\right)$
C(5)	0.4	$l_{inlet} = C(5)(l_{nac} - C(11)r_{fan})$
C(6)	0.86	$r_{inlet,throat} = (C(6) + 2(1 - C(6))\text{atan}(1/l_{inlet})/\pi)r_{fan}$
C(7)	0.3	$f_{max,inlet} = C(7) - C(8)h_{cowl}/l_{inlet}$
C(8)	0.2	
C(9)	0.28	$r_{spinner} = C(9)r_{fan}$
C(10)	1.5	$l_{spinner} = C(10)r_{spinner}$
C(11)	0.4	$l_{fan\ system} = C(11)r_{fan}$
C(12)	$\pi/2$	angle of fan inlet face
C(13)	$\pi/2$	angle of fan exit face
C(14)	0.7	$r_{max,core\ cowl} = C(14)r_{fan}$
C(15)	0.19	$r_{IPC,tip} = C(15)\sqrt{\dot{m}_{25R}}$
C(16)	2.1	$l_{core\ cowl} = C(16)r_{IPC,tip}$
C(17)	0.7	$f_{max,core\ cowl}$, relative the length of the bypass
C(18)	0.64	$r_{inner,core\ nozzle} = C(18)r_{outer,core\ nozzle}$
C(19)	$(\pi(1 - C(18)^2))^{-1/2}$	$r_{outer\ core\ nozzle} = C(19)\sqrt{A_8}$
C(20)	1.7	$l_{plug} = C(20)r_{inner\ core\ nozzle}$
C(21)	0.6	$f_{max,outer\ bypass}$
C(22)	0.4	$r_{max,outer\ bypass} = r_{fan} + C(22)h_{cowl}$
C(23)	2	$\beta_{nac} = \text{atan}(C(23)(r_{max} - r_{te})/(l_{nac}(1 - f_{max,nac})))$

Some of these parameter values are taken from the preliminary design, but some needed to be adapted so that for example the fan cowl profile does not become a bad representation of an actual fan cowl when an input parameter is changed. Therefore the position of the highlight and the fan cowl rear angle were set as a function of the cowl thickness. The variable C(23) makes the rear profile of the core cowl similar to a parabolic curve, since the derivative at some point along the curve is double the slope of a line between this point and the maximum. To limit the curvature of the aft core cowl, C(4) is a lower value than that of a parabolic curve. This value was changed several times while designing test cases. At the start, the same value as for the aft core cowl was used, but as this caused separations and then instabilities

of the bypass jet, the slope was lowered. If the value was too low so that the aft core cowl becomes s-shaped, similar problems arose. This was seen already in the preliminary design, as the aft core cowl on the CFM56-7B sketch ends at a very low slope.

There was some trouble in parameterising the input for the inlet CST curve, as it needed to give a good design both for long and short fan cowls and thus inlets. The function

$$r_{inlet,throat} = \left(C(6) + 2(1 - C(6)) \frac{\text{atan}\left(\frac{1}{l_{inlet}}\right)}{\pi} \right) r_{fan}, \quad (3.2)$$

was used because it means that, as $l_{inlet} \rightarrow 0$, $r_{inlet,throat} \rightarrow r_{fan}$, and as l_{inlet} becomes large $r_{inlet,throat}$ increases. Still if $l_{inlet} \rightarrow \infty$, $r_{inlet,throat} \rightarrow C(6)$. This value of this constant was based on $r_{inlet,throat}$ at the length of the inlet in the preliminary design of CFM56-7B. The complexity of designing a profile for a short inlet also lead to the use of two constants for the position of the throat radius, $C(7)$ and $C(8)$, which made it possible to move it with small adjustments around a base value.

It was desired that the size of the core engine geometry be scaled with the required power output to the fan. This was achieved by scaling the length of the core to the tip radius of the first blade row in the intermediate pressure compressor (IPC). The radial size of the IPC is in turn proportional to the square root of the corrected mass flow through the core. From experience in cycle design, this proportion is approximately 0.19. With mass flow, total pressure, and total temperature given at the inlet to the IPC (station number 25) from cycle data, the reduced mass flow is computed as

$$\dot{m}_{25R} = \dot{m}_{25} \frac{T_{t,25}/288.15}{P_{t,25}/101325}. \quad (3.3)$$

3.1.5 Boundary Layer Ingestion Test Case Design

The nacelle case design was used as a baseline for generating the geometries for the BLI cases, but the parameterisation was changed in some aspects. Furthermore, no actual cycle data was available for these cases as the tool used in this project can not create a cycle without a core. The fan at the rear end of the nacelle is assumed to be powered by an electric motor driven by power transfered from the engines under the wings. This also means that the shape of the aft core cowl changes, and no core nozzle or exhaust plug exist for these geometries. To create the aft core cowl, the core cowl was extended to where the exhaust plug would have been and then rounded off in the same way as the exhaust plug for the nacelle geometries. That was, a circular arc was placed at a certain slope of the core cowl curve. The modified MATLAB function used to create the core geometry can be seen in Appendix D. Furthermore, the design of the inlet needed to change to accommodate for the flow in the boundary layer at the rear of the fuselage. Figure 3.5 shows the nacelle geometry at the rear of the fuselage and the code used to generate these can be seen in Appendix E.

Both the fan cowl and the core engine geometries were generated using the same

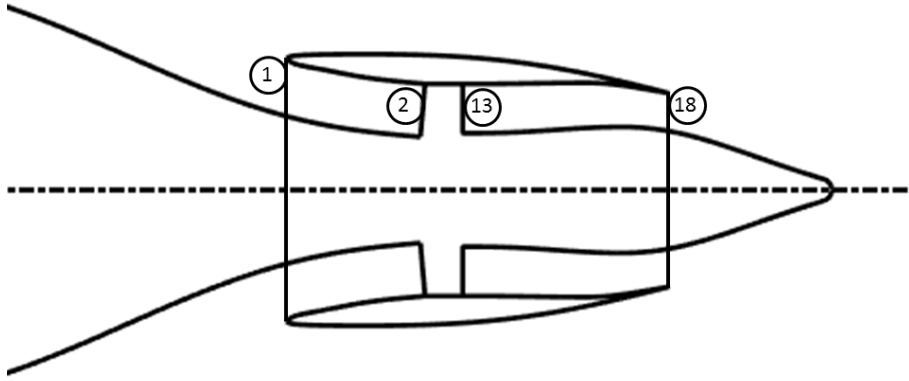


Figure 3.5: The BLI nacelle and rear fuselage geometry, with station numbering

MATLAB functions as the nacelle test cases, but some parts of the function for the core geometry were altered. The spinner was removed, but only its length was removed from the input, since the radius of the spinner still is used to determine the fan hub radius. The core nozzle was removed and the radius of the nozzle outer part was removed from the input. The length and radius of the exhaust plug were used to determine the length of the new core cowl and where the aft core cowl should be rounded off in a circular arc. The angle at the rear of the core cowl was used to determine at what angle the circular arc starts. Therefore, these input also are left in the MATLAB function used to create the core geometry for the BLI cases.

As no cycle data was available, the mass flow from the FPR 1.3 cycle at cruise (nacelle test case 3.0), which is needed to compute the area of the fan system outlet, was estimated by assuming a lower total pressure into the fan due to the boundary layer. The Mach number at the fan system outlet was assumed to the same value as in nacelle test case 5. If, for example, the total pressure is 10% lower, the mass flow also becomes 10% lower, so a parameter $C_{flow} = P_{t,BLI}/P_{t,nacelle\ case}$ is used to scale the mass flow. Also, as the area of the fan system inlet here is specified by a fan hub to tip ratio and diameter, the mass flow is also scaled by the ratio of the area in the nacelle test case and this new area. The new mass flow in the BLI system can be computed as

$$\dot{m}_{BLI} = \dot{m}_{2,nacelle\ case} C_{flow} \frac{A_{2,BLI}}{\pi(1 - 0.28^2)} \quad (3.4)$$

since the radius of the fan is 1 and the hub to tip ratio is 0.28 in the nacelle cases. When the mass flow is changed, the nozzle exit area also needs to be scaled in a similar manner, first to include the flow that before went through the core and not the bypass, and secondly the change of flow due to the area change at the fan inlet face.

3.1.5.1 Fuselage Design

The fuselage was made to be of similar size as an Airbus A320 neo aircraft, but axisymmetric. The diameter was chosen as $D_{fuselage} = 4.05 [m]$, and the base length

as $L_{fuselage} = 37.57[m]$. Figure 3.6 shows the fuselage together with a nacelle at the rear. Note that the length $L_{fuselage}$ is measured from the front of the fuselage, to the end of the aft core cowl. To create the fuselage curve, again the CST curve method was used. The front of the fuselage is the fore-body of a CST curve profile, and the rear part that ends at the fan inlet face is the after-body of a different CST curve. These parts are separated by a cylindrical body, which would be the part that can take passengers on an aircraft.

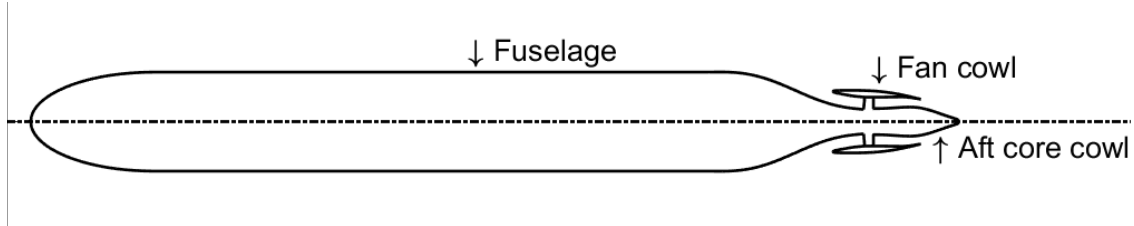


Figure 3.6: The fuselage geometry of the BLI cases

3.1.5.2 Parameterisation

The input for a BLI test case should be only the fan diameter, so all other parameters need to be fixed or parameterised. As already mentioned the length of the whole body and the diameter of the fuselage were fixed to certain values. Table 3.5 shows the parameterisation constants used to compute all needed input variables. Most parameters can be recognized from the nacelle test case parameterisation, but here they were also indexed to make it easier to identify to what part a certain parameter belongs to. The parameters for the fuselage were estimated from a sketch of the Airbus A320 neo aircraft, but the initial fore-body radius was adapted for a axisymmetric fuselage.

The biggest difference to the nacelle test case parameterisation is the way the highlight, inlet throat, and bypass maximum radius are defined. For the BLI, these are defined from defining how large the areas at these sections are relative the fan inlet face for the inlet parameters and relative the fan exit face for the bypass parameter. The inlet was assumed to be contracting and the area at the highlight was said to be 40% larger and the throat 20% larger than the fan inlet face. The maximum radius of the bypass was defined from a 5% smaller area compared to the fan exit face. If this value is low, the nozzle becomes convergent-divergent, but this is not the case for the geometries generated for the test cases.

As previously mentioned the parameter C_{flow} is related to the decreased mass flow if the BLI nacelle, compared to that of the cycle for nacelle test case 5. An initial guess of a 7% decrease was made, but CFD showed a decrease in total pressure at the inlet face of about 13% in BLI case 1. This result was then used in the a new simulation, where the mass flow was decreased by 13% instead of 7%. As more of the boundary layer is ingested with a larger fan, the total pressure at the inlet for the cases with larger fans were assumed to be a few percent higher. There was no time to iterate the C_{flow} parameter with a new value found in the CFD simulations for

Table 3.5: Constants used to parameterise the BLI case geometries

Variable	Value	Description
C_fan(1)	0.5	$r_{inner,fan\ inlet} = C_{fan}(1)r_{fan}$
C_fan(2)	0.4	$l_{fan\ system} = C_{fan}(2)r_{fan}$
C_fan(3)	85°	angle of fan inlet face
C_fan(4)	90°	angle of fan exit face
C_nac(1)	0.4	$l_{inlet} = C_{nac}(1)(l_{nac} - l_{fan\ system})$
C_nac(2)	0.25	$f_{max,inlet}$, assumed constant
C_nac(3)	1.4	$r_{hi} = \sqrt{r_{fuselage,nozzle}^2 + (C_{nac}(3)A_2)/\pi}$
C_nac(4)	1.2	$r_{inlet,throat} = \sqrt{r_{fuselage,nozzle}^2 + (C_{nac}(4)A_2)/\pi}$
C_nac(5)	0.2	$f_{max,nac}$, assumed constant
C_nac(6)	3	f_{if} , assumed constant
C_nac(7)	0.6	$f_{max,bypass}$, assumed constant
C_nac(8)	0.95	$r_{max,bypass} = \sqrt{r_{engine,max,bypass}^2 + (C_{nac}(8)A_{13})/\pi}$
C_nac(9)	2	$\beta_{nac} = \text{atan}(C_{nac}(9)(r_{max} - r_{te})/(l_{nac}(1 - f_{max,nac})))$
C_core(1)	3.1	$l_{core\ cowl} = C_{core}(1)r_{fan}$
C_core(2)	0.7	$f_{max,core\ cowl}$, as part of the length of the bypass
C_core(3)	0.6	$r_{max,core\ cowl} = C_{core}(3)r_{fan}$
C_core(4)	0.1	$l_{plug} = C_{core}(4)l_{core\ cowl}$
C_core(5)	0.1	$r_{plug} = C_{core}(5)r_{fan}$
C_core(6)	1.2	$\beta_{rear,core\ cowl} = \text{atan}\left(C_{core}(6)\frac{r_{max,core\ cowl} - r_{plug}}{l_{core\ cowl}(1 - f_{max,core\ cowl})}\right)$
C_fuselage(1)	0.8	$r_{if,fuselage}$
C_fuselage(2)	0.1495	fore-body length as portion of fuselage length
C_fuselage(3)	0.19	after-body length as portion of fuselage length
C_flow(1)	0.87/0.89/0.91	$C_{flow}(1) = P_{t,BLI\ cycle}/P_{t,nacelle\ cycle}$

these cases, but the estimated values were a better fit than keeping the same value as in BLI case 1.

3.2 Case Definitions

This section summarises the computed cases. The cases are defined either by some design parameters such as nacelle length and thickness relative the fan diameter, or flow conditions such as flight Mach number and altitude. Nacelle test cases refer to investigations of different nacelle sizes and shapes, and for these an isolated axisymmetric nacelle is simulated. Boundary layer ingestion, or BLI, test cases refer to investigations of effects on drag for an axisymmetric aircraft fuselage with a nacelle mounted at the rear.

3.2.1 Nacelle Test Cases

Five different parameters were varied to generate different nacelle test cases: fan pressure ratio, Mach number, flight altitude, cowl length over fan diameter, and thickness over fan diameter. Table 3.6 shows the outline of the cases that were considered. The first seven cases are of different nacelle geometries, while the rest are at different operating conditions, that is flight Mach number, altitude, and fan throttle. Cases 2.1 and 2.2 use the same geometry as in test case 2.0, but the flight Mach number is changed, and cases 3.1, 3.2, 3.3, and 3.4 the same geometry as test case 3.0, but the engine cycle is throttled to a lower FPR. Cases beginning with "TO" use the same case geometries as the following number implies, but are simulated at end of runway take-off flow conditions. The last case in Table 3.6 2.B is the exact same case as 2.0, but a NACA 1 cowl profile is used for the fan cowl instead of CDT method profile.

Table 3.6: Definitions of nacelle test cases

Case no.	FPR	M_{inf}	$Altitude [m]$	l_{cowl}/D_{fan}	h_{cowl}/D_{fan}
1	1.4	0.8	10668	2.5	0.18
2.0	1.4	0.8	10668	1.8	0.14
3.0	1.4	0.8	10668	1.3	0.09
4	1.4	0.8	10668	0.6	0.03
5	1.3	0.8	10668	1.3	0.09
6	1.4	0.8	10668	1.3	0.12
7	1.4	0.8	10668	1.3	0.06
2.1	1.4	0.75	10668	1.8	0.14
2.2	1.4	0.85	10668	1.8	0.14
TO 1	1.4	0.25	0	2.5	0.18
TO 2.0	1.4	0.25	0	1.8	0.14
TO 3.0	1.4	0.25	0	1.3	0.09
TO 4	1.4	0.25	0	0.6	0.03
3.1	1.3	0.8	10668	1.3	0.09
3.2	1.2	0.8	10668	1.3	0.09
3.3	1.1	0.8	10668	1.3	0.09
3.4	1.032	0.8	10668	1.3	0.09
2.B	1.4	0.8	10668	1.8	0.14

3.2.1.1 Nacelle Test Cases Motivation

The choice of fan pressure ratio was based on current technology and the trend of low fan pressure ratio. Case number 5 has an even lower FPR, corresponding to an engine with ultra high bypass ratio. This case also incorporates a short and thin nacelle, making it similar to the Rolls-Royce UltraFan [5].

Typical cruise Mach numbers are in the range 0.76 to 0.82, which was why the Mach number in most cases were set to 0.8. To study the effects of higher and lower flight

Mach numbers, cases 2.1 and 2.2, respectively, were constructed. At end of runway during take-off a typical Mach number is approximately 0.25. Case TO 1 through TO 4 were studied to evaluate the flow around the nacelle in this condition. Since all simulations are axisymmetric, this case does not consider the angle off attack and is thus a great simplification.

The effects of relative length and thickness were studied in cases 1 to 4 at cruise, and TO 1 to 4 at take-off. The length and thickness of the nacelle relative to the fan diameter of the CFM56-7B engine are approximately that of case 1. In the mentioned cases, both length and thickness are varied to avoid unrealistically long and thin, and short and thick nacelles. The cases 6 and 7 were constructed to examine the effects of changing only the thickness.

3.2.1.2 Turbofan Engine Cycle Design

From the design parameters for each case defined in Table 3.6 two turbofan engine cycles were created using GasTurb 9. The details of the cycles are given in Appendix F, but Table 3.7 shows the main engine parameters. Both engines were based on a fan with a diameter of 2 meters, and a hub tip ratio of 0.28. The cycle with a FPR of 1.4, which was used for cases 1, 2, 3, 4, 6, and 7, was tuned to give roughly the same propulsive characteristics as the LEAP-1A engine and the PW1100G engines, but an assumed higher efficiency of the core engine drives the FPR to a somewhat higher value. Further, this cycle was also run at Mach 0.75 and 0.85, which gives the cycle data for cases 2.1 and 2.2 respectively, and at Mach 0.25 and sea level atmospheric pressure, which gives the TO cases. The second engine cycles is that of the engine with FPR 1.3, that is case number 5, which could represent an advanced goal engine introduced around year 2030.

Table 3.7: Summary of main parameters from cycle designs

Engine parameter	FPR=1.4	FPR =1.3
Fan size [m]	2	2
Fan hub to tip-ratio	0.28	0.28
Thrust at top of climb [kN]	28.6	22.8
Corrected mass flow at top of climb [kg/s]	630	630
Thrust mid-cruise [kN]	21.5	16.8
BPR mid-cruise	13.4	17.2
OPR mid-cruise	43.3	43.6
Thrust at end of runway [kN]	113.9	90.5
Bypass exhaust area [m^2]	1.73	1.89
Core exhaust area [m^2]	0.258	0.217

To specify cycle thrust for the engine with FPR 1.4, requirements were taken from the CFM56-5B3 engine used on the Airbus A321 aircraft. This is an older engine, used on similar aircrafts as the LEAP-1A and PW1100G, but for this engine there are published data which was found in [15, 18]. Since there are several CFM56-5B3 engines, but they only differ 2-3% in for example pressure and bypass ratio,

a compromise was made for the data which was used in the GasTurb cycle design. The thrust level of the model is expected to be within 3-5%, and the airflow within 1-2% of published engine performance data. The cycle with FPR 1.3 gets a lower thrust as the fan diameter and airflow is kept constant. If a similar thrust level is needed, the fan diameter of this engine would have to be approximately 2.25 meters.

3.2.1.3 The Eight Test Case Nacelles

Figure 3.7 shows the eight different geometries used in the nacelle test cases. In Figure 3.7(a) are the geometries that was used for difference fan cowl length and thickness. In Figure 3.7(b) is the geometry that was used in the test case with lower designed FPR, that is test case 5, with the geometry from test case 3 to show the difference to the FPR 1.4 nacelle with similar geometric input. Figure 3.7(c) shows the fan cowls of test cases 3, 6, and 7. For these cases the core is the same, and only the thickness of the fan cowl is varied. Finally, Figure 3.7(d) shows the nacelle where a NACA 1 cowl profile is used and it is compared to the CST method fan cowl profile.

Here it can be seen that the main difference between the FPR 1.3 and FPR 1.4 (test case 5 and 3 respectively) is the length of the core. The lower FPR engine only has a shorter core due to the fact that the fan diameter of both the engines are the same. As mentioned earlier, the thrust levels of the two engines are not the same. To achieve this the whole engine and nacelle of test case 5 needs to be scaled up, thus increasing the flow through the engine. Other differences are the areas at the fan system exit face and the nozzles. The higher bypass ratio of case 5 (see Table 3.7) result in a larger bypass nozzle area and a smaller core nozzle area.

Figure 3.7(a) shows that the total length of the turbofan is shorter in test case 4. The core cowl has the same length as the other cases, but the fan system is shorter. The length of these two parts were not connected in the code. The reason for this was that the method was made so that parameters can be changed to mimic the size of the fan system and core cowl length of an existing design. The location of the maximum radius was also moved back in this test case to give a more even area change through the bypass channel.

3.2.2 Boundary Layer Ingestion Test Cases

Only one parameter was varied for the BLI test cases: the fan diameter of the rear mounted engine. Table 3.8 shows a summary of the test cases which were used in this project. As can be seen, the fan cowl length and thickness relative the fan diameter was taken from test case 2 in the nacelle cases, which represents a fan cowl on a state of the art turbofan. All test cases were also chosen to be simulated at cruise at 35 000 ft (10668 m), and at Mach 0.8. As a base for the geometry the cycle with FPR 1.3 was used.

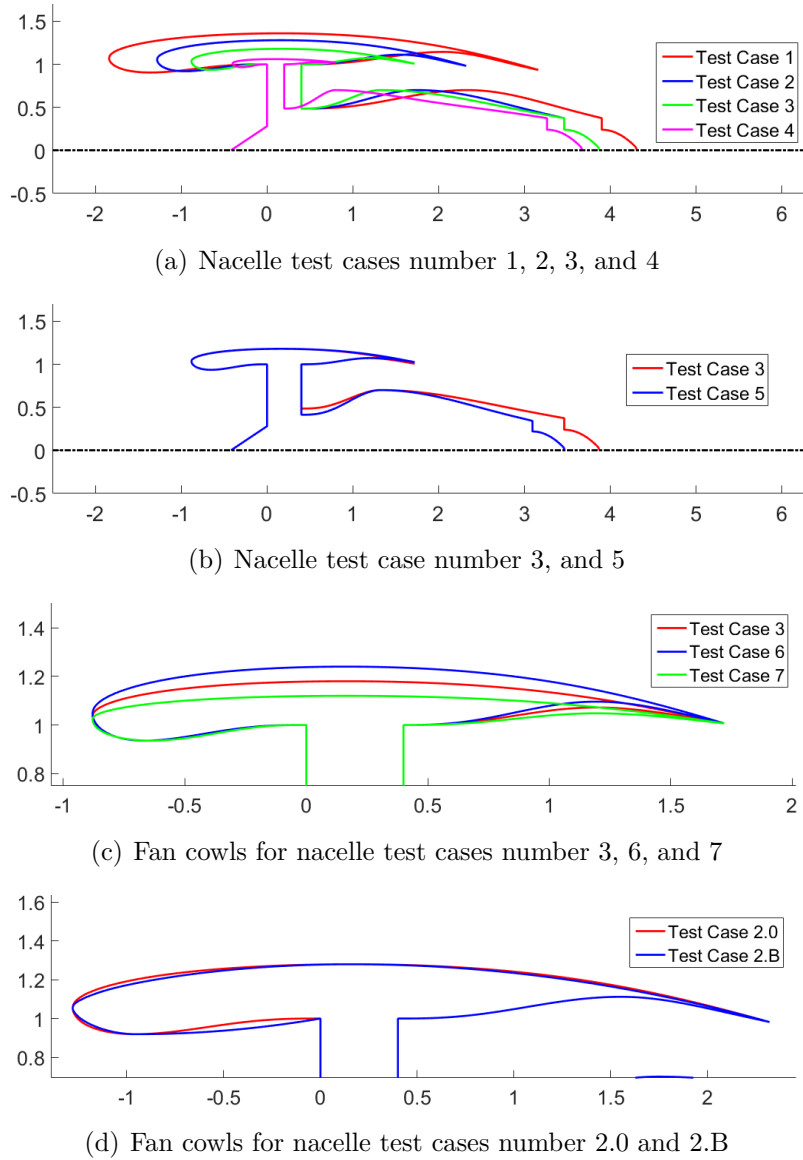


Figure 3.7: Geometries used in nacelle test cases

3.2.2.1 Motivation of BLI Test Cases

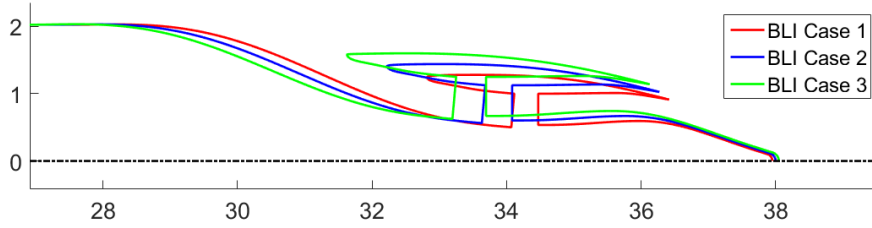
The choice to vary the fan diameter was based on creating test cases which ingest different amounts of the boundary layer of the fuselage. An alternative would have been to change the cycle, so a fan of the same size would ingest different amount of flow, but this would be limited by choking in the engine nozzle. The first case was based on the idea of using an engine of similar size as was designed for the nacelle test cases. As it was seen that this engine did not ingest the whole boundary layer, the test cases with larger fan diameter were constructed. To be able to have a reference of how large the benefit is in each case, the BLI case 0 was added. This case consist only of a fuselage at the same flow conditions as the other cases.

Table 3.8: Definitions of nacelle test cases

Case no.	D_{fan}	M_{inf}	Altitude [m]	FPR	l_{cowl}/D_{fan}	h_{cowl}/D_{fan}
BLI 0	0	0.8	10668	1.3	1.8	0.14
BLI 1	2	0.8	10668	1.3	1.8	0.14
BLI 2	2.25	0.8	10668	1.3	1.8	0.14
BLI 3	2.5	0.8	10668	1.3	1.8	0.14

3.2.2.2 The Four BLI Test Case Geometries

Figure 3.8 shows the geometries of BLI test cases 1, 2, and 3. The geometry for BLI case 0 is the same as that from BLI case 1, but the fan system and cowl is removed and the gap later filled in with a spline in the meshing tool. The total length of the fuselage was approximately the same for all cases, and the fore-body and cylindrical part of the fuselage is identical. The total length of the fuselage and nacelle is longer than the base fuselage length $L_{fuselage} = 37.57[m]$. This is because a portion was added so the slope would not be too great at the aft core cowl. The length of the core cowl is also scaled to the fan diameter and this explains that the fan system is located further towards the cylindrical part for the larger fans.

**Figure 3.8:** Geometries used in boundary layer ingestion test cases

3.3 Computational Fluid Dynamics

In this section the CFD simulations of the test cases presented above is described.

3.3.1 Meshing

The meshing was done using the meshing tool ANSYS ICEM and either a 3D axisymmetric CFX mesh or a 2D ANSYS Fluent mesh was exported. The latter was used later in the project for the BLI test cases, since this meant that the manual process of creating the meshes was faster. All parts of the domain were considered stationary. The spinner in front of the fan is actually rotating, but this was not considered.

A mesh of around 823 000 nodes, and a section of 5° consisting of six layers was used in the nacelle test cases. The longer fan cowl and inlet in test case 1 required

more nodes along the fan cowl and aft core cowl, and that an extra block was put in the inlet. This increased the total number of nodes to approximately 968 000. The long aft core cowl of test case 4 also caused the number of nodes for this case to increase to approximately 862 000. The same section was used in the BLI cases, but it contained approximately 1 030 000 nodes since the domain is larger and the boundary layer along a larger surface needs to be resolved.

3.3.1.1 Geometry

The geometry was generated using the methods presented earlier, and exported from MATLAB as formatted data points sets. These can then be imported in ICEM CFD. The formatted data point input consist of the points of the curves created in MATLAB and a line telling ICEM how many points should be used to create one line. For example if 1000 points were used to generate the outer fan cowl curve, the point data file consist of three columns containing the x, y, and z coordinates of each point. Before that a row with two columns, with the values 1000 and 1, is added. This tells ICEM to create 1 line from 1000 points listed below.

The precision of the data is important. If the points are not exact, the points might lie outside the curve or the curve might become uneven. This was experienced as highly fluctuating pressures along the curves in the simulations, or in some cases negative cells. It was sufficient to import the data points in millimeters and include three decimals, that is the precision is in the size of one micrometer.

To avoid getting cells with one side being close to zero, a one millimeter cylinder was cut away from the center of the domain. The improvements to the mesh cells was considered to outweigh the small error introduced by removing a very small portion of the domain. The fan diameter being one meter, the area of cut away cylinder is only 0.001% of the fan surface and it should not affect the results.

3.3.1.2 Mesh Strategy

The meshing was done using blocks. O-grids were created around the geometries, and further O-grids were also placed around the fan cowl and around the exhaust plug. This way the wall refinement at the plug was limited to only the blocks at this part. As the drag was an important parameter, the boundary layer needed to be sufficiently resolved. The first node from the wall was placed around $y^+ = 1$, which for the nacelle cases were around $1\mu m$ and for the BLI cases around $5\mu m$, and the growth rate for the cells was 20%. The nacelle and BLI wall distance were first approximated to $5\mu m$ and $6.5\mu m$, respectively, but was later decreased due to high velocities at the front of the fan cowl. Because the stagnation point on was located on the outside of the fan cowl in the BLI cases, the velocities were not as high and it was not required to lower the wall distance as much as for the nacelle cases.

Figure 3.9 shows the mesh around the nacelle in one of the test cases. The same structure was used in all cases, but the number of nodes along different curves was changed so that the cells were kept roughly the same size. A similar structure was

used also for the BLI cases, but an O-grid was also placed around the fuselage.

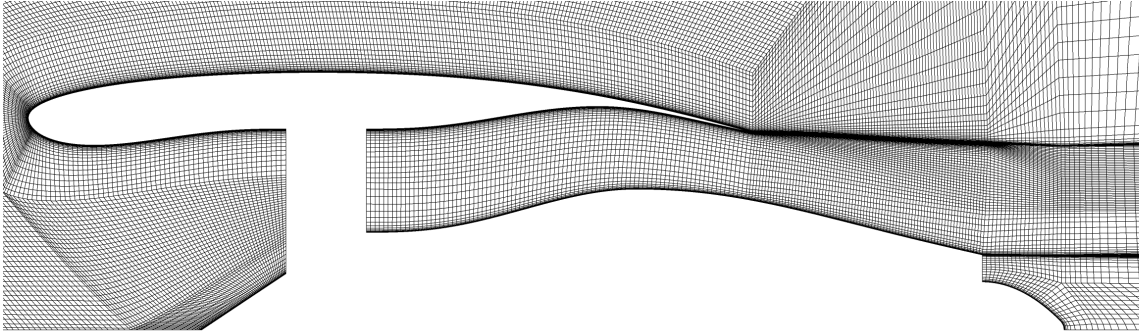


Figure 3.9: Mesh around the nacelle in test case 2

The size of the computational domain was initially 50 fan diameters radially and axially both in front and behind the nacelle, corresponding to what was used in [19, 6]. The domain was later expanded to 70 fan diameters radially and 60 fan diameters in front and behind the nacelle in the BLI test cases.

3.3.1.3 Mesh Convergence Study

Three different levels of mesh resolution was tested: 17 000, 62 000, and 245 000 nodes per rotational layer. For both course and finer meshes fluctuations of pressure along the nacelle surface was experienced while running the simulations. These fluctuations were around 1% for all meshes and the results showed a decrease of around 5% in pressure forces between the coarse and medium fine mesh. The difference between the medium fine and fine mesh was approximately the size of the fluctuations. Also, the fine mesh seemed to stabilize in fewer iterations. Therefore a mesh with around 120 000 nodes per rotational layer, was later used, since this allowed a decrease in number of iterations, but not as large increase in computational time as the fine mesh used earlier.

Most cells were required to achieve a low y^+ value and growth rate of the cells near walls, but the portions of the domain further from the geometries a course mesh was sufficient. The size of the outer cells was limited by aspect ratio and jump in cell size. A growth rate of approximately 20% was used in the whole domain. Some meshes that were tested also had different section angle. This was done to study the convergence time and influence on the fluctuations in pressure along nacelle surfaces, but no significant difference could be found.

The number of cells in the lengthwise direction of the fan cowl was increased from an initial value of around 100 cells in the initial meshes to around 200 cells in the mesh later used. This was to resolve shocks which appeared along the fan cowl surface, so that the pressure change over a shorter distance, which was needed to get a representative value of the drag on the fan cowl. The same was also done at the aft core cowl, as in some cases shocks were present in the bypass nozzle jet.

3.3.2 Model setup

The CFD model was created in CFX-pre and then solved using CFX. Either a 3D axisymmetric mesh consisting of a slice of 5° was imported as a CFX mesh, or a 2D ANSYS Fluent mesh was imported and a slice of 5° was created in the CFX pre environment. The fluid was modelled using NASA polynomials with 7 coefficients.

3.3.2.1 Schemes

For turbulence the $k-\omega$ SST model was used. Also, the Spalart-Allmaras turbulence model developed for aerospace applications was used in some case, mainly to test for improvements of convergence time, but no such improvement was seen. For the turbulence and the advection scheme high resolution were used.

3.3.2.2 Boundary Conditions

The inlet boundary to the domain was set to a velocity inlet, where the axial velocity component was given by flight Mach number and the speed of sound of air at the altitude specified by the test case. The domain outlet was set to a average static pressure outlet, where the pressure was specified from the altitude in the test case. The far field boundary and the small cylinder surface at the center was set to free slip walls. The sides of the domain were connected through rotational periodicity.

The boundaries of the fan were defined using mass flow boundary conditions. The fan inlet face was a mass flow outlet and the fan exit face a mass flow inlet, where the flow was defined by \dot{m}_2 and \dot{m}_{13} , respectively, from cycle design (see Appendix F). To get convergence while using a mass flow outlet at the fan proved to be difficult in some cases, especially for the cases at end of runway conditions. A adaptive pressure boundary condition, where the static pressure at the boundary is changed stepwise to get the correct mass flow, was used for these cases. The pressure is changed by specifying an expression in CFX that give the new pressure for each iteration.

With the mass flow boundary conditions, the flow direction needs to be specified. The normal to boundary option was used, but this meant that if for example the fan exit face was tilted Mach numbers going towards infinity was needed to turn the flow to the axial direction in the first part of the bypass channel. Therefore a exit face at 90° angle to the axial direction was used, which also gives a 90° angle between the fan exit face and the bypass curves. The same was done at the core nozzle exit face, where the exhaust plug curve begin at a 90° angle to the nozzle face. An alternative would have been to specify a direction of the flow at the boundary, but this was never done.

The BLI test cases does not cycle data from GasTurb as the nacelle cases. The mass flow obtained from equation (3.4) during the geometry generation is then used (see Table G.2 in Appendix G). The inputs to the function are taken from nacelle test case 3.0 (see Appendix F.2.2).

3.3.2.3 Convergence

To check for convergence the fluctuations of the pressure force on the nacelle was monitored. Convergence was then checked by four criteria. The difference of both the average value over 25 and 50, and 50 and 100 iterations should be less than 0.001%. Also, the standard deviation for the last 50 and 100 iterations should be less than 0.001%. These criteria can be described as

$$\begin{aligned} 1. \quad & |Average_{50} - Average_{25}| / Average_{25} < 10^{-5}, \\ 2. \quad & |Average_{100} - Average_{50}| / Average_{50} < 10^{-5}, \\ 3. \quad & StandardDeviation_{50} / Average_{50} < 10^{-5}, \\ 4. \quad & StandardDeviation_{100} / Average_{100} < 10^{-5}. \end{aligned} \tag{3.5}$$

For the BLI test cases the FPR was also monitored, since this was a good way to detect any instabilities around the rear of the fuselage. For some of the cases it was difficult to evaluate convergence in this way, but the criteria in equation (3.5) were always evaluated when a solution was terminated.

An automatic time step calculated in the solver was used and was for most cases in the order of 10^{-4} second. Still, the option of using a more aggressive timescale was turned on, and a timescale factor of 6 was applied for the nacelle test cases. A larger time scale did in some cases cause problems with convergence and for the BLI cases the time scale was even more critical. To resolve the wall scales, a physical timescale of 10^{-5} was initially used, and when the solution had stabilized, a conservative automatic timescale with timescale factor 2 could be used to speed up convergence.

3.3.3 Post Processing

The results from the CFX simulations were post processed using CFD post. The equations for drag and thrust were put in a table where all different components of forces on different surfaces were computed separately. The components were divided in pressure and wall shear forces in the axial direction, and also the impulse through the inlet and nozzle surfaces were computed. Separating all variables made it possible to change the accounting system of drag and thrust without having to introduce new equations. In this project the accounting system using the hybrid definition of drag, presented in Section 2.2.3, was implemented.

To evaluate the pressure recovery in the inlet and the pressure ratio in the bypass, the total pressure at all stations were also listed. Furthermore, the flow, total temperature, area, and C_P at the bypass and core nozzle were listed so that discharge and thrust coefficient could be calculated for the nozzles. This was done using the equations in Section 2.1.2. Since mass flow boundary conditions were used for the fan system boundaries, the FPR was also computed. This was expected to differ from the cycle design, but the alternative of specifying the FPR with pressure boundary conditions at the fan faces would possibly make the mass flow differ from the cycle design.

Chapter 4

Results

In this chapter the results of the CFD simulations done in this project are presented. Tables of thrust and discharge coefficients for engine nozzles, drag and thrust components, and pressure ratios of inlet and bypass nozzle are summarised in G, Appendix H, and I respectively.

4.1 Convergence

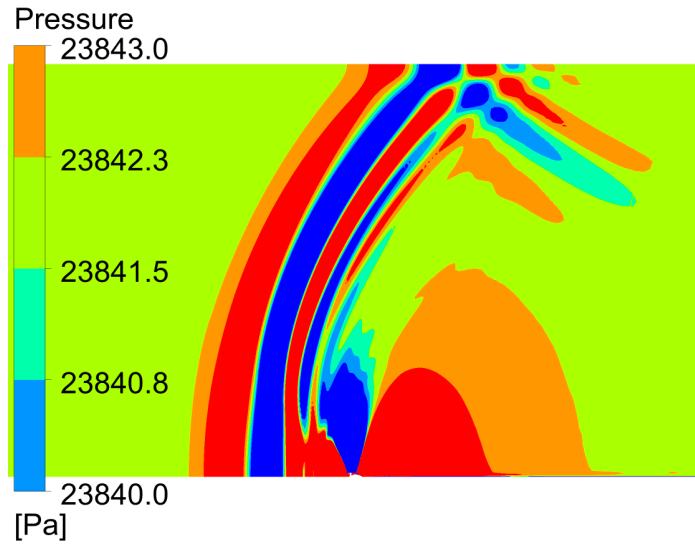
The CFD simulations for the different cases were terminated at different levels of convergence. The convergence criteria described by equation (3.5) are fulfilled in most simulations of nacelles, but some did not fulfill convergence. Table 4.1 lists these simulations, and the extent to which the convergence criteria are fulfilled. For these cases the drag was computed for a minimum of four different iterations in an interval of approximately 200 iterations, and if the maximum difference in drag was around 1%, the results were accepted. The nacelle cases not mentioned in the table have fulfilled the convergence criteria.

Table 4.1: Status on convergence criteria in simulation cases

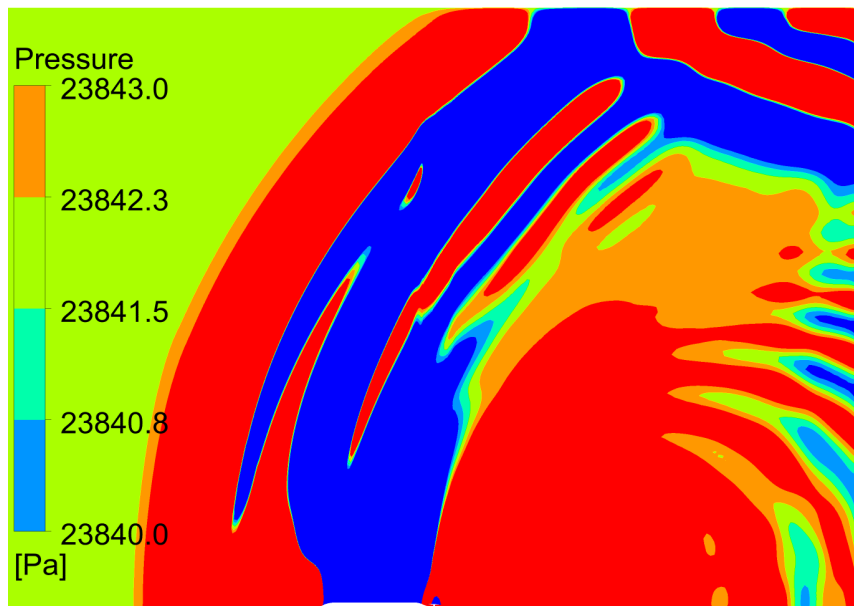
Case	Value of convergence criteria				Convergence
	1	2	3	4	
1	1.2E-05	3.0E-05	2.0E-05	3.3E-05	accepted
2.0	4.2E-05	2.0E-05	5.0E-05	5.2E-05	accepted
2.B	1.1E-05	1.1E-05	8.5E-06	1.3E-05	accepted
2.2	5.4E-05	8.5E-05	6.2E-05	1.0E-04	not converged
TO 3	2.8E-07	1.4E-05	3.0E-07	3.6E-07	accepted
3.2	7.0E-06	1.4E-05	1.5E-05	1.5E-05	accepted

The reason these simulations were stopped and could not reach convergence, was instabilities in the computational domain. At the start of the simulations a pressure wave is created at the engine, moving outwards in the domain. It is reflected in the boundaries and when it returns to the engine, it influences the pressure distribution on its surface. Figure 4.1 shows this wave, after it has been reflected in the outer boundaries, both for a nacelle test case and a BLI test case. This pressure wave results in fluctuations in drag of up to 10%, thus affecting the convergence of the

simulation. The computation is therefore stopped before the reflection of the wave reaches the nacelle. The cases are considered to have reached a satisfactory convergence for this project, with exception from test case 2.2. The results for this case is presented in Section 4.5.



(a) Nacelle test case (5)



(b) BLI test case (3)

Figure 4.1: Pressure wave propagation in computational domain

It could be expected that the pressure waves would be dissipated if the simulations were run for sufficiently many iterations, but as shown by Figure 4.2 the fluctuations in integrated pressure on the nacelle outside surface does not seem to diminish during any reasonable simulation time. Note that the pressure force shown in the figure is only the total pressure force, and not the resulting force in axial direction which is used as a part in the drag calculations. Furthermore, it is only integrated over the area in the computational domain, that is a slice of 5° .

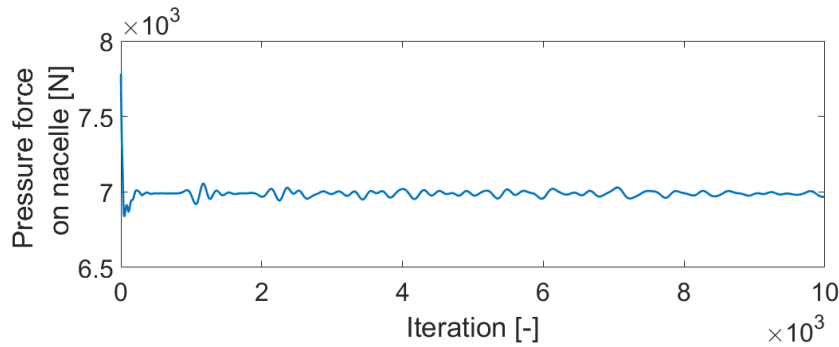


Figure 4.2: Development of integrated pressure on nacelle surface during simulation

The problem mentioned above is even more prominent in the BLI cases, where the domain is not scaled with the size of the fuselage, but as before with the fan diameter. Both domains in Figure 4.1 are the same scale, so even though the BLI domain is somewhat larger, it is not enough to compensate for the much larger pressure wave. As the region of low pressure above the fuselage and the regions of higher pressure before and after the body cover a larger part of the domain, the wave start to affect the convergence pattern as soon as it is reflected. Therefore, it is not possible to evaluate the convergence after this point, and the results presented here are taken at some iterations before that. The accuracy is deemed to lie within a few percent using the same method of checking the variation of drag as for the nacelle cases that did not fulfill convergence. To improve accuracy the simulation domain needs to be expanded. A rough estimation would be to at least double the distance between the rear end of the fuselage and the outlet of the domain and the distance to the far field boundary.

Figure 4.3 shows the integrated pressure on the fuselage in BLI case 0, that is without any engine at the rear. Note here that a wider domain is used, that is a 45° slice instead of a 5° slice. As this is a much simpler geometry to simulate, a several order of magnitudes higher time step could be used thus letting the pressure wave propagate much further in only a few iterations. Furthermore, each iteration was much faster. Thus this case was run for tens of thousands of iterations to investigate what happens to the pressure wave. The pressure seems to converge to some value, and after approximately 1000 iterations the pressure fluctuations becomes much larger, but this could be an instability caused by a too large time step. Even during this first interval, the pressure wave still causes fluctuations in drag of are not lower than for the other cases.

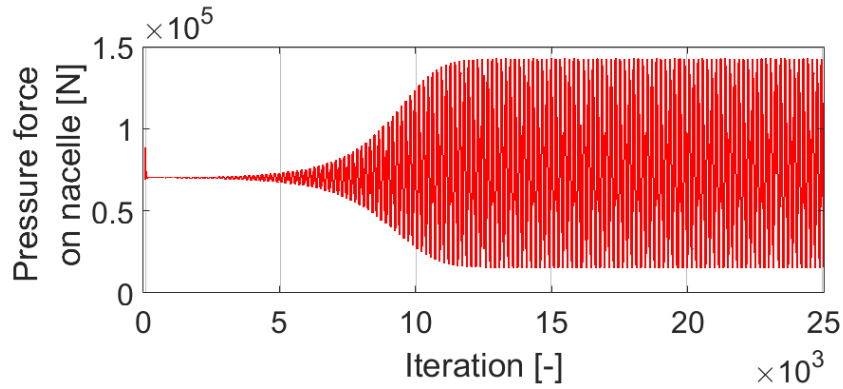


Figure 4.3: Development of integrated pressure on fuselage surface during simulation

4.2 Evaluation of Different Fan Cowl Length and Thickness

Table 4.2 shows the parameters for the test cases for which the results are presented here. In these cases the fan cowl length and thickness are decreased, while the engine cycle remains the same. Case 2.0 represents a state of the art length nacelle, and the following cases (3.0 and 4), are tests of what could be expected of some future design with a much shorter and thinner fan cowls. The thickness of the fan cowl is limited by for example parts that is needed to install the engine on an aircraft. Furthermore a very thin fan cowl, such as that in case 4, could give less noise reduction and risk have too low structural rigidity. The results from this simulation could still be used to analyze any eventual benefits to drag of such a design.

Case no.	FPR	M_{inf}	Altitude [m]	l_{cowl}/D_{fan}	h_{cowl}/D_{fan}
1	1.4	0.8	10668	2.5	0.18
2.0	1.4	0.8	10668	1.8	0.14
3.0	1.4	0.8	10668	1.3	0.09
4	1.4	0.8	10668	0.6	0.03

Table 4.2: Summary of parameters for nacelle test cases with different nacelle length and thickness

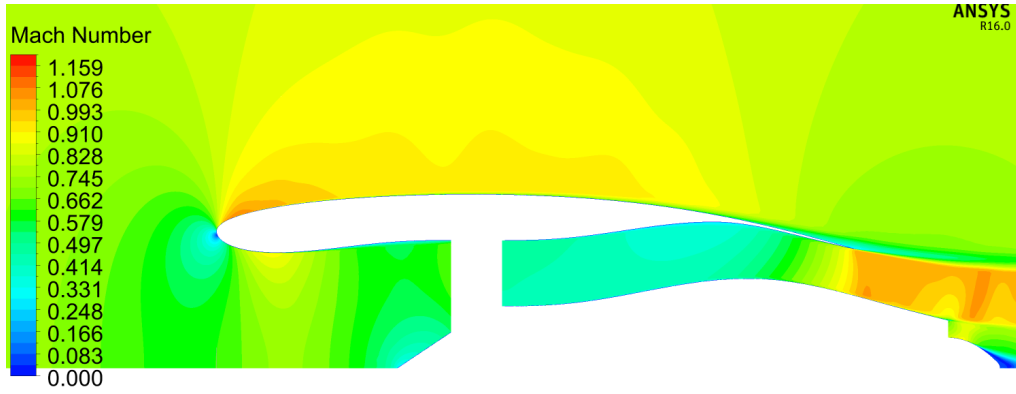
Figure 4.4 shows the Mach number contours around the nacelles of these test cases. Note that the geometries in Figure 4.4(a) are in the same scale, and that the core engine cowl is the same length in cases 2.0, 3.0, and 4. The maximum diameter of the core is the same in all four cases presented here. An important observation is the uneven contour curves at the middle and rear parts of the fan cowls. These curves are not steady, and change for each steady state iteration, indicating the presence of transient phenomena. The effects on the parameters of interest, that is thrust and drag are approximated to be less than 0.01% and thus sufficiently

small to consider the steady state simulation to have converged. The reason for these transient phenomena could be two things. Firstly, the pressure fluctuations mentioned earlier, which would mean that these phenomena might disappear if the simulations could be run further and for example with a larger domain so that the fluctuations vanishes. Secondly, unsteady flow around the front of the fan cowl. This could for example be a unsteady separation of the boundary layer. The first reason could also affect the second.

As the nacelle thickness and length parameters are reduced a higher Mach number is observed at the front of the fan cowl, and a shock appears and increases in strength in the cases with smaller nacelle. The Mach number in the bypass jet also increases in the cases with shorter nacelles, and a pattern of subsequently weaker shocks appear along the aft core cowl. Since the curvature of the aft core cowl near the bypass nozzle is higher in test case 4, the flow near the surface must change direction more rapidly resulting in a much higher Mach number in this case. This would mean a high risk of creating a transient phenomena, for example a strong shock due to high Mach numbers which causes the flow along the aft core cowl to separate. In turn, this crates a blockage for the flow, and the shock could start to move along the profile. This was experienced if the aft core cowl had a large curvature further back. The later designs therefore had a lower slope at the rear of the core cowl, and a large curvature inside the bypass channel at the maximum radius. This design created a stable jet flow.

The hybrid drag in Figure 4.5 is defined by equation (2.20). It is clear that if the forces on the aft core cowl and the plug is included in the drag, the drag increases as the nacelle is shortened. At first thought it would was assumed that a shorter fan cowl would result in a lower drag. This does not consider the influence of the aft core cowl though and this has been shown to influence the drag a great deal. Since the design parameters has not been adapted in the different test cases, it is assumed that some of these designs are closer to some optimal design than others. Especially the designs of the medium short and short nacelles, that is test case 2.0 and 3.0, is thought be have potential for reduced drag with an improved geometry. The ultra short nacelle in test case 4 is thought to be difficult to improve significantly, because of the thin fan cowl and long aft core cowl. The changes on the fan cowl only has a limited effect since it is so thin and the CST curve used for the aft core cowl has limited number of parameters to specify which limit the design of the curve.

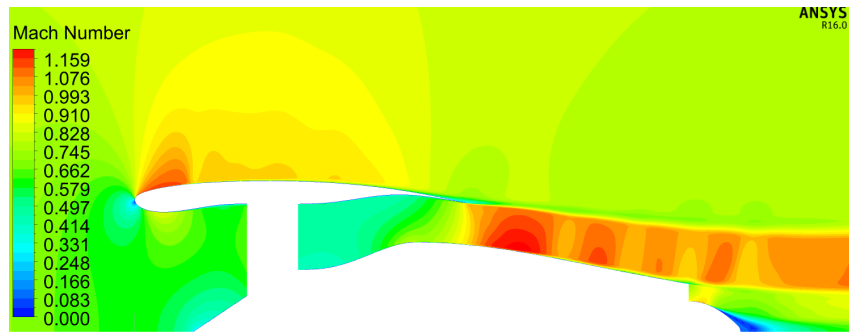
In Figure 4.5 the test case 2.B, which has a fan cowl designed with the ESDU method, is also shown. Both the hybrid drag and the fan cowl and pre-entry force are somewhat lower in this case compared to case 2.0. The reason for this is the smaller initial fore-body radius of the NACA 1 cowl profile, resulting in a lower Mach number at the front of the fan cowl. This suggests that the drag of test case 2.0 could be lowered by decreasing the curvature of the profile at the highlight.



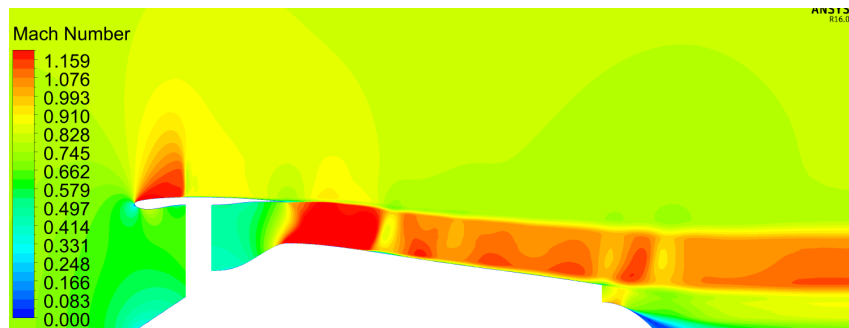
(a) Test Case 1: $L_{cowl}/D_{fan} = 2.5$, $h_{cowl}/D_{fan} = 0.18$



(b) Test Case 2.0: $L_{cowl}/D_{fan} = 1.8$, $h_{cowl}/D_{fan} = 0.14$



(c) Test Case 3.0: $L_{cowl}/D_{fan} = 1.3$, $h_{cowl}/D_{fan} = 0.09$



(d) Test Case 4: $L_{cowl}/D_{fan} = 0.6$, $h_{cowl}/D_{fan} = 0.03$

Figure 4.4: Mach number contour for different sized nacelles

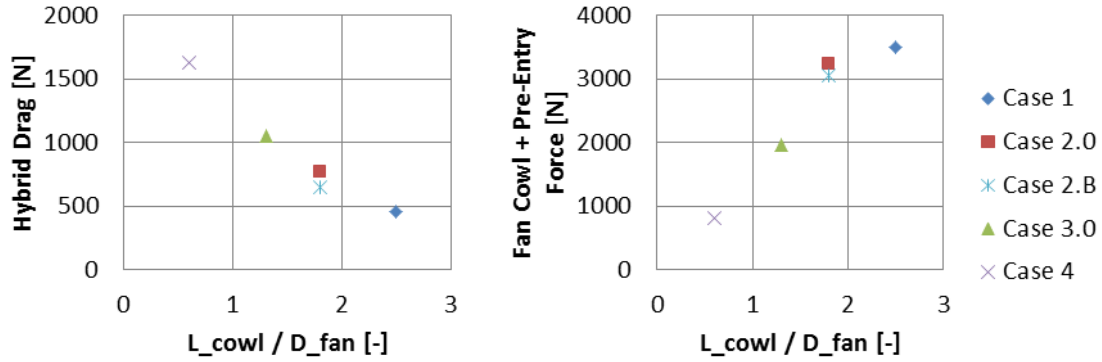


Figure 4.5: Comparison of drag for the four nacelle geometries

The sum of the pre-entry and fan cowl forces in Figure 4.5 are shown since these parameters give a suggestion towards what spillage drag can be expected. To obtain the spillage drag the force on the fore-body and after-body needs to be separated, and a reference condition without any spillage drag, which would also mean that the pre-entry force is zero, is needed. This reference condition was never created in any of the cases, but comparing the fan cowl and pre entry force to the wall shear force on the fan cowl gives some indication of spillage drag for the different cases. Table 4.3 shows the fan cowl wall shear and the portion this is of the fan cowl and pre-entry force. If the wall shear force is a large portion of the fan cowl and pre-entry force the spillage drag could be expected to be low. It would be expected that a thin cowl exhibit more spillage drag, but the ultra short and thin fan cowl of test case 4 show very low tendencies to spillage compared to for example test case 2.0. It is though that the flow state at cruise is close to the reference condition for test case 4, but that the spillage drag would increase dramatically if for example the flight Mach number is increased. This would also suggest that the design of test case 2.0 is particularly poor, and improvements for this geometry might be possible.

Table 4.3: Fan cowl wall shear and wall shear relative fan cowl and pre-entry force for nacelle test cases 1 to 4

Case	1	2.0	3.0	4
Fan cowl wall shear [N]	1029.5	755.7	533.1	242.4
Wall shear portion of fan cowl and pre-entry force [%]	29.36	23.35	27.16	29.57

4.3 Evaluation of Different Fan Pressure Ratio

The fan pressure ratio is changed in two different ways: by designing cycles with different FPR (1.4 for case 3.0 and 1.3 for case 5), and by throttling the 1.4 FPR design in steps down to 1.032, the last representing an engine in idle throttle. Table

4.4 shows the outline of these cases and the results are presented in this section. The throttled cases were mainly created to better understand spillage drag. As the flight Mach number in these cases are the same, and the flow into the engine is decreased, the flow has to turn and pass over the fan cowl. This is the basic cause of spillage drag.

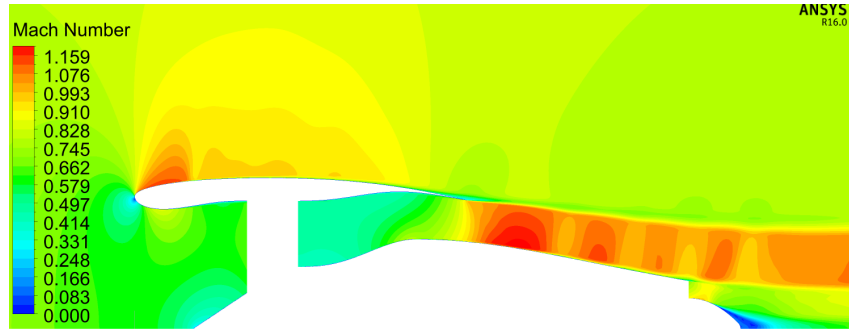
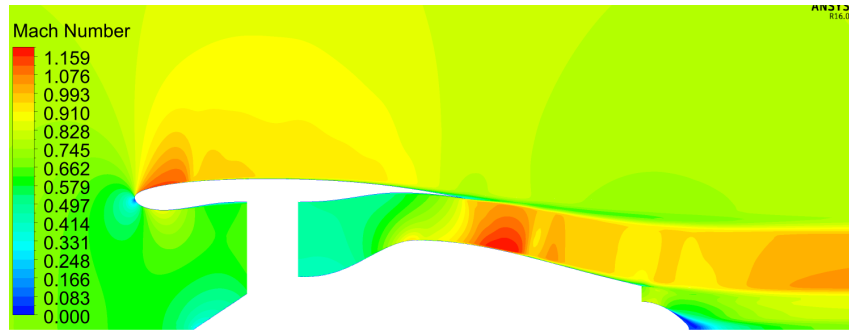
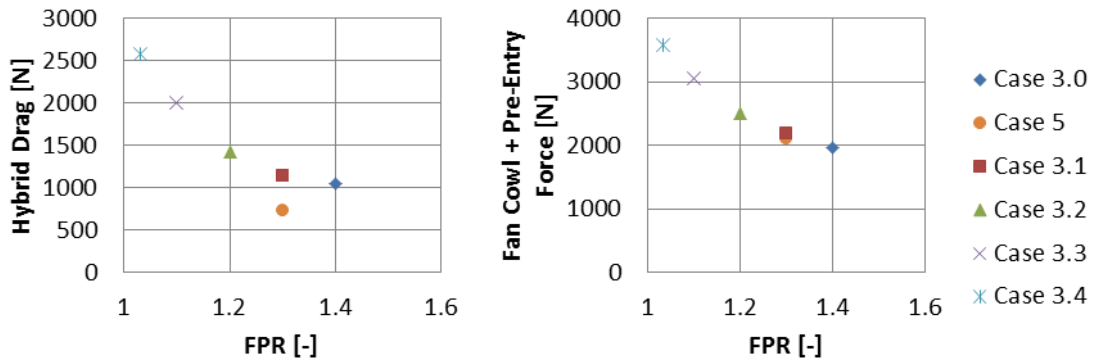
Case no.	FPR	M_{inf}	$Altitude [m]$	l_{cowl}/D_{fan}	h_{cowl}/D_{fan}
3.0	1.4	0.8	10668	1.3	0.09
5	1.3	0.8	10668	1.3	0.09
3.1	1.3	0.8	10668	1.3	0.09
3.2	1.2	0.8	10668	1.3	0.09
3.3	1.1	0.8	10668	1.3	0.09
3.4	1.032	0.8	10668	1.3	0.09

Table 4.4: Summary of parameters for nacelle test cases with different fan pressure ratios

4.3.1 Cycle Designed FPR

Figure 4.6 shows the contours of the Mach number from test cases 3.0 and 5. The contours around the fan cowls are similar for the two cases, but the bypass jet flow differs in some respects. The core engine, and thus the aft core cowl, is shorter and thus have a steeper angle in the case with lower FPR, that is test case 5. This, together with a slightly higher mass flow, could be the reason for the lower Mach number along the aft core cowl in test case 5. As the Mach number is higher in the case with higher FPR, several stronger shocks appear, which would suggest a lower forward facing force in this case. The bypass nozzle exit area is also somewhat larger in test case 5 and this could affect the direction of the flow at the outer part of the nozzle. A smaller trailing edge angle of the fan cowl would give a larger acceleration of the jet after the nozzle.

Figure 4.7 shows that the hybrid drag of test case 5 is lower than for test case 3. The geometry of test case 5 was the first to be run in CFD simulations and many parameters, such as the trailing edge angle of the aft core cowl, was changed to give a good jet flow for this case. This could be the reason why this case performs better than case 3, even if the geometries are very similar. The figure also show the throttled test cases, and as can be expected, the drag is higher for these cases. This will be discussed further below.

(a) Test Case 3.0: $FPR = 1.4$ (b) Test Case 5: $FPR = 1.3$ **Figure 4.6:** Mach number contour for different designed fan pressure ratios**Figure 4.7:** Comparison of drag for different fan pressure ratios

The right side of Figure 4.7 shows that the fan cowl and pre-entry force is higher for the nacelle with lower designed FPR. Since it corresponds well with the force seen in the case where the 1.4 FPR engine is throttled to 1.3 FPR, this is assumed to not be a cause of the small change in of the fan cowl at the trailing edge. This would suggest that the difference between these two cases is purely spillage drag. Table 4.5 shows the relative wall shear compared to the fan cowl and pre-entry force. It is expected that the wall shear would be a lesser portion of this force if spillage drag increases. This is also what is observed for these cases.

Table 4.5: Fan cowl wall shear and wall shear relative fan cowl and pre-entry force for nacelle test cases 3.0 and 5

Case	3.0	5
Fan cowl wall shear [N]	533.1	543.3
Wall shear portion of fan cowl and pre-entry force [%]	27.16	25.92

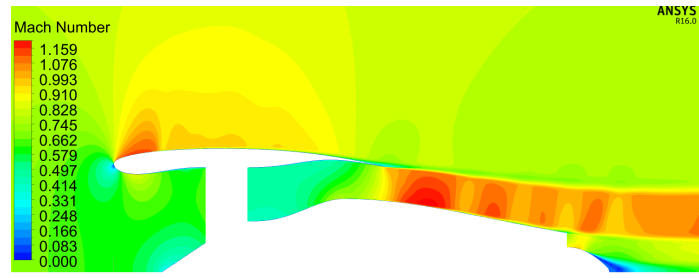
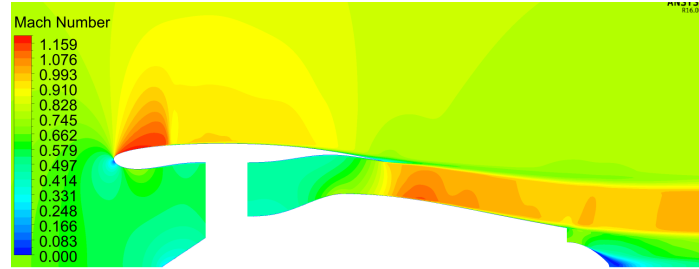
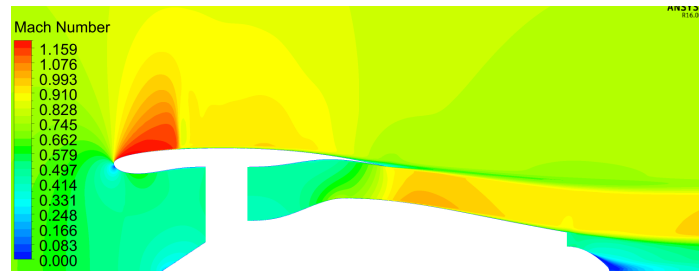
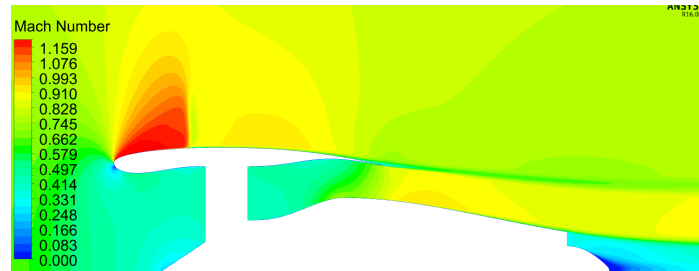
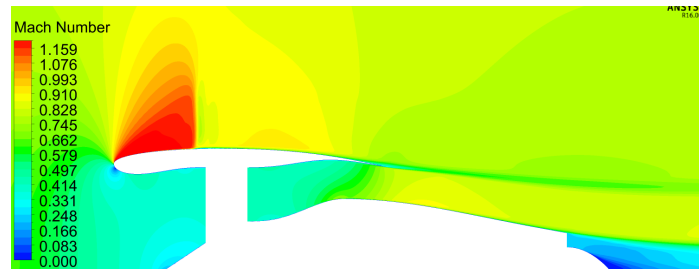
4.3.2 Throttled FPR

The cases in Figure 4.8 are based on a cycle designed for FPR 1.4 and the geometry of test case 3.0, but the FPR is throttled to 1.3, 1.2 1.1 and 1.032 (test cases 3.1, 3.2, 3.3, and 3.4 respectively). As can be expected the amount of flow entering the engine is lower for lower FPR, and while this happens the flow is directed around the nacelle. This can be compared to an increasing spillage drag. The larger flow will require a higher pressure gradient at the front of the nacelle not to separate, giving high Mach numbers around the fan cowl. This is also what can be seen in the figure.

Figure 4.7 presented earlier shows the hybrid drag and the sum of the fan cowl and pre-entry force also for the throttled FPR test cases. Previously the wall shear stress has been argued to be a lesser portion of the fan cowl and pre-entry force for cases with high spillage drag. These cases can be used to strengthen that argument since it is a fact that spillage drag increases going from test case 3.0 to 3.1 and so on. Table 4.6 show the wall shear relative the pre-entry and fan cowl force for these throttled test cases. Form this table this relation between a lower relative wall shear for higher spillage drag. It might also be worth noting that the wall shear in these cases becomes smaller as the spillage drag increases. This has not been possible to seen in previous cases as the geometries has changed between these.

Table 4.6: Fan cowl wall shear and wall shear relative fan cowl and pre-entry force for nacelle test cases 3.0, and 3.1 to 3.4

Case	3.0	3.1	3.2	3.3	3.4
Fan cowl wall shear [N]	533.1	527.5	520.3	510.5	500.9
Wall shear portion of fan cowl and pre-entry force [%]	27.16	24.22	20.80	16.74	13.96

(a) Test Case 3.0: $FPR = 1.4$ (b) Test Case 3.1: $FPR = 1.3$ (c) Test Case 3.2: $FPR = 1.2$ (d) Test Case 3.3: $FPR = 1.1$ (e) Test Case 3.4: $FPR = 1.032$ **Figure 4.8:** Mach number contour for different throttled fan pressure ratios

As can be expected for spillage drag, the increase in drag is non-linear as less flow is captured by the inlet. In the case of the nacelle designed for a lower FPR, it is interesting to note that the fan cowl force is similar to the higher FPR case, while the nacelle drag is lower. The amount of flow passing through the bypass is different in these cases, being higher in test case 5. The aft core cowl is most often subject to a forward facing pressure force. The pressure in the bypass nozzle jet in test case 5 is higher due to the larger mass flow, and this will result in a greater pressure force in the forward direction in this case compared to case 3.1.

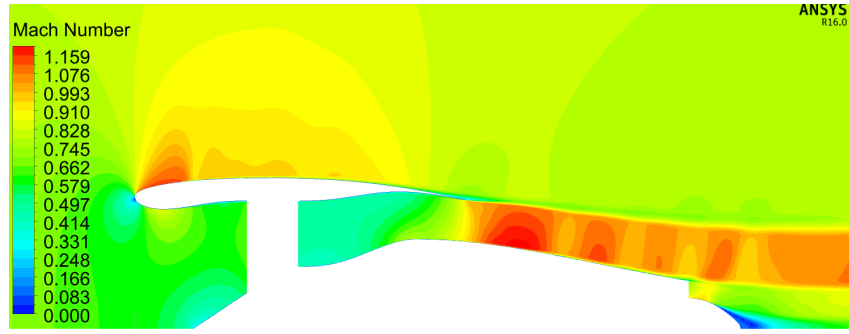
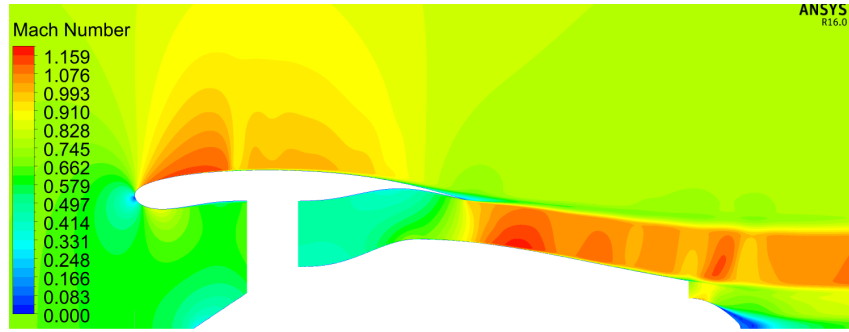
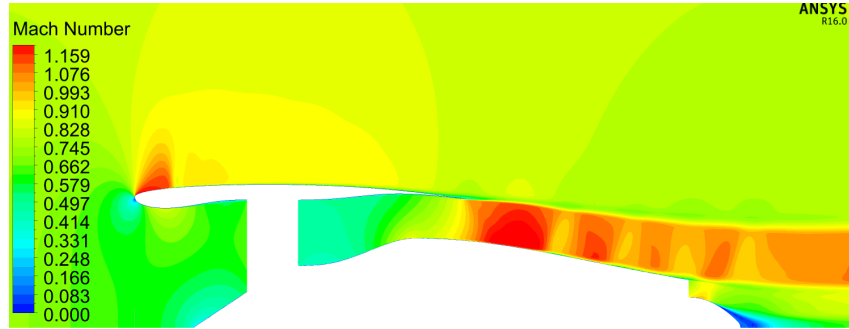
4.4 Evaluation of Only Changing Fan Cowl Thickness

Previously in this chapter the effects of changing the overall size of the nacelle on an engine was shown. Here, the results from cases where only the fan cowl thickness is changed are presented. The cases are summarised in Table 4.7. A thinner fan cowl could give less drag since the flow needs to turn less to pass over the cowl, but the flow at the inlet could be affected if the highlight radius is lowered. As this was done in the design method developed in this project, the thinner nacelle would have a greater risk of being affected by spillage drag.

Case no.	FPR	M_{inf}	$Altitude [m]$	l_{cowl}/D_{fan}	h_{cowl}/D_{fan}
3.0	1.4	0.8	10668	1.3	0.09
6	1.4	0.8	10668	1.3	0.12
7	1.4	0.8	10668	1.3	0.06

Table 4.7: Summary of parameters for nacelle test cases with different nacelle thickness

In Figure 4.9 the flow around nacelles with only varying thickness is shown. The thicker fan cowl profile is more evenly curved and the area of high Mach number at the front is larger, while the thinner nacelle is almost flat causing the acceleration of the flow to be lower. The Mach number at the front is still higher in this case since the initial radius of curvature is almost the same, since this is related to the length of the cowl, which is the same, and the highlight radius, which is only lowered very little compared to the cases with thicker fan cowl. The flow after the shock at the front is more stable in case 7, and much less of the uneven contour curves at the rear part of the fan cowl is seen in this case.

(a) Test Case 3.0: $h_{cowl}/D_{fan} = 0.09$ (b) Test Case 6: $h_{cowl}/D_{fan} = 0.12$ (c) Test Case 7: $h_{cowl}/D_{fan} = 0.06$ **Figure 4.9:** Mach number contour for different thickness of nacelles

The Mach number at the external part of the bypass jet is higher in the case of a thin nacelle profile, suggesting it is affected by the direction of the flow at the trailing edge of the fan cowl. The core geometry is the same in the three cases, but the angle of the rear fan cowl depend on the thickness. This would affect the streamlines along the rear of the fan cowl, making the jet flow expand more rapidly in the case where the angle is lower, thus causing a higher Mach number in the jet when the bypass nozzle is choked. This expansion could both affect the thrust of the bypass nozzle and the pressure along the aft core cowl and thus the drag. If the expansion is rapid as in test case 7, a stronger shock appears, which could cause and increased drag.

As shown to the right in Figure 4.10, the fan cowl and pre-entry force increases as the thickness increases. Most of this change is expected to come from the fan cowl

pressure force, since this term can become large if the fan cowl is curved as in case 6 and small for a flat fan cowl as in test case 7. To the left in the figure the hybrid drag is shown. The fact that this drag is lower for the fan cowl of middle thickness could be explained by the nacelle design and its influence on the bypass jet flow and the pressure on the aft core cowl. Since the fan cowl and pre-entry force is lower for the thin cowl, only increase of spillage drag could not explain the increased drag in this case. More likely it depends on the pressure along the aft core cowl. In the case of the thick fan cowl in case 6, the increased drag is probably an effect of the long curved profile of the cowl.

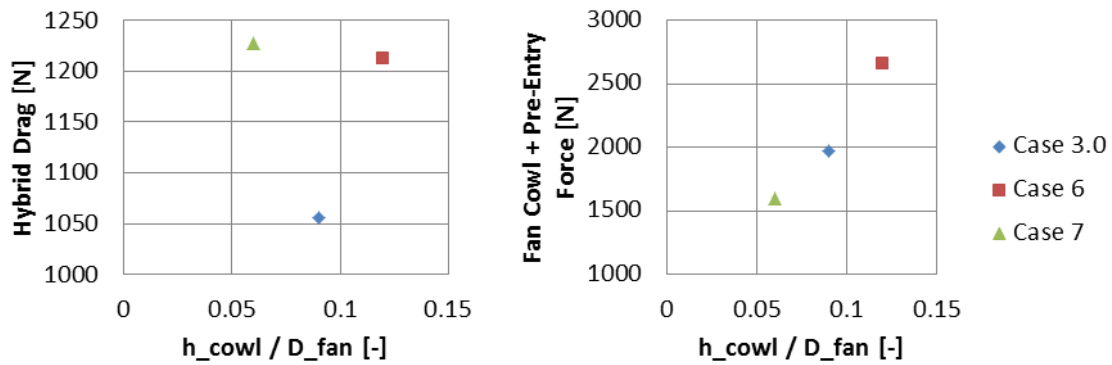


Figure 4.10: Comparison of drag for different thickness of nacelles

Table 4.8 show the wall shear of these three fan cowls relative the fan cowl and pre-entry force. Surprisingly, the relative wall shear in the case of the thin nacelle is high, indicating low spillage drag. Of course, this is in a axisymmetric cruise case, and the thinner fan cowl could still exhibit much more spillage drag at an angle of attack. It is possible that the reason for the high spillage drag in the case of the thick fan cowl is related to a large initial fore-body radius. Compared to the NACA-1 cowl design, this radius is much larger relative the fan cowl length and thickness. For the thinner cowl designs, not only case 3.0 and 7, this might not be a problem, but for a thick relatively short fan cowl as in case 6 it have caused a bad cowl design.

Table 4.8: Fan cowl wall shear and wall shear relative fan cowl and pre-entry force for nacelle test cases 3.0, 6, and 7

Case	3.0	6	7
Fan cowl wall shear [N]	533.1	563.5	492.4
Wall shear portion of fan cowl and pre-entry force [%]	27.16	21.28	30.96

4.5 Evaluation of Effects from Flight Mach Number

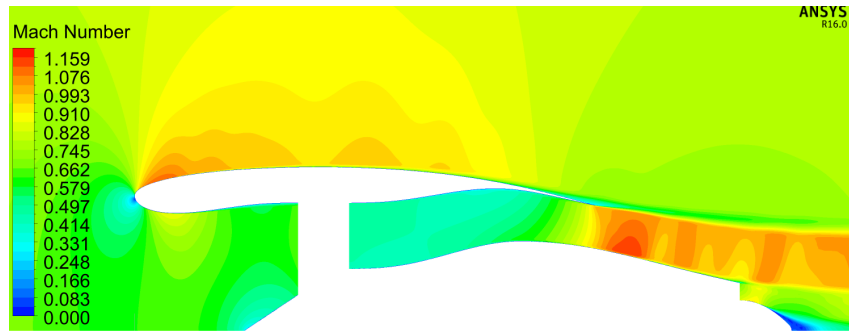
The flight Mach number for previously presented cases is 0.8. Table 4.9 shows the main parameters for the cases where the cruise Mach number is decreased and increased. The geometry used in all these cases is the one from case 2.0, representing a state of the art sized nacelle. Previously the spillage drag of different cases has been discussed. Again this becomes an interesting parameter, since a higher flight Mach number could give a rise in spillage drag. The risk for shocks along the fan cowl surface would also increase, which could cause increased drag and areas of higher Mach number along the cowl which should not be considered spillage drag.

Case no.	FPR	M_{inf}	$Altitude [m]$	l_{cowl}/D_{fan}	h_{cowl}/D_{fan}
2.0	1.4	0.8	10668	1.8	0.14
2.1	1.4	0.75	10668	1.8	0.14
2.2	1.4	0.85	10668	1.8	0.14

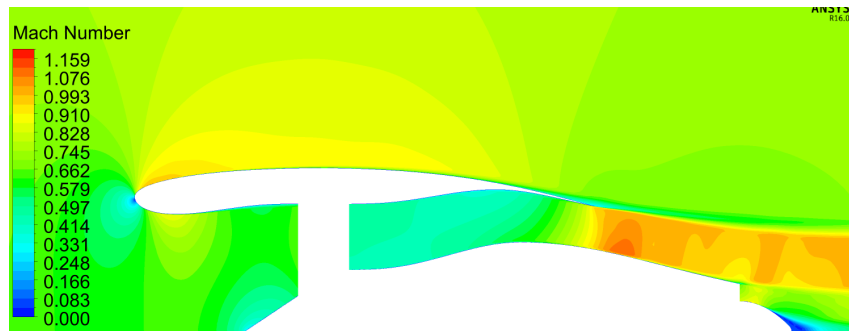
Table 4.9: Summary of parameters for nacelle test cases with different nacelle thickness

Figure 4.11 shows the Mach number contours around the nacelle. Looking at the contours for test case 2.1, the transient phenomena above the fan cowl mentioned earlier is now gone. Furthermore, no shock is observed in this region, indicating that these two are related. The same conclusion can be made by looking at test case 2.2 in Figure 4.11(c) and 4.11(d). These two contour plots show large variations in Mach number above the fan cowl at two different number of iterations, in a range where the solution is close to convergence. For this higher flight Mach number, the transient part of the solution is significant and the steady state simulation can not be considered converged.

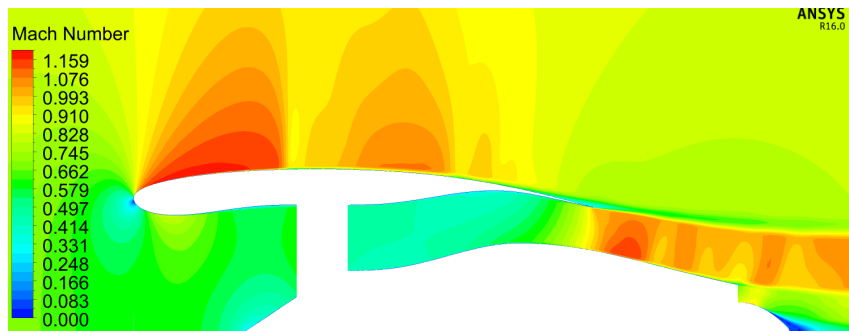
In Figure 4.12 both the hybrid drag and the fan cowl and pre-entry force increases rapidly for higher Mach number. It is important to note that the simulation for test case 2.2 is not converged, but even with an accuracy of 5 to 10% it is clear that the drag increases more between Mach 0.8 and 0.85 than between Mach 0.75 and 0.8. Transonic effects are present at the higher Mach number, which can be seen in Figure 4.11, and these contribute to an increasing drag.



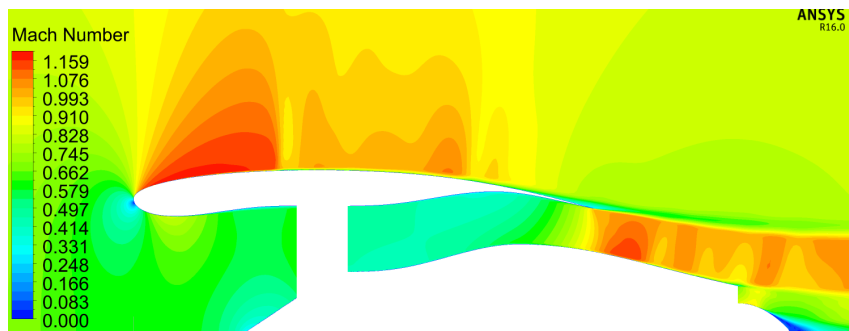
(a) Test Case 2.0: $Ma = 0.8$



(b) Test Case 2.1: $Ma = 0.75$



(c) Test Case 2.2: $Ma = 0.85$



(d) Test Case 2.2: $Ma = 0.85$

Figure 4.11: Mach number contour for different flight Mach numbers

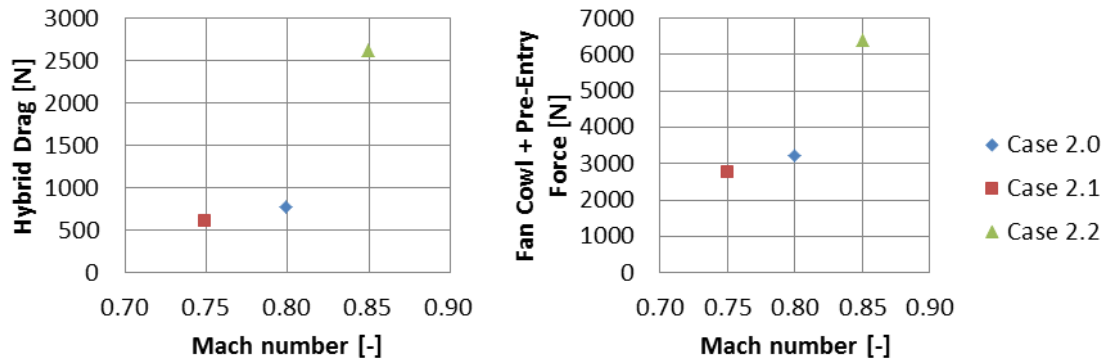


Figure 4.12: Comparison of drag for different flight Mach numbers

Because no reference condition, where there is no spillage drag, exist for these cases. The spillage drag is difficult to evaluate for the high speed cruise case, because a higher flight Mach number could give rise to shocks and thus an increase in drag, that is wave drag, even if there is no spillage. Comparing the spillage drag with wall shear force relative pre-entry and fan cowl force cannot give any clear relations of spillage drag in these cases, but only a relation of the combined effect of spillage and wave drag. Since the large increase of drag between the test cases presented here is assumed to be related to these two drag components, and it is clear that the case with lowest flight Mach number would have the lowest combined spillage and wave drag, the comparison is not carried out here. The very large increase of drag between Mach 0.8 and 0.85 could be a reason to conclude that the cowl is not well adapted to high speed cruise conditions, and thus have a poor design compared to a fan cowl on a turbofan used today. As was discussed for the fan cowl of different thicknesses, the initial radius of curvature of the cowl could be an important parameter to look at.

4.6 Evaluation of Different Nacelle Length and Thickness at End of Runway

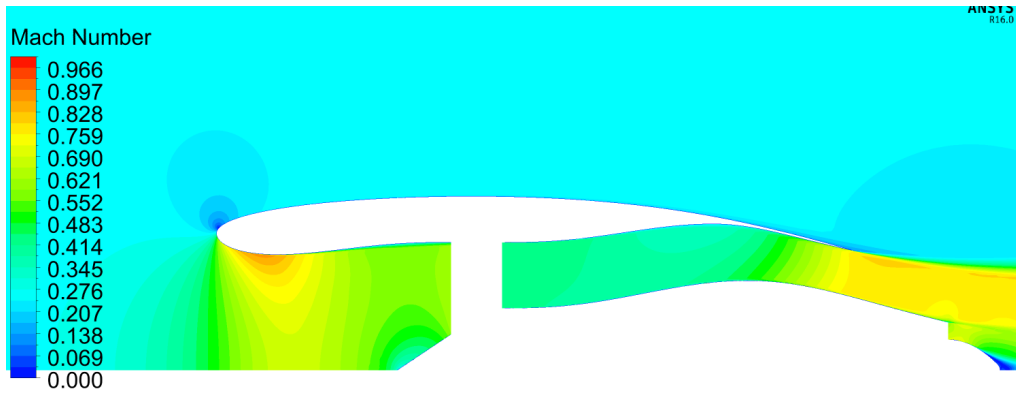
The cases presented here are similar to those presented in Section 4.2, but simulated at end of runway off conditions. This means flight Mach number 0.25 and sea level atmospheric condition. The simulations are still 2D axisymmetric and no angle of attack is considered. Table 4.10 lists the parameters for these cases. As the thrust needed at this point is very large a very high mass flow is also sucked into the engine. It is therefore expected that the force on the surface at the inlet will be negative.

Case no.	FPR	M_{inf}	$Altitude [m]$	l_{cowl}/D_{fan}	h_{cowl}/D_{fan}
TO 1	1.4	0.25	0	2.5	0.18
TO 2.0	1.4	0.25	0	1.8	0.14
TO 3.0	1.4	0.25	0	1.3	0.09
TO 4	1.4	0.25	0	0.6	0.03

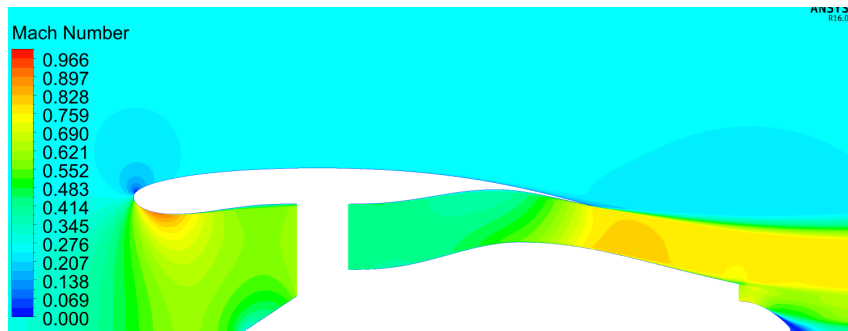
Table 4.10: Summary of parameters for nacelle test cases with different nacelle length and thickness

Figure 4.13 shows the Mach number contours for the cases at end of runway conditions. Note that the geometries in Figure 4.13(a) is the same scale. From the contours it can be seen that the flow is sucked into the engine, as was expected, placing the stagnation point at the front of the fan cowl above the highlight. This would also mean that the stream tube entering the inlet is larger further toward the free stream. This means that the pre-entry force would become negative, that is directed forwards, causing a negative contribution to drag. From the definition of spillage drag, if this would be evaluated for these cases, it also means that this term would become negative.

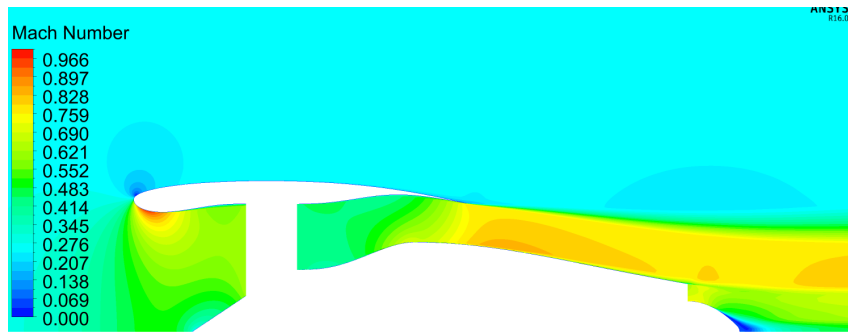
The Mach number is generally low, but in test case TO 4 the small radius at the lip of the fan cowl and the high curvature at the bypass nozzle still generates Mach numbers above 1. Since the flow around the fan cowl has a low Mach number, no small changes can be seen in the figure. At these low speeds, the pressure along the outside of the nacelle change very little, but because of the high pressure, the fan cowl pressure forces become high. As shown by Figure 4.14, the hybrid drag becomes negative in test cases TO 1 and TO 2, while the fan cowl and pre-entry force for the same cases are high. As stated previously, the pre-entry force is negative in these cases, but a very high fan cowl pressure force give a positive (rearward) combined pre-entry and fan cowl force. The pre-entry force is evaluated at the highlight radius and not the stagnation point, meaning that some of the force acting in the rearward direction is instead included in the fan cowl pressure force. Looking at the sum of these two forces, this does not make a difference, but if looking at the individual values of the forces in Appendix H it should be considered.



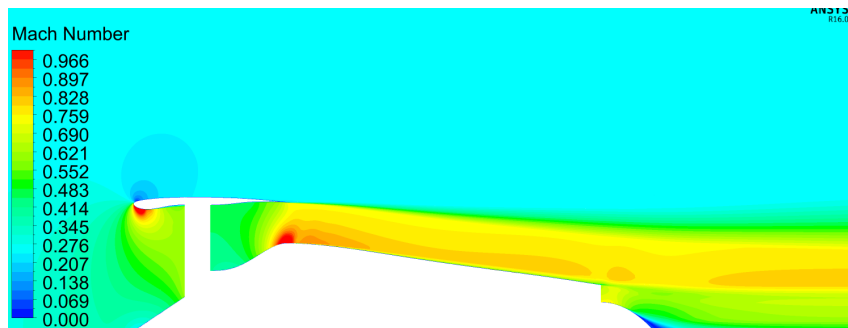
(a) Test Case TO 1: $L_{cowl}/D_{fan} = 2.5$, $h_{cowl}/D_{fan} = 0.18$



(b) Test Case TO 2: $L_{cowl}/D_{fan} = 1.8$, $h_{cowl}/D_{fan} = 0.14$



(c) Test Case TO 3: $L_{cowl}/D_{fan} = 1.3$, $h_{cowl}/D_{fan} = 0.09$



(d) Test Case TO 4: $L_{cowl}/D_{fan} = 0.6$, $h_{cowl}/D_{fan} = 0.03$

Figure 4.13: Mach number contour for different sized nacelles at end of runway

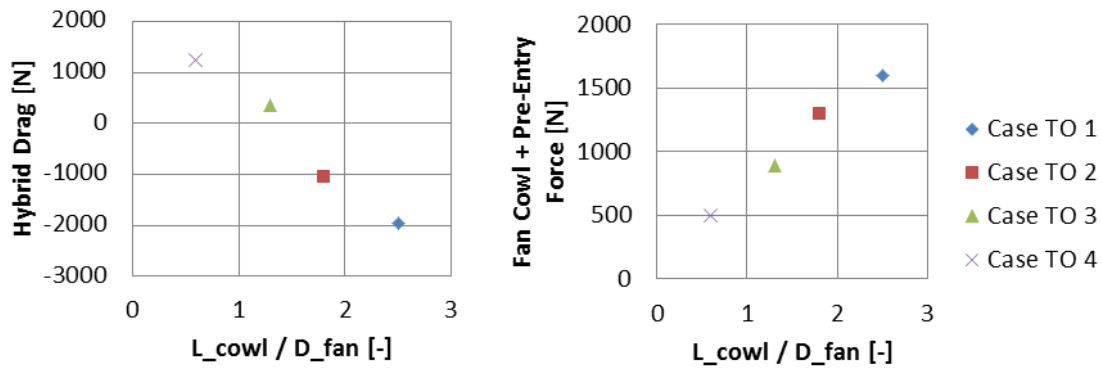


Figure 4.14: Comparison of drag for different sized nacelles at end of runway

4.7 Engine Performance of Nacelle Test Cases

In this section the results of the installation performance parameters described in Section 2.1.2 are presented. All values for these parameters are not presented here, but can be seen in Appendix H, G, and I.

4.7.1 Inlet, Fan, and Bypass Pressure Ratios

The area of the fan system exit was calculated from the total pressure, total temperature, and mass flow from cycle design, and an approximated Mach number. Since the mass flow is set on the boundary in the CFD simulations, the total pressure can change and is not fixed to the cycle design value. This led to deviations in FPR off up to 3% in some case. Table 4.11 shows the fan pressure ratios obtained in the simulations. The pressures at the fan faces can be seen in Appendix I. The FPR for the TO cases should be 1.444 according to cycle data (see Appendix F), but the FPR obtained is still larger in all these cases. To get the FPR closer to cycle design, the area of the fan system exit face would have to be changed, for example by changing the fan exit face hub radius. However if the nozzle is choked, this would also affect the pressure at the fan system exit since the mass flow is determined beforehand. So also the minimum area in the bypass, in these cases the nozzle, needs to be considered.

Table 4.11: Fan pressure ratios obtained in simulations for the nacelle test cases

Case	1	2.0	3.0	4	5	6
FPR	1.4307	1.4177	1.4071	1.4106	1.3097	1.4169
Case	7	2.1	2.2	TO1	TO2	TO3
FPR	1.3999	1.4211	1.3735	1.4786	1.4703	1.4648
Case	TO4	3.1	3.2	3.3	3.4	
FPR	1.4378	1.3136	1.2225	1.1285	1.0637	

The difference in FPR could also potentially come from a too high or too low pressure

at the fan system inlet face. If the inlet of the geometry performs poorly and the pressure recovery is low, the total pressure is lower than expected at the fan inlet face and the FPR would become higher even if the correct total pressure was obtained at the fan system exit. Both the inlet pressure recovery and the bypass nozzle pressure ratio are close to the cycle design, with an approximate deviation of 0.06%. This would suggest that these effects are smaller and cannot be the only reason for the difference between the FPR in the cycle and that from the CFD simulations.

The inlet pressure recovery in the cases with a longer inlet is lower than the cycle design, while the pressure recovery for the short inlets are higher than cycle design. In nacelle test case 1 it is 0.143% lower than cycle design, while for test case 4 it is 0.098% higher. Table 4.12 shows the inlet pressure recovery from the simulations. Considering that the cycle design pressure recovery is 0.998, the increase in test case 4 means that the inlet pressure recovery of this case is closer to 0.999. Also worth noting is that even though the inlets in test case 3.0 and test case 5 are the same, since only the FPR change between these cases, the inlet performs better with a lower FPR, that is in test case 5. The same can also be observed as the FPR is throttled in cases 3.1, 3.2, 3.3, and 3.4, with an increasing performance as the FPR is lowered. Since the flow in these cases are lower, the pressure is affected less. If there was no flow, the pressure recovery would naturally be 1, and because of the lower mass flow in the throttled engines, the pressure recovery increases up to approximately 0.9993 for case 3.4.

Table 4.12: Inlet pressure recovery obtained in simulations for the nacelle test cases

Case	1	2.0	3.0	4	5	6
Inlet PR	0.9966	0.9976	0.9981	0.9990	0.9980	0.9981
Case	7	2.1	2.2	TO1	TO2	TO3
Inlet PR	0.9982	0.9976	0.9979	0.9979	0.9980	0.9975
Case	TO4	3.1	3.2	3.3	3.4	
Inlet PR	0.9973	0.9985	0.9989	0.9992	0.9993	

As both the inlet pressure recovery and the FPR is different than the cycle design, it can be expected that also the pressure ratio in the bypass is different from cycle design. Table 4.13 shows the bypass pressure ratios for the different nacelle test cases. As mentioned above these differences are around 0.06% in average for the different cases. If the nozzle is choked a change in total pressure at the outlet will also mean that the static pressure would change. This would then affect the thrust obtained from the nozzle. The bypass pressure ratio in all cases except case 1 and 2.1 is larger than the cycle data, which would result in a higher thrust if the nozzle is choked and the fan system exit pressure is the same as in cycle design. Since both the pressure at the fan system and nozzle exit is generally higher than cycle values, the thrust must also become higher in these cases.

Table 4.13: Bypass pressure ratio obtained in simulations for the nacelle test cases

Case	1	2.0	3.0	4	5	6
Bypass PR	0.9940	0.9951	0.9960	0.9966	0.9954	0.9959
Case	7	2.1	2.2	TO1	TO2	TO3
Bypass PR	0.9951	0.9950	0.9951	0.9955	0.9960	0.9969
Case	TO4	3.1	3.2	3.3	3.4	
Bypass PR	0.9965	0.9960	0.9961	0.9962	0.9964	

4.7.2 Discharge Coefficient

The discharge coefficient for both bypass and core nozzle is lower than the cycle design in all test cases (see Appendix G), suggesting a lower nozzle performance. In the case of the bypass channel, which is included in the geometries, this would suggest that the geometries used is not representative of a state of the art nozzle with an expected discharge coefficient around 0.996 at cruise. Table 4.14 show these discharge coefficients and they are here instead around 0.985. Also, to represent the core nozzle with only a boundary at the exit does not give a good nozzle performance. For the core nozzle, a discharge coefficient of around 0.974 is expected from cycle design, while values around 0.96 or even as low as 0.91 are obtained from the CFD results. Since this nozzle is only represented by a boundary any conclusions regarding these results are difficult to make.

Table 4.14: Bypass nozzle discharge coefficients obtained in simulations for the nacelle test cases

Case	1	2.0	3.0	4	5	6
C_D	0.9774	0.9849	0.9905	0.9864	0.9887	0.9836
Case	7	2.1	2.2	TO1	TO2	TO3
C_D	0.9958	0.9828	0.9850	0.9607	0.9691	0.9722
Case	TO4	3.1	3.2	3.3	3.4	
C_D	0.9989	0.9848	0.9753	0.9636	0.9547	

The best performing bypass nozzle according to the measurement of discharge coefficient is the one in test case 7. Looking back at the Mach number contours in Figure 4.9, the most notable difference compared to test case 3 and 6 also shown is the higher Mach number after the nozzle exit. Also, the nozzle jet seem to be directed less inwards at the nozzle. If this contributes to a higher discharge coefficient, the slope of the outer part of the bypass at the nozzle could be an important parameter. Changing this angle in the other cases might increase the performance of these nozzles.

Following this logic, the discharge coefficients for cases with thick fan cowl, which with the method used for generating geometries means that the slope of the bypass at the nozzle is high, should have the worst nozzle performance. This can also be seen in the results, as the discharge coefficients for case 1, with a long thick fan cowl, and case 6, with a shorter but thick fan cowl, are some of the lowest obtained

for the cases at cruise at Mach 0.8. The angle of the outer part of the bypass is in case 1 12.68° , and in case 6 13.33° . In comparison, the case with the highest discharge coefficient at cruise, that case 7, has an angle of 6.62° .

4.7.3 Thrust

The net thrust for most cases are close to what was expected from the cycle design. A summary of the thrust for all cases can be seen in Appendix H. The cases that differ most are the throttled test cases, that is test cases 3.1 to 3.4, with an extreme of approximately 66% higher net thrust in case number 3.4. Not considering the throttled cases, the extreme is instead approximately 1.6% lower net thrust, while most fall in the range $\pm 1\%$.

The thrust coefficients for the nozzles are summarised in Appendix G. For the core nozzles the thrust coefficients obtained from the simulations are high. In general they are well above one, and thus a higher thrust than the ideal is experienced. The mass flow boundary condition representing the nozzle could enforce a different state at the nozzle outlet. This other state could have a higher ideal thrust than what is calculated here by for example assuming free stream static pressure at the outlet for a unchoked nozzle. Table 4.15 show the thrust coefficients for the bypass nozzles in the different nacelle test cases. These are somewhat lower than could be expected from cycle design, that is 0.998 for the bypass and 0.995 for the core.

Table 4.15: Bypass nozzle thrust coefficients obtained in simulations for the nacelle test cases

Case	1	2.0	3.0	4	5	6
C_F	0.9809	0.9867	0.9926	0.9940	0.9904	0.9921
Case	7	2.1	2.2	TO1	TO2	TO3
C_F	0.9942	0.9862	0.9874	0.9775	0.9833	0.9912
Case	TO4	3.1	3.2	3.3	3.4	
C_F	0.9954	0.9927	0.9928	0.9930	0.9933	

An important note when comparing the thrust coefficient to cycle data, is that GasTurb calculates this coefficient differently for choked nozzles. With the definition used here, the cycle data would give a somewhat higher bypass nozzle thrust coefficient (since these are choked in most cases). If this definition would be used in the cycle design the coefficients would probably be close to 0.998, but cases with FPR 1.4 at cruise would have a thrust coefficient around 0.9984. The definition used in GasTurb comes from

$$F_G = A(P_s - P_t) + C_F V_{ideal} \dot{m} \quad (4.1)$$

and since the first term is not included for an unchoked nozzle, the definition does not differ in that case. The differences to the definition used here is that the actual area of the nozzle is used for the first term and not the ideal area, and that only the second term is multiplied by C_F and not both.

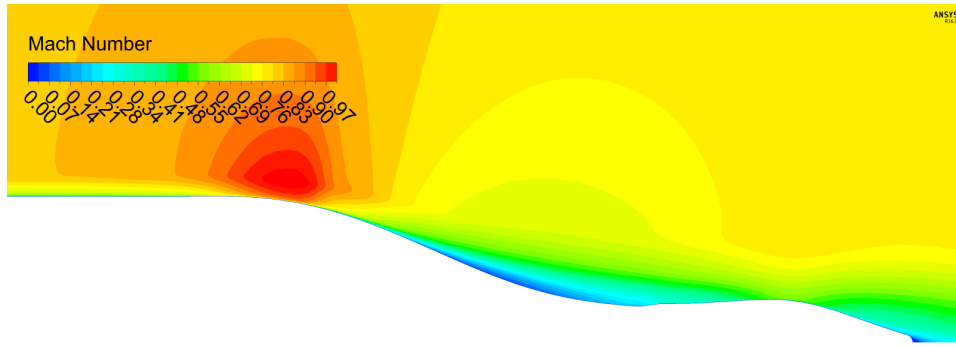
As was the case with the discharge coefficient, test case 7, with a thinner fan cowl, shows the highest performance also with respect to thrust coefficient. Because of this, the previous hypothesis that the angle of the bypass curve at the nozzle could affect the nozzle performance still holds. But, for this case the thrust is still one of the lowest for the cases simulated at cruise, around 1% lower than cycle data. The reason for the high thrust coefficient is then that the calculated ideal thrust is also lower in this case.

4.8 Boundary Layer Ingestion

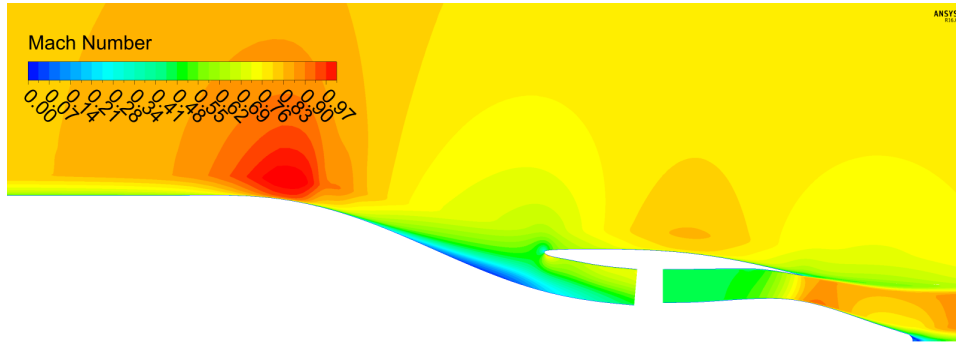
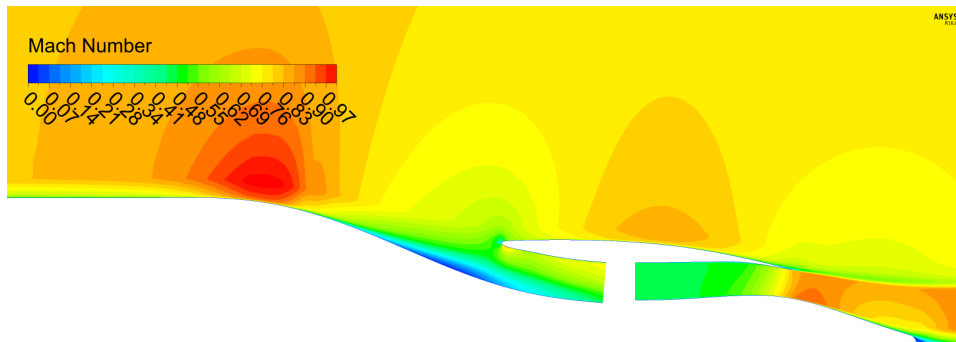
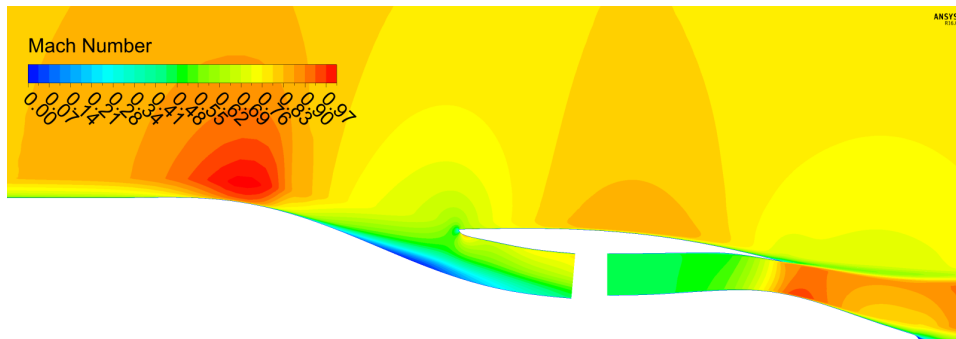
Thus far in this chapter only the nacelle test cases have been considered. In this section the BLI cases are presented. The case 0 represents a axisymmetric fuselage similar to that in case number 1, but without the engine. The results of this case is used as a baseline to get a better understanding of how much the drag could be reduced by introducing BLI. The BLI cases 1 to 3 have a nacelle and fan of varying diameter at the rear of the fuselage. BLI case 1 has a fan diameter of 2 meters, making the fan cowl of similar size to the nacelle test case 2.0, while the diameter is increased in cases 2 and 3 to 2.25 meters and 2.5 meters, respectively.

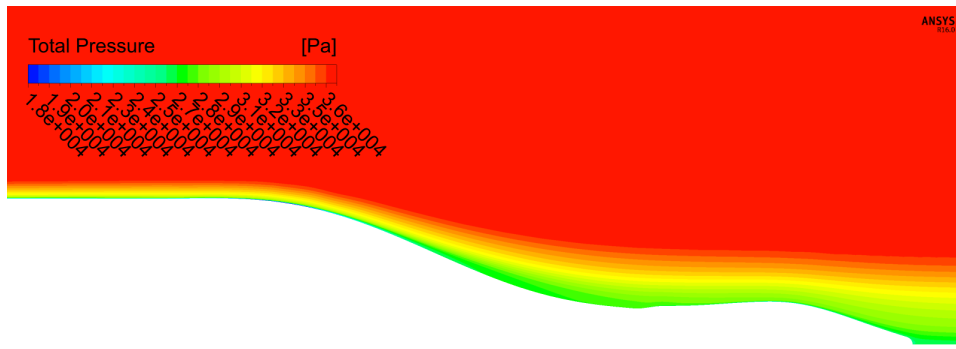
Figure 4.15 shows the contours of Mach number around the BLI engine. It is clear that a high Mach number, near sonic, is reached where the fuselage is curved at the rear. For the cases with BLI, this region persists as the flow still needs to turn into the engine. In a similar manner the Mach number is high at the rear of the fan cowl, but as in both case 1 and 2 the fan cowl lies within the boundary layer of the fuselage, the region remains relatively small because of the lower velocity. In the third case the region becomes large since the velocity around the fan cowl is higher.

In respect to these results, it is interesting to look at how much of the boundary layer from the fuselage that is captured by the rear mounted engine. Figure 4.16 shows the contours of the total pressure. The boundary layer is seen as the lower contours, while the free stream and jet from bypass nozzle is represented by the highest contour. In both case 1 and 2 it is here clear that, as previously stated, the fan cowl lies inside the boundary layer from the fuselage, while in case 3 the entire boundary layer seems to be ingested by the engine.

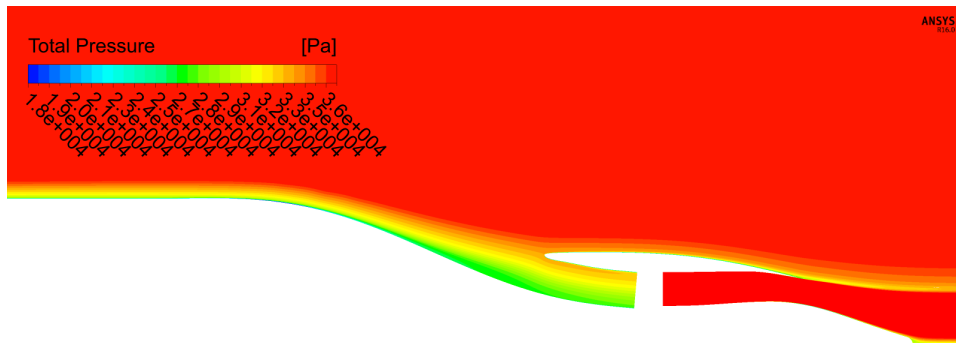


(a) Case 0: no engine

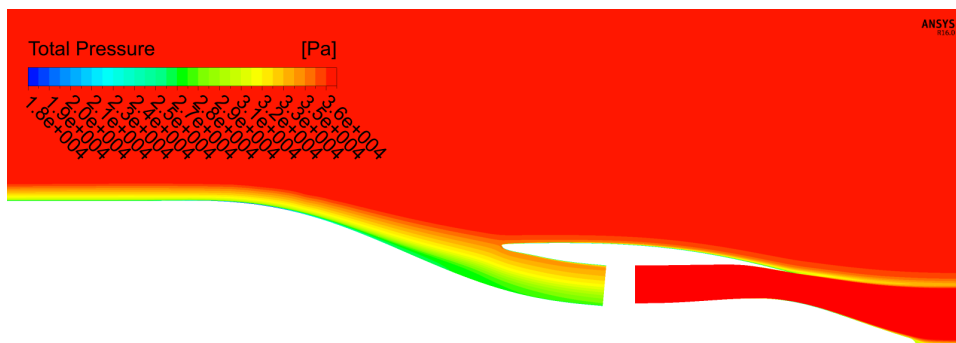
(b) Case 1: $D_{fan} = 2$ (c) Case 2: $D_{fan} = 2.25$ (d) Case 3: $D_{fan} = 2.5$ **Figure 4.15:** Contours of Mach number around BLI



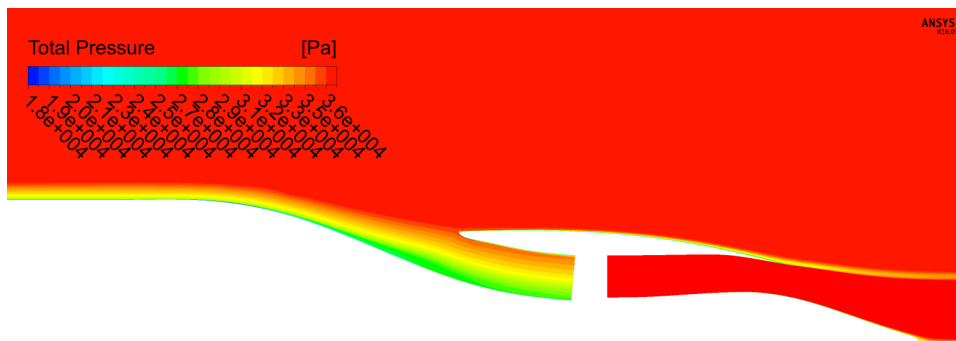
(a) Case 0: no engine



(b) Case 1: $D_{fan} = 2$



(c) Case 2: $D_{fan} = 2.25$



(d) Case 3: $D_{fan} = 2.5$

Figure 4.16: Contours of total pressure around BLI

Figure 4.17 shows the hybrid drag of the BLI cases 1 to 3. The dashed line in the figure shows the drag of BLI case 0 as a reference. The components of the hybrid drag can be seen in Appendix H. Looking at the pre-entry and the fan cowl force for case 1 and 2, they are very similar, but increase rapidly in case 3. This could be the result of spillage drag. As the fan cowl is moved further out in the boundary layer, the static pressure at the inlet increases and a larger spillage drag term would be expected. Also, a higher velocity above the fan cowl would contribute to this. Considering the hybrid drag, it is lower in case 2, than both case 1 and 3. This suggest an optimum fan radius could be found so that the fan cowl force remains low relative the possible extra forward force from the nozzle jet interacting with the aft core cowl.

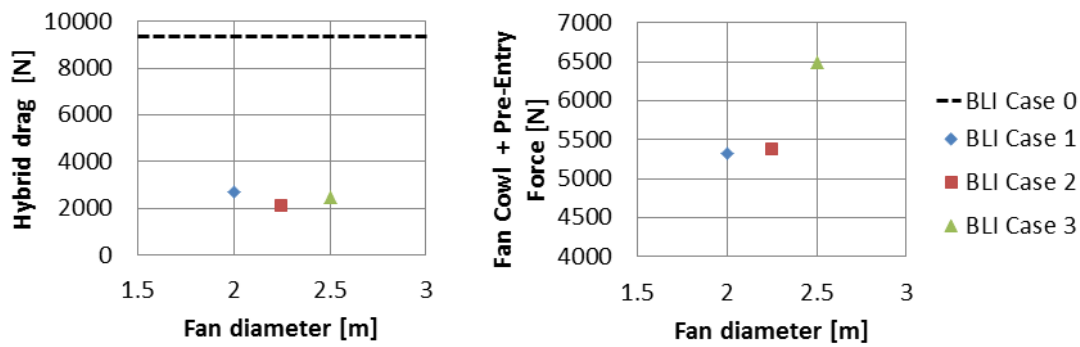


Figure 4.17: Comparison of drag for boundary layer ingestion

To look closer into the spillage drag contribution the fan cowl wall shear force relative fan cowl and pre-entry force is considered. Firstly it should be noted that the pre-entry force for these cases is negative and that this will mean that the spillage drag will not be a drag as such. For these cases it therefore makes more sense to talk about a fan suction force at the inlet. Also when making the comparison of this suction force relative the wall shear the drag from the fuselage is not considered. Table 4.16 shows the fan cowl wall shear force and the fan suction force, which is the pre-entry and fan cowl force minus the contributions from the fuselage. Since the wall shear is a much larger portion of the fan suction force in the third case, the fan suction force is much less in this case (compare to high spillage drag).

Table 4.16: Fan cowl wall shear and wall shear relative fan suction force for BLI test cases

Case	BLI 1	BLI 2	BLI 3
Fan cowl wall shear [N]	645.3	846.1	1027.6
Wall shear portion of fan suction force [%]	12.00	16.56	41.96

Figure 4.18 show the decrease of drag in the three BLI test cases relative the increase of net propulsive force F_{nps} . The increase of F_{nps} could be seen as the force which

is added to the system. As can be seen, in case 2 and 3 the force required to reduce the drag is higher. The trend seem to be that a larger fan with the same FPR less drag reduction relative the added net propulsive force to the BLI system. In that case a smaller fan, which does not ingest as much of the boundary layer could give relaiely high drag reduction. The slope between the points of case 1 and 2 is smaller compared to the slope between the points of case 2 and 3. This might suggest a optimal fan diameter, related to drag reduction per increase of net propulsive force, which is smaller than 2 meters. Although, to find this optimum other facors such as weight increase for a larger fan and the electrical system would need to be considered which is not done here.

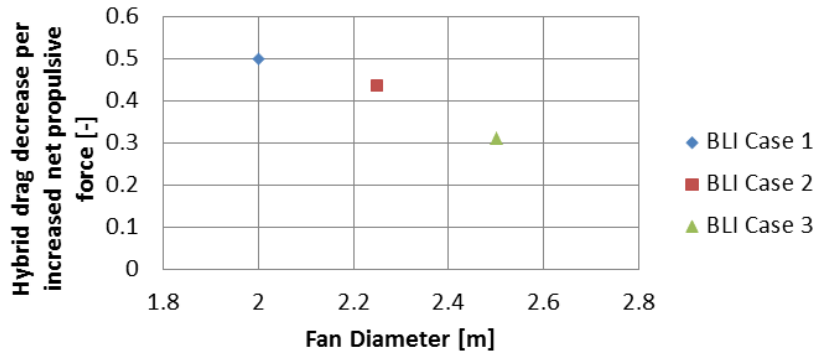


Figure 4.18: The decrease of drag relative the increase of F_{nps} for the BLI test cases

4.8.1 BLI Engine Performance

For these cases there are no real cycle data to compare the performance parameters to, but as they are based on the turbofan cycle with FPR 1.3 used in the nacelle cases the parameters from this cycle is used as reference. Table 4.17 shows the pressure ratios for inlet, nozzle, and the fan, and the discharge and thrust coefficients for the nozzles. The inlet pressure recovery is lower for the BLI cases compared to the nacelle test cases, for example 0.9980 in test case 5. These recovery ratios are defined from the total pressure at the inlet plane and fan inlet face, but the last row of the table also show the pressure recovery defined from the free stream to the fan inlet face. The bypass pressure ratio is similar to that in the nacelle cases.

Table 4.17: Engine performance parameters for the BLI cases

Case	1	2	3
Inlet PR	0.9918	0.9920	0.9747
Bypass PR	0.9940	0.9947	0.9949
FPR	1.3498	1.3438	1.3632
C_D	0.9618	0.9649	0.9674
C_F	0.9888	0.9909	0.9902
Overall inlet PR	0.8582	0.8759	0.8791

The nacelle test cases did not obtain the correct FPR, but the difference is larger in the BLI cases. A contribution to this could be the lower overall inlet pressure recovery. The design of the inlet is in these cases very different and the way the inlet geometry is created could be improved. These designs are based on an estimation of the overall inlet pressure recovery, but the as the guess was too high the outlet pressure also became too high, while the inlet pressure was determined from the flow. Since the inlet pressure recovery was lower in the simulations the FPR became approximately 4% higher than desired.

Table 4.18 shows the energy put into the fluid by the engine calculated from the difference in total temperature between the free stream and the nozzle exit. A small error might be introduced due to the total temperature in the boundary layer of the fuselage differing from the free stream. The free stream temperature is 246.88K at 35 000 feet and Mach 0.8. Other quantities needed to calculate the energy input can be seen in Appendix G. Since the temperature difference is close to constant for the different cases, the increase of energy input is due to higher mass flow. The increase of energy input is thus proportional to the mass flow increase.

Table 4.18: Fan energy output for BLI test cases

Case	1	2	3
Energy input [kJ/s]	3262.001	4222.896	5327.536

The thrust and discharge coefficients of the bypass nozzles are for the BLI cases much lower than for the nacelle test cases. As the performance of those cases were considered lower than what can be expected, the performance of the BLI nozzles can be considered poor. Before further investigations are done around these geometries, the reason for this poor performance should be determined.

Chapter 5

Conclusion

5.1 Concluding Remarks on the Nacelle Test Cases

There has been little or no effort put into optimising the nacelle geometries. Therefore the results obtained from the CFD simulations are just a first investigation into how the size of the fan cowl affect the nacelle drag. If only the fan cowl is considered, it is natural to assume that the drag would decrease if the fan cowl is shorted. Since also the forces on the aft core cowl and the exhaust plug are counted to the drag of the whole nacelle, an increase in drag can be expected if the fan cowl is shortened. But, as mentioned, the geometries has not been optimised and a lower drag could perhaps be obtained for the medium short nacelle in this project, which represent a state of the art nacelle.

The design of the aft core cowl has shown to be an important parameter for the drag. The method used in this project, that is constructing a core cowl curve from a CST method with Bernstein polynomials as shape functions, is perhaps not the best choice. A higher order polynomial where the curvature of the cowl could be better designed might be better suited for this part of the geometry. Also using a representative class function would probably remove the need to use two of these CST curves to create the core cowl. However, using a higher order polynomial for the fan cowl would require more constraining parameters. The parameters used for a fourth order polynomial are clear and uncomplicated, while the higher order constraints might be less intuitive.

The geometries generated in this project exhibit poor installation performance. The reason for this is assumed to be a combination of the geometry and the boundary conditions used in the CFD simulations. Forcing a given mass flow through a inlet and bypass channel that are not well designed has given some total pressures, and thrust and discharge coefficients that differ from the cycle design. Shortening the bypass so that the fan system outlet boundary better represents the position of the guide vanes could perhaps affect the performance parameters of the bypass.

5.2 Concluding Remarks on the BLI Test Cases

The designs used in this project show low performance parameters, but some reservations related to pressures around the nacelle are made. The CFD simulations still

show around 1% fluctuations in drag, which mean that the pressures around the fan cowl, inlet and nozzle are not completely stable. Since a large portion of the drag in these cases come from the fuselage, if this part is stable a 1% change means that larger fluctuations around the fan cowl. The results from this part of the project should be seen as a base for future work.

5.3 Future Work

In this section some suggestions are made on what can be developed further from this project. As more work has been done in this project on the topic of nacelle geometries, the developed method could be refined to get better performing nacelles. The work done with BLI in the project could be seen as an introduction to the subject and there is lots of room for improvements and investigations of other parameters to better understand this concept.

5.3.1 Improvements and Further Investigations of Nacelles

Some of the parameters which define the fan cowl has not been changed in the different test cases. For example the initial fore-body radius and the position of the location of the maximum radius. The effects of these parameters, along with the other input parameters to the fan cowl curve, would be interesting to investigate. Possibly these parameters could also be optimised for a nacelle of modern size, and this could give a better sense of how low drag could be achieved with this design method. This would require some atomisation of the processes used in this project.

If the fan cowl profile is optimised, it could be of interest to also optimise the aft core cowl at the same time, since this part has been shown to affect the drag. It might be possible to optimise the two parts separately, which would make the process easier. If a core cowl profile created from a higher order polynomial the number of optimisation parameters would increase. As the method is now, there would be around 20 parameters to consider, but some of these are not parameters that could be optimised, such as fan cowl length relative fan diameter or length of the core relative the tip radius of the IPC. In this sense, increasing the number of parameters might not be too difficult.

5.3.2 Improvements and Further Investigations of BLI

In the cases in this project only the fan diameter was changed to ingest different portions of the boundary layer. This could also be done by changing the design FPR and thus the mass flow through the fan. The difference between these two ways of altering the amount of boundary layer captured by the fan could be interesting to look at. The inlet could be designed to compensate for any spillage drag which arises as less flow is captured in a larger fan. To also evaluate cases with smaller fan diameter to find any optimum fan diameter, which ingests a smaller portion

of the boundary layer, can be found. It could also be interesting to compare the power needed to drive the different fans. Relating to any further simulations using CFX, the domain should be dramatically increased so that proper convergence can be obtained.

For the nacelle cases an optimisation of parameters could be interesting, but the design of the fan cowl and aft core cowl of the BLI should, at least to some degree, be optimised and the design method reviewed. Some performance parameters show very low values and to get a better representation of the fan and nacelle in any future work related to this design method, these need to be addressed.

Bibliography

- [1] European Commission. (2015) Paris Agreement. [Online]. Available: http://ec.europa.eu/clima/policies/international/negotiations/paris_en, Accessed:2016-12-14
- [2] ——. (2016) Reducing emissions from aviation. [Online]. Available: http://ec.europa.eu/clima/policies/transport/aviation_en, Accessed:2016-12-14
- [3] N. A. Cumpsty, “Preparing for the Future: Reducing Gas Turbine Environmental Impact—IGTI Scholar Lecture,” *Journal of Turbomachinery*, vol. 132, October 2010.
- [4] B. MacIsaac and R. Langton, *Gas Turbine Propulsion Systems*. West Sussex, United Kingdom: John Wiley & Sons, 2011.
- [5] Rolls-Royce. (2016) UltraFan. [Online]. Available: <http://www.rolls-royce.com/products-and-services/civil-aerospace/products/future-products/ultrafan.aspx>, Accessed:2016-10-03
- [6] A. Peters, Z. S. Spakovszky, W. K. Lord, and B. Rose, “Ultrashort Nacelles for Low Fan Pressure Ratio Propulsors,” *Journal of Turbomachinery*, vol. 137, February 2015.
- [7] G. Norris. (2016, Feb.) NASA ‘Surprised’ By Hybrid Power Study Results. [Online]. Available: <http://aviationweek.com/technology/nasa-surprised-hybrid-power-study-results>, Accessed:2016-04-07
- [8] R. W. Johnson, *The Handbook of Fluid Dynamics*, 1st ed. CRC press LLC, 1998.
- [9] MIDAP Study Group, “Agardograph no. 237: Guide to In-Flight Thrust Measurement of Turbojets and Fan Engines,” London, UK, Technical Report AGARD-AG-237, 1979.
- [10] ESDU, “Drag of Axisymmetry Cowls at Zero Incidence for Subsonic Mach Numbers,” ESDU International, London, UK, Technical Report ESDU 81024, 1981.
- [11] D. D. Baals, N. E. Smith, and J. B. Wright, “The Development and Application of High-Critical-Speed Nose Inlets,” *NACA Report No. 920*, 1976.
- [12] F. Zhu and N. Qin, “Intuitive Class/Shape Function Parameterization for Airfoils,” *AIAA Journal*, vol. 52, January 2014.

- [13] R. Christie, A. Heidebrecht, and D. MacManus, “An Automated Approach to Nacelle Parametrisation using Intuitive Class Shape Transformation Curves,” *ASME*, 2016.
- [14] Boeing. (2016) Next-Generation 737 Design Highlights. [Online]. Available: <http://www.boeing.com/commercial/737ng/#/design-highlights/characteristics/>, Accessed: 2016-11-22
- [15] Safran Aircraft Engines. (2016) CFM56-7B: the exclusive Boeing 737NG engine. [Online]. Available: <http://www.safran-aircraft-engines.com/commercial-engines/single-aisle-commercial-jets/cfm56/cfm56-7b>, Accessed: 2016-11-22
- [16] Rolls-Royce. (2014) Advance and UltraFan engine designs. [Online]. Available: <https://www.flickr.com/photos/rolls-royceplc/14151526910/in/album-72157644584413758/>, Accessed: 2016-11-22
- [17] A. Heidebrecht, T. Stankowski, and D. MacManus, “Parametric Geometry and CFD Process for Turbofan Nacelles,” *ASME*, 2016.
- [18] EASA. (2016) ICAO Aircraft Engine Emissions Databank. [Online]. Available: <https://www.easa.europa.eu/document-library/icao-aircraft-engine-emissions-databank>, Accessed: 2016-07-30
- [19] A. Peters, “Ultra-Short Nacelles for Low Fan Pressure Ratio Propulsors,” Ph.D. dissertation, Massachusetts Institute of Technology, February 2014.

Appendix A

MATLAB function used to generate cowl profiles

```
function [Phi,Xi] = ProfileGenerator(g,n,nacelle_type)
% INPUT
% g - vector containning the parameters needed to generate
    the curve
%
% n - number of points per curve
%
% nacelle_type - specified if a CST curve or a NACA-1
    profile should be
% used
%
% OUTPUT
% Phi - axial ordinates of the profile
%
% Xi - radial ordinates of the profile
%
```

CST curve

```
if strcmp(nacelle_type,'CST')
```

Cowl parameters

```
h = g(1);
l = g(2);
f_max = g(3);
f_if = g(4);
Delta_Xi = g(5);
beta = g(6);
```

Class function:

```
Phi = linspace(0,1,n);
C = (Phi.^0.5.*(1-Phi)); % Describes a round-nosed
    airfoil
```

Shape functions (Bernstein polynomials)

```
order = 4;
BP = zeros(order,length(Phi));
for iter_1 = 0:order
    K_in = factorial(order)/(factorial(iter_1)*factorial
        (order-iter_1));
```

```

        BP(iter_1+1,:) = K_in*(Phi.^iter_1.*(1-Phi).^(order-
            iter_1));
    end
    order = order + 1;

```

Constraints

```

% First and second derivative of the class function
C_p = gradient(C,Phi);
C_pp = gradient(C_p,Phi);
% First and second derivatives of the Bernstein
    polynomials
BP_p = gradient(BP,Phi,1);
BP_pp = gradient(BP_p,Phi,1);

A = zeros(3);
% Weighting coefficient for the first Bernstien
    polynomial
A_0 = sqrt(2*(f_if*(h-1)^2/(f_max*l))/l);
% Weighting coefficient for the last(fifth) Bernstien
    polynomial
A_n = (tan(beta) + Delta_Xi);

% constraints on position (local max)
% at Phi = f_max,
    iter = 1;
while Phi(iter) < f_max;
    iter = iter + 1;
end
% Xi = Xi_max
Xi_max = (h-1)/l;
for iter_1 = 2:order-1
    A(1,iter_1-1) = (BP(iter_1,iter))*C(iter);
end
B(1,1) = Xi_max - Phi(iter)*Delta_Xi - A_0*(BP(1,iter))*
    C(iter) -...
    A_n*(BP(order,iter))*C(iter);

% constraints on gradient (local max)
% at Phi = f_max, Xi' = 0;
for iter_1 = 2:order-1
    A(2,iter_1-1) = (BP_p(iter_1,iter))*C(iter) +...
        (BP(iter_1,iter))*C_p(iter);
end
B(2,1) = 0 - Delta_Xi - A_0*(BP(1,iter))*C_p(iter) -...
    A_n*(BP(order,iter))*C_p(iter) - A_0*(BP_p(1,iter))
        *C(iter) -...

```



```

A_n*(BP_p(order , iter))*C(iter);

% constraints on 2nd derivative (trailing edge)
% at Phi = 1, Xi'' = 0
for iter_1 = 2:order-1
    A(3,iter_1-1) = (BP_pp(iter_1 , end))*C(end) + ...
        2*(BP_p(iter_1 , end))*C_p(end) + (BP(iter_1 , end))*
        C_pp(end);
end
B(3,1) = 0 - A_0*(BP(1 , end))*C_pp(end) - A_n*(BP(order ,
end))*C_pp(end) - ...
    2*(A_0*(BP_p(1 , end))*C_p(end) + A_n*(BP_p(order , end
    ))*C_p(end)) - ...
    A_0*(BP_pp(1 , end))*C(end) - A_n*(BP_pp(order , end))*
    C(end);

% Solvning the rest of the weightiing coefficients
X = A\B;

```

Weighting shape function with Bernstein coefficients

```

bp(1) = A_0;    % curvature at leading edge (fourth
    order constraint)
bp(2) = X(1);   %
bp(3) = X(2);   %
bp(4) = X(3);   %
bp(5) = A_n;    % gradient at triling edge

S = zeros(size(Phi));
for iter_1 = 1:order
    S = S + (bp(iter_1)*BP(iter_1 , :));
end

Xi = S.*C + Phi*Delta_Xi;

```

NACA-1 cowl profile

```
elseif strcmp(nacelle_type , 'NACA1')
```

Cowl parameters

```

L.f = g(1);
L.c = g(2);
L.a = g(3);
DeDm = g(4);
delta = g(5);

```

Cowl geometry

NACA-1 cowl ordinates

```
Ordinates = load('Ordinates_NACA_1_cowls.txt');
x.naca1 = L.f*Ordinates(:,1)'/100;
y.naca1 = Ordinates(:,2)'/100;

n_x = length(x.naca1);

% center of cowl
if L.c > 0
    x.center = linspace(L.f,L.f+L.c,n_x);
    y.center = ones(n_x,1);
else
    x.center = [];
    y.center = [];
end

% rear cowl (parabolic)
x.rear = linspace(0,1,n_x);
y.rear = 1 - (1-delta)*x.rear.^2;
x.rear = L.f + L.c + L.a*x.rear;

Phi = [x.naca1 x.center x.rear];
Xi = [y.naca1 y.center y.rear];

end
```

Appendix B

MATLAB function for generating core geometries

```
function [x,y] = CenterGeometryGenerator(center_input,n)

r_spinner = center_input(1);
l_spinner = center_input(2);
r_fan = center_input(3);
alpha_fan_inlet_face = center_input(4);
l_fan_system = center_input(5);
alpha_fan_exit_face = center_input(6);
r_outer_fan_exit = center_input(7);
r_inner_fan_exit = center_input(8);
r_max_core_cowl = center_input(9);
l_core_cowl = center_input(10);
f_max_core_cowl = center_input(11);
beta_rear_core_cowl = center_input(12);
r_outer_core_nozzle = center_input(13);
r_inner_core_nozzle = center_input(14);
l_rear_step = center_input(15);

x(1:n) = linspace(0,l_spinner,n);
x(n+1:2*n) = linspace(x(n),x(n) + (r_fan-r_spinner)/tan(
    alpha_fan_inlet_face),n);
x(2*n+1:3*n) = linspace(x(2*n),x(2*n) + l_fan_system,n);
x(3*n+1:4*n) = linspace(x(3*n),x(3*n) - (r_outer_fan_exit-
    r_inner_fan_exit)/tan(alpha_fan_exit_face),n);
x(4*n+1:5*n) = linspace(x(4*n),x(4*n) + l_core_cowl,n);
x(5*n+1:6*n) = linspace(x(5*n),x(5*n),n);
x(6*n+1:7*n) = linspace(x(6*n),x(6*n) + l_rear_step,n);

y(1:n) = linspace(0,r_spinner,n); % spinner
y(n+1:2*n) = linspace(y(n),r_fan,n); % fan inlet face
y(2*n+1:3*n) = linspace(y(2*n),y(2*n),n); % tip of fan
    system
y(3*n+1:4*n) = linspace(y(3*n),r_inner_fan_exit,n); % fan
    exit face
% Core cowl
g(1) = r_max_core_cowl/r_inner_fan_exit;
g(2) = l_core_cowl/r_inner_fan_exit;
g(3) = f_max_core_cowl;
g(4) = 1;% assuming some radius of curvature (this end is
    not used) to improve curve
g(5) = (r_outer_core_nozzle-r_inner_fan_exit)/l_core_cowl;
g(6) = beta_rear_core_cowl;% gradient on trailing edge
```

```

[~,Xi_1] = ProfileGenerator(g,n);
g(1) = r_max_core_cowl/r_inner_fan_exit;
g(2) = l_core_cowl/r_inner_fan_exit;
g(3) = (1-f_max_core_cowl);
g(4) = 0;% assuming zero radius of curvature (this end is
    not used)
g(5) = 0;% assuming no height difference of end points
g(6) = 0;% assuming zero angle out from fan
[~,Xi_2] = ProfileGenerator(g,n);
Xi = [Xi_2(n:-1:round((1-f_max_core_cowl)*n+1)) Xi_1(round(
    f_max_core_cowl*n+1):n)];
y(4*n+1:5*n) = y(4*n)+Xi*l_core_cowl;
%
y(5*n+1:6*n) = linspace(y(5*n),r_inner_core_nozzle,n); %
    core nozzle
% Exhaust plug
intersect_angle = pi/4;
arc_angle = pi/2-intersect_angle;
pi_temp = linspace(arc_angle,0,round(n*1/3));
r = 1e-5;
delta_y = 1;
while delta_y > 1e-4
    r = r + 1e-5;
    x_temp_2 = r*(cos(pi_temp)-1)+x(7*n);
    y_temp_2 = r*sin(pi_temp);
    gamma = (l_rear_step-(x_temp_2(end)-x_temp_2(1)))/
        l_rear_step;
    x_temp_1 = linspace(x(6*n),x_temp_2(1),round(n*2/3));
    A = [2*x(6*n)+gamma*l_rear_step 1 0; x(6*n)^2 x(6*n) 1;
        2*x(6*n) 1 0];
    b = [-tan(intersect_angle)/2;y(6*n);0];
    c = A\b;
    y_temp_1 = c(1)*x_temp_1.^2 + c(2)*x_temp_1 + c(3);
    delta_y = abs(y_temp_1(end) - y_temp_2(1));
end
x(6*n+1:7*n) = [x_temp_1 x_temp_2];
y(6*n+1:7*n) = [y_temp_1 y_temp_2];
%

```

Appendix C

MATLAB script for generating nacelle test cases

```
clear variables
close all
clc
```

Constants

```
R_air = 287;
gamma_air = 1.4;
```

The parameters used to specify the nacelle geometry:

Nacelle type:

```
nacelle_type = 'CST'; % NACA1 or CST
% Number of points in each curve:
n_points_curve = 1000;
```

Parameters for scaling

```
C(1) = 0.2; % r_hi = r_fan + C
            (1)*h_cowl
C(2) = 0.4; % f_max_nac, assumed
            constant
C(3) = 1.092; % f_if, assumed
            constant
C(4) = 1.2; %
            beta_rear_core_cowl = atan(C(4)*(r_max_core_cowl-
            r_outer_core_nozzle)/(l_core_cowl*(1-f_max_core_cowl)))
C(5) = 0.4; % l_inlet = C(5)*(
            l_nac-C(11)*r_fan)
C(6) = 0.86; % r_inlet_throat = (
            C(6)+2*(1-C(6))*atan(1/l_inlet)/pi)*r_fan
C(7) = 0.3;
C(8) = 0.2; % f_max_inlet = C(7)
            - C(8)*h_cowl/l_inlet
C(9) = 0.28; % r_spinner = C(9)*
            r_fan
C(10) = 1.5; % l_spinner = C(10)*
            r_spinner
C(11) = 0.4; % l_fan_system = C
            (11)*r_fan
```

```

C(12) = pi/2; % angle of fan inlet
           face (pi/2 => perpendiculat to axial direction)
C(13) = pi/2; % angle of fan exit
           face
C(14) = 0.7; % r_max_core_cowl =
           C(15)*r_fan
C(15) = 0.19; % r_IPC_tip = C(16)*
           sqrt(m_25R)
C(16) = 2.1; % l_core_cowl = C
           (17)*r_IPC_tip
C(17) = 0.7; % location of
           maximum radius of core cowl as part of the length of the
           bypass
C(18) = 0.64; %
           r_inner_core_nozzle = C(19)*r_outer_core_nozzle
C(19) = 1/sqrt(pi*(1-C(18)^2)); %
           r_outer_core_nozzle = C(20)*sqrt(A_8)
C(20) = 1.7; % l_rear_step = C
           (21)*r_inner_core_nozzle
C(21) = 0.6; % f_max_outer_bypass
           = C(22)
C(22) = 0.4; % r_max_outer_bypass
           = r_fan + C(23)*h_cowl
C(23) = 2; % beta_nac = atan(C
           (4)*(r_max-r_te)/(l_nac*(1-f_max_nac)))

```

Generating case geometries

```

line_spec = {'r' 'b' 'g' 'm'};
loop_nr = 1;
for test_case = [% enter number from nacelle test case table
]

```

Case parameters

```

CaseParameters = load('TestCases.txt');
FanDiameter = CaseParameters(test_case,6);
CowlLength_FanDiameter_ratio = CaseParameters(test_case
,8);
CowlThickness_FanDiameter_ratio = CaseParameters(
test_case,9);

```

Input from cycle design

```

CycleParameters = load('Cycles.txt');
cycle_case = CaseParameters(test_case,2);

```

```
CoolExitArea = CycleParameters(cycle_case,2);
HotExitArea = CycleParameters(cycle_case,3);

M_13 = CycleParameters(cycle_case,4);    % [-] Guess
      !!!!!!!!!!!
W_13 = CycleParameters(cycle_case,5);
T_13 = CycleParameters(cycle_case,6);
P_13 = CycleParameters(cycle_case,7);
m_13R = W_13*sqrt(T_13/288.15)/(P_13/101325);
A_13 = W_13*sqrt(R_air*T_13)/(P_13*sqrt(gamma_air) *
      M_13*(1 + (gamma_air-1)/2*M_13^2) ^(-(gamma_air+1)
      /(2*(gamma_air-1))));

W_25 = CycleParameters(cycle_case,8);
T_25 = CycleParameters(cycle_case,9);
P_25 = CycleParameters(cycle_case,10);
m_25R = W_25*sqrt(T_25/288.15)/(P_25/101325);
```

Scaling parameters

```
r_fan = FanDiameter/2;
l_nac = CowlLength_FanDiameter_ratio*FanDiameter;
h_cowl = CowlThickness_FanDiameter_ratio*FanDiameter;
r_hi = r_fan + C(1)*h_cowl;
r_max = r_fan + h_cowl;
f_max_nac = C(2);
f_if = C(3);
l_fan_system = C(11)*r_fan;
if test_case == 4                                % Shorter fan system for
    case 4 to have room for the bypass channel
    l_fan_system = l_fan_system/2;
end
l_inlet = C(5)*(l_nac-l_fan_system);
r_inlet_throat = (C(6)+(1-C(6))*atan(1/l_inlet)*2/pi)*
    r_fan; % So that r_inlet_throat -> r_fan when l_inlet
    -> 0
f_max_inlet = C(7) - C(8)*h_cowl/l_inlet;
r_spinner = C(9)*r_fan;
l_spinner = C(10)*r_spinner;
r_outer_fan_exit = r_fan;
alpha_fan_inlet_face = C(12);
alpha_fan_exit_face = C(13);
r_inner_fan_exit = sqrt(r_outer_fan_exit^2 - A_13/pi);
l_rear_nac = l_nac-l_inlet-l_fan_system;
r_max_core_cowl = C(14)*r_fan;
if test_case == 14                                % Higher maximum radius
    of core cowl for CFM56-7B
```

```
    r_max_core_cowl = r_max_core_cowl*8/7;
end
r_IPC_tip = C(15)*sqrt(m_25R);
l_core_cowl = C(16)*2*r_IPC_tip;
if test_case == 1 % Longer core cowl for
    case 1
        l_core_cowl = l_core_cowl*2.4/C(16);
    elseif test_case == 14 % and shorter for CFM56
        -7B
        l_core_cowl = l_core_cowl*1.65/C(16);
    end
f_max_core_cowl = C(17)*l_rear_nac/l_core_cowl;
if test_case == 4 % placing maximum radius exactly at
    exit for case 4
        f_max_core_cowl = l_rear_nac/l_core_cowl;
end
r_outer_core_nozzle = C(19)*sqrt(HotExitArea);
r_inner_core_nozzle = C(18)*r_outer_core_nozzle;
beta_rear_core_cowl = atan(C(4)*(r_max_core_cowl-
    r_outer_core_nozzle)/(l_core_cowl*(1-f_max_core_cowl)
));
l_rear_step = C(20)*r_inner_core_nozzle;
f_max_rear_nac = C(21);
r_max_rear_nac = r_fan + C(22)*h_cowl;
```

Centerbody/Core engine

```
center_input(1) = r_spinner;
center_input(2) = l_spinner;
center_input(3) = r_fan;
center_input(4) = alpha_fan_inlet_face;
center_input(5) = l_fan_system;
center_input(6) = alpha_fan_exit_face;
center_input(7) = r_outer_fan_exit;
center_input(8) = r_inner_fan_exit;
center_input(9) = r_max_core_cowl;
center_input(10) = l_core_cowl;
center_input(11) = f_max_core_cowl;
center_input(12) = beta_rear_core_cowl;
center_input(13) = r_outer_core_nozzle;
center_input(14) = r_inner_core_nozzle;
center_input(15) = l_rear_step;

[x_center, y_center] = CenterGeometryGenerator(
    center_input, n_points_curve);
x_center = x_center + l_inlet - x_center(2*
    n_points_curve);
```



```

index = 1;
while x_center(index) < l_nac
    index = index + 1;
end
r_te = sqrt(CoolExitArea/pi + y_center(index)^2);
beta_nac = atan(C(23)*(r_max-r_te)/(l_nac*(1-f_max_nac)))
);

```

Outside of nacelle

% A CST curve or a NACA 1-series cowl profile can be used.

```

if strcmp(nacelle_type, 'CST')
    g(1) = r_max/r_hi;
    g(2) = l_nac/r_hi;
    g(3) = f_max_nac;
    g(4) = f_if;
    g(5) = (r_te-r_hi)/l_nac;
    g(6) = beta_nac;
elseif strcmp(nacelle_type, 'NACA1')
    g(1) = f_max_nac;
    g(2) = 0; % assuming no cylindrical mid-body
    g(3) = 1-f_max_nac-g(2);
    g(4) = r_te/r_max;
    g(5) = (r_te-r_hi)/(r_max-r_hi);
end

```

```

[Phi, Xi] = ProfileGenerator(g, n_points_curve,
    nacelle_type);

```

```

x_nac = Phi*l_nac;
if strcmp(nacelle_type, 'CST')
    y_nac = r_hi + Xi*l_nac;
elseif strcmp(nacelle_type, 'NACA1')
    y_nac = r_hi + Xi*(r_max-r_hi);
end

```

Inlet

%A CST curve or a NACA 1-series cowl profile can be used.

```

if strcmp(nacelle_type, 'CST')
    g(1) = (2*r_hi-r_inlet_throat)/r_hi;
    g(2) = l_inlet/r_hi;
    g(3) = f_max_inlet;
    g(4) = f_if;
    g(5) = (r_hi-r_fan)/l_inlet;
    g(6) = 0; % assuming zero angle onto fan face

```

```

elseif strcmp(nacelle_type, 'NACA1')
    g(1) = f_max_inlet;
    g(2) = 0; % assuming no cylindrical mid-body
    g(3) = 1-f_max_inlet-g(2);
    g(4) = r_te/r_inlet_throat;
    g(5) = (r_hi-r_fan)/(r_hi-r_inlet_throat);
end

[Phi, Xi] = ProfileGenerator(g, n_points_curve,
    nacelle_type);

x_inlet = Phi*l_inlet;
if strcmp(nacelle_type, 'CST')
    y_inlet = r_hi - Xi*l_inlet;
elseif strcmp(nacelle_type, 'NACA1')
    y_inlet = r_hi - Xi*(r_hi-r_inlet_throat);
end

```

Nacelle inside

Two curves are combined to ensure that the flow is straight at the exit of the fan. It also gives a smoother bypass channel. (The same is also done in the centerbody function, so this way they are more similar.) A difference between the slope at the rear end of the outside and inside is introduced to avoid that the two curves cross and to give the nacelle a thicker end.

```

Delta_beta_nac = 0.8;
g(1) = r_max_rear_nac/r_fan;
g(2) = l_rear_nac/r_fan;
g(3) = f_max_rear_nac;
g(4) = 0; % assuming zero radius
g(5) = (r_te-r_fan)/l_rear_nac;
g(6) = Delta_beta_nac*beta_nac;
[Phi, Xi_1] = ProfileGenerator(g, n_points_curve);
g(1) = r_max_rear_nac/r_fan;
g(2) = l_rear_nac/r_fan;
g(3) = (1-f_max_rear_nac);
g(4) = 0; % assuming zero radius
g(5) = 0; % assuming no height difference between end
    points
g(6) = 0; % assuming zero radius/gradient on trailing
    edge
[~, Xi_2] = ProfileGenerator(g, n_points_curve);
Xi = [Xi_2(n_points_curve:-1:round((1-f_max_rear_nac)*
    n_points_curve)) Xi_1(round(f_max_rear_nac*
    n_points_curve)+2:n_points_curve)];

```

```
x_rear_nac = l_inlet + l_fan_system + Phi*l_rear_nac;  
y_rear_nac = r_fan + Xi*l_rear_nac;
```

Domain for CFD analysis

```
Domain_size = 50;  
Ref_size = FanDiameter;  
x_domain = [-Domain_size*Ref_size Domain_size*Ref_size+  
            x_center(end)];  
y_domain = [0.001 1.2*Domain_size*Ref_size];  
xn_domain = [1 2 2 2 2 1 1 1];  
yn_domain = [1 1 1 2 2 2 2 1];  
  
plot(x_domain(xn_domain),y_domain(yn_domain),'r')
```

Line for meshing

```
pi_mesh_line = linspace(pi,0);  
radius_mesh_line = 7*Ref_size;  
center_mesh_line = x_center(end)/2;  
x_mesh_line = radius_mesh_line*cos(pi_mesh_line) +  
              center_mesh_line;  
y_mesh_line = radius_mesh_line*sin(pi_mesh_line) +  
              y_domain(1);  
  
plot(x_mesh_line,y_mesh_line,'r')
```

File to ICEM

```
if test_case == 14  
    filename = ['CFM56_7B_' nacelle_type '  
              _parametric_geometry.txt'];  
else  
    filename = ['TestCase_' num2str(test_case) '_'  
              nacelle_type '_geometry.txt'];  
end  
% Nacelle  
if strcmp(nacelle_type,'CST')  
    dlmwrite(filename,[n_points_curve,3])  
    dlmwrite(filename,[x_nac,x_inlet,x_rear_nac];[y_nac,  
            y_inlet,y_rear_nac];zeros(size([x_nac,x_inlet,  
            x_rear_nac]))]*1e3,'-append')  
elseif strcmp(nacelle_type,'NACA1')  
    n_points_NACA1_curve = 168;  
    dlmwrite(filename,[n_points_NACA1_curve,2])
```

```

    dlmwrite(filename,[x_nac,x_inlet];[y_nac,y_inlet];zeros(
        size([x_nac,x_inlet]))]*1e3,'-append')
    dlmwrite(filename,[n_points_curve,1],'-append')
    dlmwrite(filename,[x_rear_nac];[y_rear_nac];zeros(size([
        x_rear_nac]))]*1e3,'-append')
end
% Centerbody
    dlmwrite(filename,[n_points_curve,length(x_center)/
        n_points_curve],'-append')
    dlmwrite(filename,[x_center;y_center;zeros(size(x_center)
        )]*1e3,'-append')
% Domain
    dlmwrite(filename,[2,length(x_domain(xn_domain))/2],'-
        append')
    dlmwrite(filename,[x_domain(xn_domain);y_domain(yn_domain
        )];zeros(size(x_domain(xn_domain)))]*1e3,'-append')
% Mesh line
    dlmwrite(filename,[length(x_mesh_line),1],'-append')
    dlmwrite(filename,[x_mesh_line;y_mesh_line;zeros(size(
        x_mesh_line))]*1e3,'-append')

end

```

Appendix D

MATLAB code for generating core geometries for BLI cases

```
function [x,y] = BLI_EngineGeometryGenerator(center_input,n)

% Fan
r_fuselage_fan_face = center_input(1);
r_fan = center_input(2);
alpha_fan_inlet_face = center_input(3);
l_fan_system_tip = center_input(4);
alpha_fan_exit_face = center_input(5);
r_outer_fan_exit = center_input(6);
r_inner_fan_exit = center_input(7);
% Core cowl
r_max_core_cowl = center_input(8);
l_core_cowl = center_input(9);
f_max_core_cowl = center_input(10);
beta_rear_core_cowl = center_input(11);
% Core nozzle
l_rear_step = center_input(12);
r_rear_step = center_input(13);

x(1:n) = linspace(0,(r_fan-r_fuselage_fan_face)/tan(
    alpha_fan_inlet_face),n);
x(n+1:2*n) = linspace(x(n),x(n) + l_fan_system_tip,n);
x(2*n+1:3*n) = linspace(x(2*n),x(2*n) - (r_outer_fan_exit-
    r_inner_fan_exit)/tan(alpha_fan_exit_face),n);
x(3*n+1:4*n) = linspace(x(3*n),x(3*n) + l_core_cowl+
    l_rear_step,n);

y(1:n) = linspace(r_fuselage_fan_face,r_fan,n); % fan inlet
    face
y(n+1:2*n) = linspace(y(n),y(n),n); % tip of fan system
y(2*n+1:3*n) = linspace(y(2*n),r_inner_fan_exit,n); % fan
    exit face
% Core cowl
g(1) = r_max_core_cowl/r_inner_fan_exit;
g(2) = (l_core_cowl+l_rear_step)/r_inner_fan_exit;
g(3) = f_max_core_cowl;
g(4) = 1;% assuming some radius of curvature (this end is
    not used) to improve curve
g(5) = (r_rear_step-r_inner_fan_exit)/l_core_cowl;
g(6) = beta_rear_core_cowl;% gradient on trailing edge
[~,Xi_1] = ProfileGenerator(g,n);
g(1) = r_max_core_cowl/r_inner_fan_exit;
```

```

g(2) = (l_core_cowl+l_rear_step)/r_inner_fan_exit;
g(3) = (1-f_max_core_cowl);
g(4) = 0;% assuming zero radius of curvature (this end is
    not used)
g(5) = 0;% assuming no hight difference of end points
g(6) = 0;% assuming zero angle out from fan
[~,Xi_2] = ProfileGenerator(g,n);
Xi = [Xi_2(n:-1:round((1-f_max_core_cowl)*n+1)) Xi_1(round(
    f_max_core_cowl*n+1):n)];

y(3*n+1:4*n) = y(3*n)+Xi*l_core_cowl;
%
% Exhaust plug/ end of aft core cowl
intersect_angle = beta_rear_core_cowl;%pi/4;
arc_angle = pi/2-intersect_angle;
pi_temp = linspace(arc_angle,0,n);
r = y(4*n);
delta_y = 1;
while delta_y > 1e-6
    r = r + 1e-8;
    y_temp = r*sin(pi_temp);
    delta_y = abs(y(4*n) - y_temp(1));
end
pi_temp = linspace(arc_angle,atan(1e-3/r),n);
x_temp = x(4*n) + r*(cos(pi_temp)-cos(pi_temp(1)));
y_temp = r*sin(pi_temp);

x(4*n+1:5*n) = x_temp;
y(4*n+1:5*n) = y_temp;
%
```

Appendix E

MATLAB script for generating geometries of BLI test cases

```
clear variables
close all
clc
```

Constants

```
R_air = 287;
gamma_air = 1.4;
```

The parameters used to specify the nacelle geometry:

```
%Nacelle type:
nacelle_type = 'CST'; % NACA1 or CST

% Number of points in each curve:
n_points_curve = 1000;

% Test Case:
test_case = 3;
```

Case parameters

```
CaseParameters = load('BLI_TestCases.txt');

FanDiameter = CaseParameters(test_case,6);
CowlLength_FanDiameter_ratio = CaseParameters(test_case,8);
CowlThickness_FanDiameter_ratio = CaseParameters(test_case,9);

FuselageDiameter = CaseParameters(test_case,10);
FuselageLength = CaseParameters(test_case,11);
```

Parameters for scaling

```
% Fan
C_fan(1) = 0.5; % r_inner_fan_inlet = C_fan()*r_fan
C_fan(2) = 0.4; % l_fan_system = C_fan()*r_fan
C_fan(3) = 85*pi/180;% angle of fan inlet face (pi/2 =>
    perpendicular to axial direction)
C_fan(4) = pi/2; % angle of fan exit face

% Nacelle
C_nac(1) = 0.4; % l_inlet = C_nac()*(l_nac-l_fan_system)
```

```

C_nac(2) = 0.25; % f_max_inlet, assumed constant
C_nac(3) = 1.4; % r_hi = sqrt(y_fuselage(index)^2 + (C_nac()
    *A_2)/pi)
C_nac(4) = 1.2; % r_inlet_throat = sqrt(y_fuselage(index)^2
    + (C_nac()*A_2)/pi)
C_nac(5) = 0.2; % f_max_nac, assumed constant
C_nac(6) = 3; % f_if, assumed constant
C_nac(7) = 0.6; % f_max_rear_nac, assumed constant
C_nac(8) = 0.95; % r_max_rear_nac = sqrt(y_engine(
    index)^2 + (C_nac()*A_2)/pi)
C_nac(9) = 2; % beta_nac = atan(C_nac()*(r_max-r_te)/(
    l_nac*(1-f_max_nac)))

```

% Core

```

C_core(1) = 3.1; % l_core_cowl = C_core()*r_fan
C_core(2) = 0.7; % location of maximum radius of core
    cowl as part of the length of the bypass
C_core(3) = 0.6; % r_max_core_cowl = C_core()*r_fan
C_core(4) = 0.1; % l_rear_step = C_core()*l_core_cowl
C_core(5) = 0.1; % r_rear_step = C_core()*r_fan
C_core(6) = 1.2; % beta_rear_core_cowl = atan(C_core
    ()*(r_max_core_cowl-r_rear_step)/(l_core_cowl*(1-
    f_max_core_cowl)))

```

% Fuselage

```

C_fus(1) = 0.8; % r_if_fuselage
C_fus(2) = 0.1495; % part of fuselage length of the
    front
C_fus(3) = 0.19; % part of fuselage length of the
    rear (changed to get sufficient height at rear door)

```

% Pressure ratio P_2_BLI/P_2_engine

```

if test_case == 1
    C_flow(1) = 0.87; % C_flow() = P_2_BLI/P_2_engine =
        P_13_BLI/P_13_engine
elseif test_case == 2
    C_flow(1) = 0.89; % 0.8808 from cfd (~0.887 earlier)
elseif test_case == 3
    C_flow(1) = 0.91; % approximated from increase in two
        previous cases (~0.903 from CFD)
end

```

Input from cycle design

```

CycleParameters = load('BLI_Cycles.txt');
cycle_case = CaseParameters(test_case,2);

```



```

BPR = CycleParameters(cycle_case,10);
CoolExitArea = (1+BPR)/BPR * CycleParameters(cycle_case,2);
W_13 = (1+BPR)/BPR * CycleParameters(cycle_case,7);

M_13 = CycleParameters(cycle_case,6);    % [-] Guess
!!!!!!!
T_13 = CycleParameters(cycle_case,8);
P_13 = C_flow(1) * CycleParameters(cycle_case,9);

```

Scaling parameters

```

% Fan
r_fan = FanDiameter/2;
l_fan_system_hub = C_fan(2)*r_fan;
% Core
l_core_cowl = C_core(1)*r_fan;
% Fuselage
l_fuselage = FuselageLength - (l_core_cowl+l_fan_system_hub)
;
r_max_fuselage = FuselageDiameter/2;

```

Scaling parameters

```

% Fan
r_inner_fan_inlet = C_fan(1)*r_fan;
A_2 = pi*(r_fan^2-r_inner_fan_inlet^2);
MassFlow_BLI = W_13*C_flow(1)*A_2/(pi*(1-0.28^2));
alpha_fan_inlet_face = C_fan(3);

A_18 = A_2/(pi*(1-0.28^2)) * CoolExitArea;
A_13 = MassFlow_BLI*sqrt(R_air*T_13) / (P_13*sqrt(gamma_air)
    *M_13*(1 + (gamma_air-1)/2*M_13^2) ^(-(gamma_air+1)/(2*(
    gamma_air-1)))));

```

```

% Nacelle
beta_inlet = alpha_fan_inlet_face - pi/2;

```

```

% Fuselage
r_fuselage_fan_face = r_inner_fan_inlet;
r_hi_fuselage = 0;
r_if_fuselage = C_fus(1);
l_fuselage_front = C_fus(2)*l_fuselage;
l_fuselage_rear = C_fus(3)*l_fuselage;
l_fuselage_cylinder = (1-C_fus(2)-C_fus(3))*l_fuselage;
beta_rear_fuselage = pi/2 - alpha_fan_inlet_face;

```

Fuselage Geometry

```

f_max_temp_front = 0.25;
l_temp_front = 1/f_max_temp_front*l_fuselage_front;
g(1) = 2*r_max_fuselage/r_max_fuselage;
g(2) = l_temp_front/r_max_fuselage;
g(3) = f_max_temp_front;
g(4) = r_if_fuselage*f_max_temp_front*l_temp_front/(
    r_max_fuselage-r_hi_fuselage)^2;
g(5) = 0;
g(6) = 0;
[Phi_front, Xi_front] = ProfileGenerator(g, n_points_curve,
    nacelle_type);

f_max_temp_rear = 0.4;
f_if_temp = 25; % f_max_temp_rear and f_if_temp are
    changed to obtain sufficient diameter at the rear door
l_temp_rear = 1/(1-f_max_temp_rear)*l_fuselage_rear;
g(1) = 2*r_max_fuselage/r_max_fuselage;
g(2) = l_temp_rear/r_max_fuselage;
g(3) = f_max_temp_rear;
g(4) = f_if_temp;
g(5) = (r_fuselage_fan_face-r_hi_fuselage)/l_temp_rear;
g(6) = beta_rear_fuselage; % assuming zero angle into fan
[Phi_rear, Xi_rear] = ProfileGenerator(g, n_points_curve,
    nacelle_type);

n_points_curve_front = round(n_points_curve*f_max_temp_front
    )+1;
n_points_curve_rear = (n_points_curve-round(n_points_curve*
    f_max_temp_rear));
x_fuselage(1:n_points_curve_front) = Phi_front(1:
    n_points_curve_front)*l_temp_front;
x_fuselage(end+1:end+n_points_curve) = linspace(Phi_front(
    n_points_curve_front)*l_temp_front, Phi_front(
    n_points_curve_front)*l_temp_front+l_fuselage_cylinder,
    n_points_curve);
x_fuselage(end+1:end+n_points_curve_rear) =
    l_fuselage_cylinder + Phi_front(n_points_curve_front)*
    l_temp_front + (Phi_rear((n_points_curve-
    n_points_curve_rear+1):n_points_curve)-Phi_rear(
    n_points_curve-n_points_curve_rear+1))*l_temp_rear;

l_fuselage = x_fuselage(end); % to avoid gaps in the
    geometry

y_fuselage(1:round(n_points_curve*f_max_temp_front+1)) =
    Xi_front(1:round(n_points_curve*f_max_temp_front+1))*

```

```

    l_temp_front;
y_fuselage(end+1:end+n_points_curve) = r_max_fuselage;
y_fuselage(end+1:end+(n_points_curve-round(n_points_curve*
    f_max_temp_rear)))) = Xi_rear(round(n_points_curve*
    f_max_temp_rear)+1:n_points_curve)*l_temp_rear;

y_fuselage(1) = 1e-3; % to get a 1 mm cylindrical center
    axis in mesh

```

Scaling parameters

```

% Fan
r_outer_fan_exit = r_fan;
alpha_fan_exit_face = C_fan(4);
r_inner_fan_exit = sqrt(r_outer_fan_exit^2 - A_13/pi);
delta_fan_system_inlet = (r_fan-r_fuselage_fan_face)/tan(
    alpha_fan_inlet_face);
delta_fan_system_exit = (r_fan-r_inner_fan_exit)/tan(pi-
    alpha_fan_exit_face);
l_fan_system_tip = l_fan_system_hub - (
    delta_fan_system_inlet+delta_fan_system_exit);

% Nacelle
l_nac = CowlLength_FanDiameter_ratio*FanDiameter;
h_cowl = CowlThickness_FanDiameter_ratio*FanDiameter;
l_inlet = C_nac(1)*(l_nac-l_fan_system_tip);
f_max_inlet = C_nac(2);

index = 1;
while x_fuselage(index) < l_fuselage - l_inlet
    index = index + 1;
end
r_hi = sqrt(y_fuselage(index)^2 + (C_nac(3)*A_2)/pi);

index = 1;
while x_fuselage(index) < l_fuselage - (1-f_max_inlet)*
    l_inlet
    index = index + 1;
end
r_inlet_throat = sqrt(y_fuselage(index)^2 + (C_nac(4)*A_2)/
    pi);

r_max = r_fan + h_cowl;
f_max_nac = C_nac(5);
f_if = C_nac(6);
l_rear_nac = l_nac-l_inlet-l_fan_system_tip;
f_max_rear_nac = C_nac(7);

```

```
% Core cowl parameters
f_max_core_cowl = C_core(2)*l_rear_nac/l_core_cowl;
r_max_core_cowl = C_core(3)*r_fan;
l_rear_step = C_core(4)*l_core_cowl;
r_rear_step = C_core(5)*r_fan;
beta_rear_core_cowl = atan(C_core(6)*(r_max_core_cowl-
    r_rear_step)/(l_core_cowl*(1-f_max_core_cowl)));
```

Centerbody

```
center_input(1) = r_fuselage_fan_face;
center_input(2) = r_fan;
center_input(3) = alpha_fan_inlet_face;
center_input(4) = l_fan_system_tip;
center_input(5) = alpha_fan_exit_face;
center_input(6) = r_outer_fan_exit;
center_input(7) = r_inner_fan_exit;
center_input(8) = r_max_core_cowl;
center_input(9) = l_core_cowl;
center_input(10) = f_max_core_cowl;
center_input(11) = beta_rear_core_cowl;
center_input(12) = l_rear_step;
center_input(13) = r_rear_step;

[x_engine,y_engine] = BLI_EngineGeometryGenerator(
    center_input,n_points_curve);
```

Scaling parameters

```
% Nacelle
index = 1;
while x_engine(index) < l_fan_system_hub + f_max_rear_nac*
    l_rear_nac
    index = index + 1;
end
r_max_rear_nac = sqrt(y_engine(index)^2 + (C_nac(8)*A_13)/pi
    );

index = 1;
while x_engine(index) < l_nac - l_inlet
    index = index + 1;
end
r_te = sqrt(A_18/pi + y_engine(index)^2);
beta_nac = atan(C_nac(9)*(r_max-r_te)/(l_nac*(1-f_max_nac)))
    ;
```

```
x_engine = x_engine + l_fuselage;
```

Nacelle outside

```
% A CST curve cowl profile is used.
g(1) = r_max/r_hi;
g(2) = l_nac/r_hi;
g(3) = f_max_nac;
g(4) = f_if;
g(5) = (r_te-r_hi)/l_nac;
g(6) = beta_nac;

[Phi,Xi] = ProfileGenerator(g,n_points_curve,nacelle_type);

x_nac = Phi*l_nac + l_fuselage + delta_fan_system_inlet -
    l_inlet;
y_nac = r_hi + Xi*l_nac;
```

Inlet

A CST curve cowl profile is used. The curve is created assuming no difference between r_{hi} and r_{te} , then the curve is rotated to fit to the fan radius. This means that the radius of curvature at the front will not match that of the external part of the nacelle. However, this is not done even if the curve is not rotated as the radius of curvature is scaled with length and height of the profile (which are not proportional for inlet and external nacelle).

```
alpha_hi_to_fan = atan(abs(r_hi-r_fan)/l_inlet);
delta_alpha = alpha_hi_to_fan + alpha_fan_inlet_face - pi/2;
g(1) = (2*r_hi-r_inlet_throat-f_max_inlet*l_inlet*sin(
    alpha_hi_to_fan))/r_hi;
g(2) = l_inlet/r_hi;
g(3) = f_max_inlet;
g(4) = f_if;
g(5) = 0;
g(6) = delta_alpha; % angle onto fan face

[Phi,Xi] = ProfileGenerator(g,n_points_curve,nacelle_type);

x_inlet = Phi*l_inlet + l_fuselage - l_inlet + (
    l_fan_system_hub-l_fan_system_tip);
y_inlet = r_hi - Xi*l_inlet - linspace(0,l_inlet,length(Xi))
    *tan(alpha_hi_to_fan);
```

Nacelle inside

Two curves are combined to ensure that the flow is straight at the exit of the fan. It also gives a smoother bypass channel. (The same is also done in the centerbody function, so this way they are more similar.) A difference between the slope at the rear end of the outside and inside is introduced to avoid that the two curves cross and to give the nacelle a thicker end.

```
Delta_beta_nac = 0.7;
g(1) = r_max_rear_nac/r_fan;
g(2) = l_rear_nac/r_fan;
g(3) = f_max_rear_nac;
g(4) = 0; % assuming zero radius
g(5) = (r_te-r_fan)/l_rear_nac;
g(6) = Delta_beta_nac*beta_nac;
[Phi,Xi_1] = ProfileGenerator(g,n_points_curve);
g(1) = r_max_rear_nac/r_fan;
g(2) = l_rear_nac/r_fan;
g(3) = (1-f_max_rear_nac);
g(4) = 0; % assuming zero radius
g(5) = 0; % assuming no height difference between end points
g(6) = 0; % assuming zero radius/gradient on trailing edge
[~,Xi_2] = ProfileGenerator(g,n_points_curve);
Xi = [Xi_2(n_points_curve:-1:round((1-f_max_rear_nac)*
    n_points_curve)) Xi_1(round(f_max_rear_nac*n_points_curve
    )+2:n_points_curve)];

x_rear_nac = Phi*l_rear_nac + l_fuselage + l_fan_system_hub;
y_rear_nac = r_fan + Xi*l_rear_nac;
```

Domain for CFD analysis

```
n_points_mesh = 10;
Domain_size_x = 60; % 50 in nacelle test cases
Domain_size_y = 70; % 50 in nacelle test cases
Ref_size = FanDiameter;
center_mesh = [l_fuselage 1e-3];

x_min = center_mesh(1) - Domain_size_x*Ref_size;
x_max = center_mesh(1) + Domain_size_x*Ref_size;
y_min = center_mesh(2);
y_max = Domain_size_y*Ref_size;

x_mesh_line = [linspace(x_min,x_max,n_points_mesh),linspace(
    x_max,x_max,n_points_mesh),linspace(x_max,x_min,
    n_points_mesh),linspace(x_min,x_min,n_points_mesh)];
```

```
y_mesh_line = [ linspace(y_min,y_min,n_points_mesh) , linspace (
    y_min,y_max,n_points_mesh) , linspace (y_max,y_max,
    n_points_mesh) , linspace (y_max,y_min,n_points_mesh) ];
```

File to ICEM

```
filename = [ 'BLI_Case_' num2str(test_case) '_' nacelle_type
    '_geometry.txt '];
scale = 1e3; % 1e3->mm, 1e6->um

% Nacelle
dlmwrite(filename,[n_points_curve,3])
dlmwrite(filename,[x_nac,x_inlet,x_rear_nac];[y_nac,y_inlet
    ,y_rear_nac];zeros(size([x_nac,x_inlet,x_rear_nac]))] '*
    scale','precision',10,'-append')

% Fuselage
l_fuselage_external = l_fuselage - l_inlet + (
    l_fan_system_hub-l_fan_system_tip);
index = 1;
while x_fuselage(index) < l_fuselage_external
    index = index + 1;
end
dlmwrite(filename,[length(x_fuselage(1:index)),1],'-append')
dlmwrite(filename,[x_fuselage(1:index);y_fuselage(1:index);
    zeros(size(x_fuselage(1:index)))] '*scale','precision
    ',10,'-append')
dlmwrite(filename,[length(x_fuselage(index:end)),1],'-append
    ')
dlmwrite(filename,[x_fuselage(index:end);y_fuselage(index:
    end);zeros(size(x_fuselage(index:end)))] '*scale','
    precision',10,'-append')

% Engine
dlmwrite(filename,[n_points_curve,3],'-append')
dlmwrite(filename,[x_engine(1:3*n_points_curve);y_engine
    (1:3*n_points_curve);zeros(size(x_engine(1:3*
    n_points_curve)))] '*scale','precision',10,'-append')

index = 1;
while x_engine(index) < l_fuselage_external + l_nac
    index = index + 1;
end
range_internal_core_cowl = 3*n_points_curve+1:index;
dlmwrite(filename,[length(range_internal_core_cowl),1],'-
    append')
dlmwrite(filename,[x_engine(range_internal_core_cowl);
```

```

        y_engine(range_internal_core_cowl); zeros(size(
        range_internal_core_cowl))]*scale,'precision',10,'-
        append')
range_external_core_cowl = index:4*n_points_curve;
dlmwrite(filename,[length(range_external_core_cowl),1],'-
        append')
dlmwrite(filename,[x_engine(range_external_core_cowl);
        y_engine(range_external_core_cowl); zeros(size(
        range_external_core_cowl))]*scale,'precision',10,'-
        append')

dlmwrite(filename,[n_points_curve,1],'-append')
dlmwrite(filename,[x_engine(4*n_points_curve:5*
        n_points_curve);y_engine(4*n_points_curve:5*
        n_points_curve); zeros(size(4*n_points_curve:5*
        n_points_curve))]*scale,'precision',10,'-append')

% Mesh line
dlmwrite(filename,[n_points_mesh,length(x_mesh_line)/
        n_points_mesh],'-append')
dlmwrite(filename,[x_mesh_line;y_mesh_line; zeros(size(
        x_mesh_line))]*scale,'precision',10,'-append')

```


Appendix F

Cycle data used in the project

F.1 FPR 1.4 cycle, 2m fan

F.1.1 Design input to GasTurb 9 for FPR 1.4

Altitude	m	10668	
Delta T from ISA	K	0	
Relative Humidity [%]		0	
Mach Number		0.8	
Basic Data Intake Pressure Ratio			0.998
Inner Fan Pressure Ratio		1.45	
Outer Fan Pressure Ratio		1.5	
IP Compressor Pressure Ratio		2.5	
Compr. Interduct Press. Ratio		1	
HP Compressor Pressure Ratio		15	
Bypass Duct Pressure Ratio		0.995	
Turb. Interd. Ref. Press. Ratio		1	
Design Bypass Ratio		12	
Burner Exit Temperature	K	1650.78	
Burner Design Efficiency		0.9995	
Burner Partload Constant		1.6	
Fuel Heating Value	MJ/kg	43.124	
Overboard Bleed	kg/s	0.453592	
Power Offtake	kW	50	
HP Spool Mechanical Efficiency		1	
Gear Ratio		1	
LP Spool Mechanical Efficiency		1	
Burner Pressure Ratio		0.95	
Turbine Exit Duct Press Ratio		0.995	
Core Nozzle Thrust Coeff		0.995	
Bypass Nozzle Thrust Coeff		0.998	
Design Core Nozzle Angle [°]		10	
Design Bypass Nozzle Angle [°]		2	
Air System Rel. Handling Bleed to Bypass			0
Rel. HP Leakage to Bypass		0	
Rel. Overboard Bleed W_Bld/W25		0	
Rel. Enthalpy of Overb. Bleed		1	
NGV Cooling Air W_C1_NGV/W25		0.05	
LPT Cooling Air W_C1/W25		0.02	
Rel. Enth. of LPT Cooling Air		0.7	
HPT Cooling Air W_C1/W25		0.06	
Rel. HP Leakage to LPT exit		0	

Rel. Fan Overb.Bleed W_Bld/W13	0	
Mass Flow Input Inlet Corr. Flow W2Rstd	kg/s	630.18
LPC Efficiency Isentr.Inner LPC Efficiency		0.88
Isentr.Outer LPC Efficiency	0.91	
LPC Design Nominal LP Spool Speed		4000
IPC Efficiency Isentr.IPC Efficiency		0.84
HPC Efficiency Isentr.HPC Efficiency		0.88
HPC Design Nominal HP Spool Speed		18000
HPT Efficiency Isentr.HPT Efficiency		0.96
LPT Efficiency Isentr.LPT Efficiency		0.96

F.1.2 GasTurb output at mid cruise condition for FPR 1.4

Station	W	T	P	WRstd	FN	=	21.21
amb		218.81	23.842		TSFC	=	13.0437
2	228.640	246.88	36.281	591.040	WF	=	0.2767
13	212.733	273.16	50.794		s NOx	=	0.6705
21	15.907	271.61	49.343	31.713	Core Eff	=	0.5622
24	15.907	359.84	122.354	14.721	Prop Eff	=	0.8361
25	15.907	359.84	122.354	14.721	BPR	=	13.3737
3	15.589	774.88	1572.157	1.648	P2/P1	=	0.9980
31	13.385	774.88	1572.157		P3/P2	=	43.33
4	13.662	1482.40	1491.618	2.105	P5/P2	=	1.0838
41	14.457	1446.30	1491.618	2.200	P16/P13	=	0.99500
43	14.457	1054.08	356.015		P16/P6	=	1.29148
44	15.412	1037.70	356.015		P16/P2	=	1.39300
45	15.412	1037.70	356.015	8.324	P6/P5	=	0.99517
49	15.412	612.87	39.323		A8	=	0.25837
5	15.730	613.69	39.323	59.150	A18	=	1.72798
8	15.730	613.69	39.133	59.438	XM8	=	0.87924
18	212.733	273.16	50.540	415.258	XM18	=	1.00000
					CD8	=	0.97357
Efficiencies:	isentr	polytr	RNI	P/P	CD18	=	0.99600
Outer LPC	0.9491	0.9515	0.464	1.400	PWX	=	50.00000
Inner LPC	0.9179	0.9214	0.464	1.360	V18/V8,id=		0.80517
IP Compressor	0.9103	0.9209	0.538	2.480	WBLD/W21	=	0.00000
HP Compressor	0.8869	0.9182	0.830	12.849	WBLD/W25	=	0.02852
Burner	0.9989			0.949	Loading %	=	162.11
HP Turbine	0.9465	0.9369	0.997	4.190	WHcl/W25	=	0.06000
LP Turbine	0.9542	0.9394	0.411	9.054	WLcl/W25	=	0.02000
HP Spool mech	1.0000	Nominal Spd		4000	ZWBld	=	0.45359
LP Spool mech	1.0000	Nominal Spd		18000			
Fuel	FHV	humidity	war2				
Generic	43.124	0.0	0.0000				

Iteration Variables:

HPC Spool Speed ZXNH (0.85...1.1) = 0.905368

Iteration Targets:

LPC Outer Pressure Ratio = 1.4

F.1.3 GasTurb output at cruise, thottled to FPR 1.3

Station	W	T	P	WRstd	FN	=	14.94
amb		218.81	23.842		TSFC	=	13.6710
2	212.693	246.88	36.281	549.816	WF	=	0.2042
13	199.753	267.14	47.166		s NOx	=	0.4786
21	12.940	265.90	46.077	27.334	Core Eff	=	0.5239
24	12.940	350.01	109.489	13.198	Prop Eff	=	0.8705
25	12.940	350.01	109.489	13.198	BPR	=	15.4371
3	12.681	728.66	1226.605	1.666	P2/P1	=	0.9980
31	10.804	728.66	1226.605		P3/P2	=	33.81
4	11.008	1387.74	1163.364	2.104	P5/P2	=	0.9236
41	11.655	1353.68	1163.364	2.200	P16/P13	=	0.99500
43	11.655	989.10	279.117		P16/P6	=	1.40631
44	12.432	973.54	279.117		P16/P2	=	1.29350
45	12.432	973.54	279.117	8.295	P6/P5	=	0.99586
49	12.432	585.30	33.510		A8	=	0.25837
5	12.690	585.97	33.510	54.720	A18	=	1.72798
8	12.690	585.97	33.371	54.947	XM8	=	0.71613
18	199.753	267.14	46.930	415.257	XM18	=	1.00000
					CD8	=	0.96198
Efficiencies:	isent	polytr	RNI	P/P	CD18	=	0.99599
Outer LPC	0.9500	0.9518	0.464	1.300	PWX	=	50.00000
Inner LPC	0.9186	0.9214	0.464	1.270	V18/V8,id	=	0.93433
IP Compressor	0.8855	0.8985	0.521	2.376	WBLD/W21	=	0.00000
HP Compressor	0.8820	0.9135	0.778	11.203	WBLD/W25	=	0.03505
Burner	0.9980			0.948	Loading %	=	238.61
HP Turbine	0.9328	0.9209	0.867	4.168	WHcl/W25	=	0.06000
LP Turbine	0.9484	0.9324	0.358	8.329	WLcl/W25	=	0.02000
HP Spool mech	1.0000	Nominal	Spd	4000	ZWBld	=	0.45359
LP Spool mech	1.0000	Nominal	Spd	18000			
Fuel	FHV	humidity	war2				
Generic	43.124	0.0	0.0000				

Composed Values:

1: FN = 14.940211

Iteration Variables:

HPC Spool Speed ZXNH (0.75...1.1) = 0.842553

F. Cycle data used in the project

Iteration Targets:

LPC Outer Pressure Ratio = 1.3

F.1.4 GasTurb output at cruise, thottled to FPR 1.2

Station	W	T	P	WRstd	FN	=	9.14
amb		218.81	23.842		TSFC	=	15.3643
2	196.103	246.88	36.281	506.930	WF	=	0.1404
13	186.359	260.78	43.538		s NOx	=	0.3219
21	9.744	259.90	42.812	21.902	Core Eff	=	0.4643
24	9.744	336.64	91.330	11.684	Prop Eff	=	0.9098
25	9.744	336.64	91.330	11.685	BPR	=	19.1257
3	9.549	677.30	880.992	1.684	P2/P1	=	0.9980
31	8.024	677.30	880.992		P3/P2	=	24.28
4	8.164	1297.76	835.850	2.100	P5/P2	=	0.8030
41	8.651	1265.14	835.850	2.198	P16/P13	=	0.99501
43	8.651	928.50	202.905		P16/P6	=	1.49130
44	9.236	913.42	202.905		P16/P2	=	1.19402
45	9.236	913.42	202.905	8.212	P6/P5	=	0.99704
49	9.236	573.54	29.135		A8	=	0.25837
5	9.431	573.62	29.135	46.276	A18	=	1.72798
8	9.431	573.62	29.049	46.413	XM8	=	0.54376
18	186.359	260.78	43.320	414.668	XM18	=	0.96414
					CD8	=	0.94944
Efficiencies:	isent	polytr	RNI	P/P	CD18	=	0.99566
Outer LPC	0.9508	0.9521	0.464	1.200	PWX	=	50.00000
Inner LPC	0.9195	0.9214	0.464	1.180	V18/V8,id	=	1.13891
IP Compressor	0.8179	0.8361	0.503	2.133	WBLD/W21	=	0.00000
HP Compressor	0.8709	0.9037	0.693	9.646	WBLD/W25	=	0.04655
Burner	0.9957			0.949	Loading %	=	381.55
HP Turbine	0.9176	0.9032	0.696	4.119	WHcl/W25	=	0.06000
LP Turbine	0.9397	0.9228	0.289	6.964	WLcl/W25	=	0.02000
HP Spool mech	1.0000	Nominal	Spd	4000	ZWBld	=	0.45359
LP Spool mech	1.0000	Nominal	Spd	18000			
Fuel	FHV	humidity	war2				
Generic	43.124	0.0	0.0000				

Composed Values:

1: FN = 9.140129

Iteration Variables:

HPC Spool Speed ZXNH (0.75...1.1) = 0.784043

Iteration Targets:

XXX

LPC Outer Pressure Ratio

= 1.2

F.1.5 GasTurb output at cruise, thottled to FPR 1.1

Station	W	T	P	WRstd	FN	=	3.92
amb		218.81	23.842		TSFC	=	22.5509
2	177.485	246.88	36.281	458.802	WF	=	0.0885
13	170.892	254.80	39.909		s NOx	=	0.2027
21	6.592	254.28	39.547	15.867	Core Eff	=	0.3667
24	6.592	327.51	75.632	9.416	Prop Eff	=	0.9545
25	6.592	327.51	75.632	9.416	BPR	=	25.9223
3	6.461	622.16	563.547	1.707	P2/P1	=	0.9980
31	5.282	622.16	563.547		P3/P2	=	15.53
4	5.370	1222.59	535.457	2.093	P5/P2	=	0.7232
41	5.700	1190.36	535.457	2.192	P16/P13	=	0.99512
43	5.700	886.93	135.635		P16/P6	=	1.51615
44	6.095	870.46	135.635		P16/P2	=	1.09464
45	6.095	870.46	135.635	7.914	P6/P5	=	0.99837
49	6.095	589.23	26.237		A8	=	0.25837
5	6.227	588.11	26.237	34.357	A18	=	1.72798
8	6.227	588.11	26.195	34.413	XM8	=	0.37306
18	170.892	254.80	39.715	409.997	XM18	=	0.88557
					CD8	=	0.93935
Efficiencies:	isent	polytr	RNI	P/P	CD18	=	0.99488
Outer LPC	0.8608	0.8627	0.464	1.100	PWX	=	50.00000
Inner LPC	0.8324	0.8344	0.464	1.090	V18/V8,id	=	1.48771
IP Compressor	0.7065	0.7318	0.482	1.912	WBLD/W21	=	0.00000
HP Compressor	0.8399	0.8769	0.601	7.451	WBLD/W25	=	0.06880
Burner	0.9894			0.950	Loading %	=	674.62
HP Turbine	0.8943	0.8767	0.493	3.948	WHcl/W25	=	0.06000
LP Turbine	0.9283	0.9120	0.209	5.170	WLcl/W25	=	0.02000
HP Spool mech	1.0000	Nominal	Spd	4000	ZWBld	=	0.45359
LP Spool mech	1.0000	Nominal	Spd	18000			
Fuel	FHV	humidity	war2				
Generic	43.124	0.0	0.0000				

Composed Values:

1: FN = 3.922452

Iteration Variables:

HPC Spool Speed ZXNH (0.71...1.1) = 0.713824

Iteration Targets:

LPC Outer Pressure Ratio = 1.1

F.1.6 GasTurb output at cruise, thottled to FPR 1.032

Station	W	T	P	WRstd	FN	=	0.76
amb		218.81	23.842		TSFC	=	76.8798
2	163.336	246.88	36.281	422.227	WF	=	0.0586
13	158.997	250.90	37.479		s NOx	=	0.1340
21	4.339	250.63	37.359	10.977	Core Eff	=	0.2493
24	4.339	327.55	65.761	7.129	Prop Eff	=	0.9891
25	4.339	327.55	65.761	7.129	BPR	=	36.6395
3	4.253	578.13	352.628	1.731	P2/P1	=	0.9980
31	3.322	578.13	352.628		P3/P2	=	9.72
4	3.380	1205.77	336.129	2.084	P5/P2	=	0.6863
41	3.597	1170.63	336.129	2.186	P16/P13	=	0.99529
43	3.597	897.71	92.906		P16/P6	=	1.49930
44	3.858	877.14	92.906		P16/P2	=	1.02813
45	3.858	877.14	92.906	7.340	P6/P5	=	0.99921
49	3.858	645.53	24.899		A8	=	0.25837
5	3.944	642.53	24.899	23.969	A18	=	1.72798
8	3.944	642.53	24.880	23.988	XM8	=	0.25078
18	158.997	250.90	37.302	403.010	XM18	=	0.82561
					CD8	=	0.93424
Efficiencies:	isent	polytr	RNI	P/P	CD18	=	0.99410
Outer LPC	0.5721	0.5741	0.464	1.033	PWX	=	50.00000
Inner LPC	0.5533	0.5551	0.464	1.030	V18/V8,id	=	1.96779
IP Compressor	0.5711	0.6035	0.466	1.760	WBLD/W21	=	0.00000
HP Compressor	0.7889	0.8310	0.523	5.362	WBLD/W25	=	0.10453
Burner	0.9754			0.953	Loading %	=	1142.59
HP Turbine	0.8658	0.8458	0.318	3.618	WHcl/W25	=	0.06000
LP Turbine	0.9158	0.9012	0.142	3.731	WLcl/W25	=	0.02000
HP Spool mech	1.0000	Nominal	Spd	4000	ZWBld	=	0.45359
LP Spool mech	1.0000	Nominal	Spd	18000			
Fuel	FHV	humidity	war2				
Generic	43.124	0.0	0.0000				

Composed Values:

1: FN = 0.761913

Iteration Variables:

HPC Spool Speed ZXNH (0.63...1.1) = 0.640081

Iteration Targets:

LPC Outer Pressure Ratio = 1.032

F.1.7 GasTurb output at low speed cruise, $M = 0.75$

Station	W	T	P	WRstd	FN	=	20.97
amb		218.81	23.842		TSFC	=	12.5743
2	219.341	243.48	34.565	591.040	WF	=	0.2637
13	204.081	269.40	48.391		s NOx	=	0.6277
21	15.260	267.87	47.009	31.713	Core Eff	=	0.5566
24	15.260	354.85	116.454	14.734	Prop Eff	=	0.8227
25	15.260	354.85	116.454	14.734	BPR	=	13.3737
3	14.955	765.69	1500.411	1.646	P2/P1	=	0.9980
31	12.823	765.69	1500.411		P3/P2	=	43.41
4	13.086	1471.46	1423.886	2.104	P5/P2	=	1.0990
41	13.849	1435.44	1423.886	2.200	P16/P13	=	0.99500
43	13.849	1046.45	340.101		P16/P6	=	1.27360
44	14.765	1029.98	340.101		P16/P2	=	1.39300
45	14.765	1029.98	340.101	8.317	P6/P5	=	0.99527
49	14.765	609.95	37.986		A8	=	0.25837
5	15.070	610.67	37.986	58.520	A18	=	1.72798
8	15.070	610.67	37.806	58.798	XM8	=	0.84613
18	204.081	269.40	48.149	415.258	XM18	=	1.00000
					CD8	=	0.97141
Efficiencies:	isent	polytr	RNI	P/P	CD18	=	0.99600
Outer LPC	0.9491	0.9515	0.453	1.400	PWX	=	50.00000
Inner LPC	0.9179	0.9214	0.453	1.360	V18/V8,id	=	0.80470
IP Compressor	0.9097	0.9204	0.525	2.477	WBLD/W21	=	0.00000
HP Compressor	0.8864	0.9179	0.808	12.884	WBLD/W25	=	0.02972
Burner	0.9988			0.949	Loading %	=	174.17
HP Turbine	0.9451	0.9353	0.964	4.187	WHcl/W25	=	0.06000
LP Turbine	0.9533	0.9382	0.397	8.953	WLcl/W25	=	0.02000
HP Spool mech	1.0000	Nominal	Spd	4000	ZWBld	=	0.45359
LP Spool mech	1.0000	Nominal	Spd	18000			
Fuel	FHV	humidity	war2				
Generic	43.124	0.0	0.0000				

Composed Values:

1: FN = 20.973152

Iteration Variables:

HPC Spool Speed ZXNH (0.85...1.1) = 0.89977

Iteration Targets:

LPC Outer Pressure Ratio = 1.4

F.1.8 GasTurb output at high speed cruise, $M = 0.85$

Station	W	T	P	WRstd	FN	=	21.57
amb		218.81	23.842		TSFC	=	13.5194
2	238.818	250.49	38.174	591.023	WF	=	0.2916
13	222.207	277.16	53.443		s NOx	=	0.7193
21	16.610	275.59	51.917	31.704	Core Eff	=	0.5677
24	16.610	365.24	128.987	14.690	Prop Eff	=	0.8478
25	16.610	365.24	128.987	14.690	BPR	=	13.3777
3	16.278	784.71	1651.800	1.648	P2/P1	=	0.9980
31	13.997	784.71	1651.800		P3/P2	=	43.27
4	14.289	1495.45	1566.909	2.105	P5/P2	=	1.0715
41	15.120	1459.19	1566.909	2.200	P16/P13	=	0.99500
43	15.120	1063.66	373.691		P16/P6	=	1.30643
44	16.116	1047.29	373.691		P16/P2	=	1.39300
45	16.116	1047.29	373.691	8.331	P6/P5	=	0.99508
49	16.116	617.30	40.905		A8	=	0.25837
5	16.448	618.19	40.905	59.678	A18	=	1.72798
8	16.448	618.19	40.704	59.973	XM8	=	0.91591
18	222.207	277.16	53.176	415.256	XM18	=	1.00000
					CD8	=	0.97571
Efficiencies:	isent	polytr	RNI	P/P	CD18	=	0.99600
Outer LPC	0.9492	0.9515	0.477	1.400	PWX	=	50.00000
Inner LPC	0.9179	0.9214	0.477	1.360	V18/V8,id	=	0.80290
IP Compressor	0.9109	0.9215	0.552	2.485	WBLD/W21	=	0.00000
HP Compressor	0.8875	0.9185	0.853	12.806	WBLD/W25	=	0.02731
Burner	0.9990			0.949	Loading %	=	150.09
HP Turbine	0.9469	0.9375	1.032	4.193	WHcl/W25	=	0.06000
LP Turbine	0.9551	0.9405	0.425	9.136	WLcl/W25	=	0.02000
HP Spool mech	1.0000	Nominal	Spd	4000	ZWBld	=	0.45359
LP Spool mech	1.0000	Nominal	Spd	18000			
Fuel	FHV	humidity	war2				
Generic	43.124	0.0	0.0000				

Composed Values:

1: FN = 21.566973

Iteration Variables:

HPC Spool Speed ZXNH (0.85...1.1) = 0.910833

Iteration Targets:

LPC Outer Pressure Ratio = 1.4

F.1.9 GasTurb output at max take off, end-of-runway

Station	W	T	P	WRstd	FN	=	113.88
amb		288.15	101.325		TSFC	=	8.6082
2	602.638	291.76	105.616	581.759	WF	=	0.9803
13	557.802	326.04	152.520		s NOx	=	2.2968
21	44.836	324.05	147.829	32.589	Core Eff	=	0.5340
24	44.836	419.96	338.780	16.189	Prop Eff	=	0.4741
25	44.836	419.96	338.780	16.189	BPR	=	12.4410
3	43.939	925.08	4948.379	1.612	P2/P1	=	0.9980
31	38.554	925.08	4948.379		P3/P2	=	46.85
4	39.534	1749.40	4694.951	2.102	P5/P2	=	1.3163
41	41.776	1708.72	4694.951	2.195	P16/P13	=	0.99545
43	41.776	1250.69	1118.028		P16/P6	=	1.09641
44	44.466	1232.18	1118.028		P16/P2	=	1.43752
45	44.466	1232.18	1118.028	8.333	P6/P5	=	0.99605
49	44.466	753.39	139.024		A8	=	0.25837
5	45.363	753.89	139.024	53.477	A18	=	1.72798
8	45.363	753.89	138.475	53.689	XM8	=	0.69398
18	557.802	326.04	151.826	395.983	XM18	=	0.78264
					CD8	=	0.95994
Efficiencies:	isent	polytr	RNI	P/P	CD18	=	0.99348
Outer LPC	0.9401	0.9431	1.021	1.444	PWX	=	50.00000
Inner LPC	0.9091	0.9133	1.021	1.400	V18/V8,id	=	0.74177
IP Compressor	0.8975	0.9086	1.197	2.292	WBLD/W21	=	0.00000
HP Compressor	0.8859	0.9181	1.768	14.606	WBLD/W25	=	0.01012
Burner	0.9999			0.949	Loading %	=	35.93
HP Turbine	0.9607	0.9538	2.381	4.199	WHcl/W25	=	0.06000
LP Turbine	0.9725	0.9643	0.973	8.042	WLcl/W25	=	0.02000
HP Spool mech	1.0000	Nominal	Spd	4000	ZWBld	=	0.45359
LP Spool mech	1.0000	Nominal	Spd	18000			
Fuel	FHV	humidity	war2				
Generic	43.124	0.0	0.0000				
Iteration Variables:							
HPC Spool Speed ZXNH (0.85...1.1)						=	1.03869
Iteration Targets:							
Net Thrust				kN		=	113.876

F.2 FPR 1.3 cycle, 2m fan

F.2.1 Design input to GasTurb 9 for FPR 1.3

Altitude	m	10668	
Delta T from ISA	K	0	
Relative Humidity [%]		0	
Mach Number		0.8	
Intake Pressure Ratio		0.998	
Inner Fan Pressure Ratio		1.34	
Outer Fan Pressure Ratio		1.38	
IP Compressor Pressure Ratio		2.7	
Compr. Interduct Press. Ratio		1	
HP Compressor Pressure Ratio		15	
Bypass Duct Pressure Ratio		0.995	
Turb. Interd. Ref. Press. Ratio		1	
Design Bypass Ratio		15.5	
Burner Exit Temperature	K	1650.78	
Burner Design Efficiency		0.9995	
Burner Partload Constant		1.6	
Fuel Heating Value	MJ/kg	43.124	
Overboard Bleed	kg/s	0.453592	
Power Offtake	kW	50	
HP Spool Mechanical Efficiency		1	
Gear Ratio		1	
LP Spool Mechanical Efficiency		1	
Burner Pressure Ratio		0.95	
Turbine Exit Duct Press Ratio		0.995	
Core Nozzle Thrust Coeff		0.995	
Bypass Nozzle Thrust Coeff		0.998	
Design Core Nozzle Angle [°]		10	
Design Bypass Nozzle Angle [°]		2	
Air System Rel. Handling Bleed to Bypass			0
Rel. HP Leakage to Bypass		0	
Rel. Overboard Bleed W_Bld/W25		0	
Rel. Enthalpy of Overb. Bleed		1	
NGV Cooling Air W_C1_NGV/W25		0.05	
LPT Cooling Air W_C1/W25		0.02	
Rel. Enth. of LPT Cooling Air		0.7	
HPT Cooling Air W_C1/W25		0.06	
Rel. HP Leakage to LPT exit		0	
Rel. Fan Overb.Bleed W_Bld/W13		0	
Mass Flow Input Inlet Corr. Flow W2Rstd	kg/s		630.18
LPC Efficiency Isentr.Inner LPC Efficiency			0.88
Isentr.Outer LPC Efficiency		0.91	

LPC Design Nominal LP Spool Speed	4000
IPC Efficiency Isentr.IPC Efficiency	0.84
HPC Efficiency Isentr.HPC Efficiency	0.88
HPC Design Nominal HP Spool Speed	18000
HPT Efficiency Isentr.HPT Efficiency	0.96
LPT Efficiency Isentr.LPT Efficiency	0.96

F.2.2 GasTurb output at mid cruise condition for FPR 1.3

Station	W	T	P	WRstd	FN	=	16.85
amb		218.81	23.842		TSFC	=	12.9218
2	230.733	246.88	36.281	596.450	WF	=	0.2177
13	218.078	267.21	47.166		s NOx	=	0.6769
21	12.655	265.87	46.020	26.765	Core Eff	=	0.5546
24	12.655	363.58	126.585	11.379	Prop Eff	=	0.8662
25	12.655	363.58	126.585	11.379	BPR	=	17.2321
3	12.402	776.22	1582.459	1.303	P2/P1	=	0.9980
31	10.557	776.22	1582.459		P3/P2	=	43.62
4	10.774	1482.07	1501.190	1.649	P5/P2	=	1.0293
41	11.407	1445.75	1501.190	1.725	P16/P13	=	0.99500
43	11.407	1051.51	353.863		P16/P6	=	1.26252
44	12.166	1035.23	353.863		P16/P2	=	1.29350
45	12.166	1035.23	353.863	6.603	P6/P5	=	0.99532
49	12.166	604.10	37.346		A8	=	0.21693
5	12.420	605.14	37.346	48.831	A18	=	1.88679
8	12.420	605.14	37.172	49.060	XM8	=	0.82941
18	218.078	267.21	46.930	453.418	XM18	=	1.00000
					CD8	=	0.97028
Efficiencies:	isent	polytr	RNI	P/P	CD18	=	0.99599
Outer LPC	0.9463	0.9482	0.464	1.300	PWX	=	50.00000
Inner LPC	0.9151	0.9179	0.464	1.268	V18/V8,id	=	0.80577
IP Compressor	0.9105	0.9222	0.520	2.751	WBLD/W21	=	0.00000
HP Compressor	0.8873	0.9182	0.843	12.501	WBLD/W25	=	0.03584
Burner	0.9989			0.949	Loading %	=	160.23
HP Turbine	0.9446	0.9346	1.004	4.242	WHcl/W25	=	0.06000
LP Turbine	0.9552	0.9402	0.410	9.475	WLcl/W25	=	0.02000
HP Spool mech	1.0000	Nominal Spd		4000	ZWBld	=	0.45359
LP Spool mech	1.0000	Nominal Spd		18000			
Fuel	FHV	humidity	war2				
Generic	43.124	0.0	0.0000				
1: FN	=	16.848623					
2: FG	=	71.605026					

Iteration Variables:

F. Cycle data used in the project

HPC Spool Speed ZXNH (0.85...1.1) = 0.898778

Iteration Targets:

LPC Outer Pressure Ratio = 1.3

Appendix G

Table used to evaluate discharge and thrust coefficient

Table G.1: Nozzle quantities, and thrust and drag coefficients for nacelle test cases

Case	Nozzle	Total temperature	Total pressure	Mass flow	Cp
1	Core	613.544	40990.2	15.73	1041.91
	Bypass	273.159	51490	212.722	1002.72
2.0	Core	613.368	40420.3	15.73	1041.21
	Bypass	273.159	51135.1	212.741	1002.75
3.0	Core	613.689	39468	15.73	1039.82
	Bypass	273.16	50818.8	212.74	1002.77
4	Core	613.474	39015.2	15.73	1038.96
	Bypass	273.256	51027.7	212.738	1002.71
5	Core	605.053	38424.9	12.42	1040.47
	Bypass	267.215	47270.7	218.086	1002.66
6	Core	613.697	39549.3	15.73	1039.94
	Bypass	273.161	51171.9	212.731	1002.81
7	Core	613.697	39314.6	15.73	1039.52
	Bypass	273.16	50516.1	212.735	1002.71
2.1	Core	610.351	38879.5	15.07	1040.96
	Bypass	269.396	48831.5	204.132	1002.71
2.2	Core	617.873	42436.6	16.448	1042.13
	Bypass	277.159	53793.7	222.208	1002.8
TO 1	Core	753.765	138941	45.363	1075.43
	Bypass	326.046	155447	557.811	1004.42
TO 2	Core	753.466	137897	45.363	1075.07
	Bypass	326.024	154646	558.283	1004.44
TO 3	Core	753.889	135685	45.363	1074.43
	Bypass	326.057	154157	557.819	1004.48
TO 4	Core	753.545	134321	45.363	1073.88
	Bypass	326.052	151242	557.815	1004.2
3.1	Core	585.954	34136.8	12.69	1038.55
	Bypass	267.144	47465.1	199.759	1002.72
3.2	Core	573.514	30426.6	9.431	1039.8
	Bypass	260.786	44190.9	186.364	1002.67
3.3	Core	587.429	27896.8	6.227	1045.57
	Bypass	254.805	40813.1	170.904	1002.65
3.4	Core	640.182	26597.6	3.944	1059.23
	Bypass	250.904	38483.6	159.004	1002.64
2.B	Core	613.378	40409	15.73	1041.2
	Bypass	273.159	51123.9	212.74	1002.74

G. Table used to evaluate discharge and thrust coefficient

Case	Nozzle	Actual area	Actual thrust	Kappa	Critical PR	state
1	Core	0.25836	6710.68	1.38017777	1.880959968	unchoked
	Bypass	1.72805	68662.31	1.400994802	1.893529517	choked
2.0	Core	0.25836	6600.89	1.380530621	1.881173139	unchoked
	Bypass	1.72688	68798.68	1.400977995	1.893519374	choked
3.0	Core	0.25836	6429.88	1.38123323	1.8815976	unchoked
	Bypass	1.72777	68965.5	1.400966791	1.893512612	choked
4	Core	0.25836	6346.618	1.381669238	1.881860994	unchoked
	Bypass	1.72814	69235.61	1.401000405	1.893532898	choked
5	Core	0.21693	4938.51	1.380904349	1.881398918	unchoked
	Bypass	1.88681	66690.02	1.401028421	1.893549805	choked
6	Core	0.25836	6446.449	1.381172471	1.881560895	unchoked
	Bypass	1.72772	69202.6	1.400944385	1.893499091	choked
7	Core	0.25836	6404.568	1.381385212	1.881689414	unchoked
	Bypass	1.72774	68825.16	1.401000405	1.893532898	choked
2.1	Core	0.25836	6081.021	1.380656799	1.881249367	unchoked
	Bypass	1.72688	63726.86	1.401000405	1.893532898	choked
2.2	Core	0.25836	7235.28	1.380067008	1.880893052	unchoked
	Bypass	1.72688	74519.9	1.400949986	1.893502471	choked
TO 1	Core	0.25836	16489.04	1.364014561	1.871190836	unchoked
	Bypass	1.72805	149720.78	1.400044604	1.892956078	unchoked
TO 2	Core	0.25836	16270.912	1.364180847	1.871291384	unchoked
	Bypass	1.72688	149860.41	1.400033452	1.892949348	unchoked
TO 3	Core	0.25836	15838.328	1.364476842	1.87147036	unchoked
	Bypass	1.72777	150418.63	1.40001115	1.892935888	unchoked
TO 4	Core	0.25836	15562.252	1.364731598	1.871624397	unchoked
	Bypass	1.72814	147772	1.400167317	1.893030136	unchoked
3.1	Core	0.25836	4332.246	1.381877453	1.881986775	unchoked
	Bypass	1.72777	61383.51	1.400994802	1.893529517	choked
3.2	Core	0.25836	2683.839	1.381243358	1.881603719	unchoked
	Bypass	1.72777	53837.88	1.401022818	1.893546423	unchoked
3.3	Core	0.25836	1513.313	1.378343462	1.879851727	unchoked
	Bypass	1.72777	45812.71	1.401034025	1.893553187	unchoked
3.4	Core	0.25836	921.29	1.371650933	1.875807355	unchoked
	Bypass	1.72777	40091.21	1.401039629	1.893556569	unchoked
2.B	Core	0.25836	6599.17	1.380535667	1.881176187	unchoked
	Bypass	1.72688	68785.43	1.400983597	1.893522755	choked

G. Table used to evaluate discharge and thrust coefficient

Case	Nozzle	Static temperature	Velocity	Static pressure	Density
1	Core	528.4704507	421.0438974	23842	0.157195489
	Bypass	227.5381852	302.47282	27192.60489	0.416403744
2.0	Core	530.3084705	415.8904008	23842	0.156650658
	Bypass	227.539778	302.4720644	27005.32179	0.41353296
3.0	Core	533.9852105	407.1304322	23842	0.155572044
	Bypass	227.5416728	302.4721143	26838.37418	0.410973066
4	Core	535.4406567	402.6748622	23842	0.155149165
	Bypass	227.6184539	302.5267719	26948.40953	0.412518826
5	Core	530.4209769	394.0872521	23842	0.156617431
	Bypass	222.5837875	299.165277	24964.06478	0.390786791
6	Core	533.6975707	407.9083389	23842	0.155655891
	Bypass	227.5446293	302.4716605	27025.04599	0.413826174
7	Core	534.5451472	405.6597934	23842	0.155409082
	Bypass	227.5384872	302.4736256	26678.22675	0.408526465
2.1	Core	533.3662783	400.3448912	23842	0.155752574
	Bypass	224.4031275	300.3824336	25788.567	0.400420596
2.2	Core	527.1573449	434.8275651	23842	0.15758705
	Bypass	230.8744469	304.6773699	28409.62757	0.428753596
TO 1	Core	692.858272	361.9417702	101325	0.50955411
	Bypass	288.5161657	274.5750031	101325	1.223670707
TO 2	Core	693.9597754	357.6963987	101325	0.508745309
	Bypass	288.9235793	273.0023682	101325	1.221945198
TO 3	Core	697.3209751	348.6499188	101325	0.506293075
	Bypass	289.2158058	272.052358	101325	1.220710533
TO 4	Core	698.8594796	342.7117932	101325	0.505178495
	Bypass	290.7839043	266.1436519	101325	1.214127657
3.1	Core	530.6235798	339.0085778	23842	0.156557631
	Bypass	222.527762	299.124035	25066.99768	0.392496894
3.2	Core	536.1806181	278.6368622	23842	0.15493505
	Bypass	218.5626298	290.9849019	23842	0.380088631
3.3	Core	562.6416197	227.670557	23842	0.147648464
	Bypass	218.4655196	269.9473283	23842	0.380257584
3.4	Core	621.4888249	198.9993558	23842	0.133668004
	Bypass	218.770089	253.8454038	23842	0.379728194
2.B	Core	530.3572485	415.7913094	23842	0.15663625
	Bypass	227.5392471	302.4723162	26999.35867	0.413442611

G. Table used to evaluate discharge and thrust coefficient

Case	Nozzle	Ideal area	Ideal thrust	Thrust coefficient	Discharge coefficient
1	Core	0.237662832	6623.020507	1.013235576	0.919890199
	Bypass	1.68892913	70001.55743	0.98086832	0.977361263
2.0	Core	0.241444659	6541.956004	1.00900862	0.93452802
	Bypass	1.700809983	69728.41871	0.986666287	0.9849034
3.0	Core	0.248349676	6404.161699	1.004015873	0.961254359
	Bypass	1.711395764	69475.89966	0.992653573	0.990522908
4	Core	0.251782048	6334.075583	1.00198015	0.974539588
	Bypass	1.704658882	69654.30901	0.9939889	0.986412491
5	Core	0.201228326	4894.563671	1.0089786	0.927618705
	Bypass	1.865420417	67336.88116	0.990393657	0.988663626
6	Core	0.247742535	6416.398171	1.004683442	0.95890438
	Bypass	1.699527263	69754.77224	0.992084094	0.983682114
7	Core	0.249511382	6381.028551	1.003688974	0.965750821
	Bypass	1.721595978	69229.56329	0.994158517	0.996443896
2.1	Core	0.241681679	6033.19751	1.007926724	0.93544542
	Bypass	1.697149697	64621.28253	0.98615901	0.982783805
2.2	Core	0.240035516	7152.04379	1.011638101	0.929073834
	Bypass	1.701028996	75471.41596	0.987392366	0.985030226
TO 1	Core	0.245964683	16418.76452	1.004280193	0.952023079
	Bypass	1.660204219	153160.9571	0.977538812	0.960738531
TO 2	Core	0.249279625	16226.18174	1.002756672	0.964853789
	Bypass	1.673540628	152412.5811	0.983254853	0.969112288
TO 3	Core	0.256986443	15815.80627	1.001424001	0.994683553
	Bypass	1.679686053	151755.9743	0.991187534	0.972169938
TO 4	Core	0.262016031	15546.43507	1.001017399	1.014150917
	Bypass	1.72627398	148458.9212	0.995372988	0.998920215
3.1	Core	0.239098413	4302.018852	1.00702627	0.925446713
	Bypass	1.701448549	61836.98863	0.992666547	0.984765651
3.2	Core	0.218458777	2627.824248	1.021316019	0.845559595
	Bypass	1.685026318	54229.11025	0.992785604	0.97526078
3.3	Core	0.185243536	1417.704558	1.067438904	0.716997741
	Bypass	1.664927432	46135.0782	0.993012514	0.963627932
3.4	Core	0.148271531	784.8534594	1.173836961	0.573895074
	Bypass	1.649551588	40362.43458	0.993280272	0.954728689
2.B	Core	0.241524414	6540.397297	1.008986106	0.934836716
	Bypass	1.701172243	69719.17148	0.986607106	0.985113177

G. Table used to evaluate discharge and thrust coefficient

Case	Nozzle	Cycle data discharge coeff.	Difference in discharge coeff. [%]
1	Core	0.97357	-5.84
	Bypass	0.996	-1.91
2.0	Core	0.97357	-4.18
	Bypass	0.996	-1.13
3.0	Core	0.97357	-1.28
	Bypass	0.996	-0.55
4	Core	0.97357	0.10
	Bypass	0.996	-0.97
5	Core	0.97028	-4.60
	Bypass	0.99599	-0.74
6	Core	0.97357	-1.53
	Bypass	0.996	-1.25
7	Core	0.97357	-0.81
	Bypass	0.996	0.04
2.1	Core	0.97141	-3.84
	Bypass	0.996	-1.34
2.2	Core	0.97591	-5.04
	Bypass	0.996	-1.11
TO 1	Core	0.95994	-0.83
	Bypass	0.99348	-3.41
TO 2	Core	0.95994	0.51
	Bypass	0.99348	-2.51
TO 3	Core	0.95994	3.49
	Bypass	0.99348	-2.19
TO 4	Core	0.95994	5.35
	Bypass	0.99348	0.54
3.1	Core	0.96198	-3.95
	Bypass	0.99599	-1.14
3.2	Core	0.94944	-12.29
	Bypass	0.99566	-2.09
3.3	Core	0.93935	-31.01
	Bypass	0.99488	-3.24
3.4	Core	0.93424	-62.79
	Bypass	0.9941	-4.12
2.B	Core	0.97357	-4.14
	Bypass	0.996	-1.11

Table G.2: Nozzle quantities, and thrust and drag coefficients for BLI test cases

Case	Total temperature	Total pressure	Mass flow	Cp
BLI 1	267.177	41849.1	163.617	1002.81
BLI 2	267.211	42547.5	211.509	1002.79
BLI 3	267.208	43329.2	266.948	1002.77

G. Table used to evaluate discharge and thrust coefficient

Case	Actual area	Actual thrust	Kappa	Critical PR	state
BLI 1	1.64983	45671.79	1.400944385	1.893499091	unchoked
BLI 2	2.08802	59963.09	1.400955588	1.893505851	unchoked
BLI 3	2.57789	76708.42	1.400966791	1.893512612	unchoked

Case	Static temperature	Velocity	Static pressure	Density
BLI 1	227.4411306	282.303125	23842	0.365251309
BLI 2	226.3943996	286.1135393	23842	0.366940043
BLI 3	225.214545	290.206054	23842	0.36886237

Case	Ideal area	Ideal thrust	Thrust coefficient	Discharge coefficient
BLI 1	1.586795494	46189.5904	0.988789673	0.961793332
BLI 2	2.014630176	60515.58859	0.990870144	0.964851953
BLI 3	2.493766874	77469.92569	0.990170306	0.967367449

Appendix H

Table of drag and thrust components

Table H.1: Components of thrust and drag for nacelle test cases

Case	Pre entry drag	Fan cowl pressure force	Fan cowl scrubbing drag
1	7309.7	-4832.3	1029.5
2.0	6381.0	-3900.7	755.7
3.0	5140.6	-3710.8	533.1
4	3344.6	-2767.4	242.4
5	4971.9	-3419.0	543.3
6	5843.2	-3758.6	563.5
7	4449.1	-3351.2	492.4
2.1	4941.7	-2865.9	682.9
2.2	11693.6	-6111.3	837.7
TO 1	-2245.0	3384.0	460.7
TO 2	-1936.0	2890.9	337.4
TO 3	-1095.5	1750.3	236.3
TO 4	391.2	5.4	96.7
3.1	6547.2	-4896.7	527.5
3.2	8140.2	-6158.9	520.3
3.3	10098.1	-7558.8	510.5
3.4	11692.9	-8605.0	500.9
2.B	6246.0	-3952.4	751.6

Case	Core cowl pressure force	Core cowl scrubbing drag	Plug pressure force
1	-2384.98	93.621	-775.802
2	-2001.48	166.907	-643.776
3	-774.357	272.998	-420.841
4	738.731	365.539	-307.127
5	-998.93	177.396	-556.325
6	-1303.34	288.786	-436.504
7	-247.239	273.58	-404.656
2.1	-1741.24	157.46	-576.315
2.2	-3107.25	175.012	-884.147
TO 1	-2827.1	195.487	-978.893
TO 2	-1904.5	347.459	-839.521
TO 3	-588.307	579.738	-585.961
TO 4	355.228	764.997	-420.963
3.1	-843.842	247.13	-448.353
3.2	-873.458	219.288	-420.529
3.3	-869.486	191.461	-376.339
3.4	-846.444	172.552	-335.196
2.B	-1934.2	166.808	-641.101

H. Table of drag and thrust components

Case	Plug scrubbing drag	Ram Drag	Gross Thrust
1	15.8	54235.1	75373.0
2.0	15.7	54235.1	75399.6
3.0	15.3	54235.1	75395.4
4	15.6	54235.1	75582.2
5	12.2	54731.6	71628.5
6	15.4	54235.1	75649.0
7	15.4	54235.1	75229.7
2.1	14.9	48777.5	69807.9
2.2	16.4	60190.0	81755.2
TO 1	36.6	51270.3	166209.8
TO 2	36.4	51275.3	166131.3
TO 3	35.5	51253.0	166257.0
TO 4	35.9	51274.3	163334.3
3.1	10.3	50452.4	65715.8
3.2	6.0	46517.1	56521.7
3.3	3.0	42100.8	47326.0
3.4	1.5	38744.5	41012.5
2.B	15.8	54235.1	75384.6

Case	Hybrid Drag only considering fan cowl	Hybrid Drag	Net Propulsive Force
1	3506.9	455.6	20682.3
2.0	3235.9	773.3	20391.1
3.0	1962.9	1056.0	20104.3
4	819.6	1632.4	19714.8
5	2096.2	730.6	16166.4
6	2648.0	1212.4	20201.6
7	1590.2	1227.3	19767.3
2.1	2758.7	613.5	20416.9
2.2	6420.0	2620.1	18945.1
TO 1	1599.7	-1974.2	116913.7
TO 2	1292.3	-1067.9	115923.9
TO 3	891.1	332.1	114671.9
TO 4	493.3	1228.4	110831.5
3.1	2178.0	1143.2	14120.1
3.2	2501.6	1432.9	8571.7
3.3	3049.8	1998.5	3226.7
3.4	3588.8	2581.2	-313.2
2.B	3045.2	652.5	20497.0

Case	Net Thrust	Cycle Net Thrust	Difference
1	21137.9	21210.0	-0.34
2.0	21164.5	21210.0	-0.22
3.0	21160.3	21210.0	-0.23
4	21347.1	21210.0	0.64
5	16896.9	16850.0	0.28
6	21413.9	21210.0	0.95
7	20994.6	21210.0	-1.03
2.1	21030.4	20970.0	0.29
2.2	21565.2	21570.0	-0.02
TO 1	114939.5	113880.0	0.92
TO 2	114856.0	113880.0	0.85
TO 3	115004.0	113880.0	0.98
TO 4	112060.0	113880.0	-1.62
3.1	15263.4	14940.0	2.12
3.2	10004.6	9140.0	8.64
3.3	5225.2	3920.0	24.98
3.4	2268.0	760.0	66.49
2.B	21149.5	21210.0	-0.29

Table H.2: Components of thrust and drag for BLI test cases

Case	Pre entry drag	Fuselage pressure force	Fuselage scrubbing drag
0	0	1864.8	7692.1
1	-7784.24	3167.9	7535.5
2	-7955.5	3031.6	7453.4
3	-5200.5	1575.6	7360.6

Case	Fan cowl pressure force	Fan cowl scrubbing drag	Core cowl pressure force
BLI 0	0.0	0.0	0.0
BLI 1	1760.9	645.3	-2686.4
BLI 2	1999.5	846.1	-3374.2
BLI 3	1723.9	1027.6	-4166.4

Case	Core cowl scrubbing drag	Ram Drag	Gross Thrust
BLI 0	0.0	0.0	0.0
BLI 1	88.1	38748.0	45671.8
BLI 2	113.3	50176.9	59963.1
BLI 3	143.1	60895.3	76708.4

H. Table of drag and thrust components

Case	Hybrid Drag	Net Thrust	Net Propulsive Force
BLI 0	9556.9	0.0	-9556.9
BLI 1	2727.1	6923.8	4196.7
BLI 2	2114.2	9786.2	7672.0
BLI 3	2463.9	15813.1	13349.3

Appendix I

Table with pressures and pressure ratios

Table I.1: Pressures [Pa] and pressure ratios of nacelle test cases

Case	P1	P2	P13	P16
1	36333.1	36208.4	51802.3	51490.0
2.0	36336.4	36248.6	51388.4	51135.1
3.0	36332.2	36261.9	51023.1	50818.8
4	36334.5	36297.3	51202.3	51027.7
5	36332.1	36257.7	47487.6	47270.7
6	36333.9	36264.2	51381.2	51171.9
7	36332.7	36265.4	50767.4	50516.1
2.1	34618.9	34536.8	49078.7	48831.5
2.2	39443.2	39360.5	54060.4	53793.7
TO 1	105827.0	105607.0	156151.0	155447.0
TO 2	105826.0	105610.0	155275.0	154646.0
TO 3	105839.0	105570.0	154638.0	154157.0
TO 4	105836.0	105552.0	151767.0	151242.0
3.1	36332.8	36278.6	47656.5	47465.1
3.2	36331.1	36290.6	44365.8	44190.9
3.3	36332.0	36301.8	40968.0	40813.1
3.4	36333.0	36308.0	38621.0	38483.6
2.B	36335.8	36238.1	51376.9	51123.9

Case	Inlet PR (P2/P1)	Cycle Inlet PR (P2/P1)	Difference Inlet PR [%]
1	0.99657	0.998	-0.143
2	0.99758	0.998	-0.042
3	0.99807	0.998	0.007
4	0.99898	0.998	0.098
5	0.99795	0.998	-0.005
6	0.99808	0.998	0.008
7	0.99815	0.998	0.015
2.1	0.99763	0.998	-0.037
2.2	0.9979	0.998	-0.010
TO 1	0.99792	0.998	-0.008
TO 2	0.99796	0.998	-0.004
TO 3	0.99746	0.998	-0.054
TO 4	0.99732	0.998	-0.068
3.1	0.99851	0.998	0.051
3.2	0.99889	0.998	0.089
3.3	0.99917	0.998	0.117
3.4	0.99931	0.998	0.131
2.B	0.99731	0.998	-0.069

I. Table with pressures and pressure ratios

Case	Bypass PR (P16/P13)	Cycle Bypass PR (P16/P13)	Difference Bypass PR [%]
1	0.99397	0.995	-0.104
2	0.99507	0.995	0.007
3	0.996	0.995	0.100
4	0.99659	0.995	0.160
5	0.99543	0.995	0.043
6	0.99593	0.995	0.093
7	0.99505	0.995	0.005
2.1	0.99496	0.995	-0.004
2.2	0.99507	0.995	0.007
TO 1	0.99549	0.99545	0.004
TO 2	0.99595	0.99545	0.050
TO 3	0.99689	0.99545	0.144
TO 4	0.99654	0.99545	0.109
3.1	0.99598	0.995	0.098
3.2	0.99606	0.99501	0.105
3.3	0.99622	0.99512	0.110
3.4	0.99644	0.99529	0.115
2.B	0.99508	0.995	0.008

Case	FPR	Cycle FPR	Difference FPR [%]
1	1.430670784	1.4	2.14
2	1.417665786	1.4	1.25
3	1.407071885	1.4	0.50
4	1.410636604	1.4	0.75
5	1.309724555	1.3	0.74
6	1.416857397	1.4	1.19
7	1.39988529	1.4	-0.01
2.1	1.421055222	1.4	1.48
2.2	1.373468325	1.4	-1.93
TO 1	1.478604638	1.444	2.34
TO 2	1.470267967	1.444	1.79
TO 3	1.464791134	1.444	1.42
TO 4	1.437841064	1.444	-0.43
3.1	1.313625664	1.3	1.04
3.2	1.222514921	1.2	1.84
3.3	1.128539081	1.1	2.53
3.4	1.063704969	1.032	2.98
2.B	1.417759209	1.4	1.25

Table I.2: Pressures [Pa] and pressure ratios of BLI test cases

Case	P1	P2	P13	P16
BLI 1	31448.2	31190.1	42101.9	41849.1
BLI 2	32088.5	31831.4	42776.4	42547.5
BLI 3	32776.9	31948.6	43552.2	43329.2

Case	Inlet PR (P2/P1)	Cycle Inlet PR (P2/P1)	Difference Inlet PR [%]
BLI 1	0.99179	0.998	-0.626
BLI 2	0.99199	0.998	-0.606
BLI 3	0.97473	0.998	-2.387

Case	Bypass PR (P16/P13)	Cycle Bypass PR (P16/P13)	Difference Bypass PR [%]
BLI 1	0.994	0.995	-0.101
BLI 2	0.99465	0.995	-0.035
BLI 3	0.99488	0.995	-0.012

Case	FPR	Cycle FPR	Difference FPR [%]
BLI 1	1.349848189	1.3	3.693
BLI 2	1.343842872	1.3	3.262
BLI 3	1.363195883	1.3	4.636